

ADAPTIVE UPDATE METHOD FOR EMBEDDED REAL-TIME

JET ENGINE MODELS

by

Frederick John Pineo

B.S., Clarkson College of Technology (1980)

SUBMITTED IN PARTIAL FULFILLMENT OF

THE REQUIREMENTS OF THE

DEGREE OF

MASTER OF SCIENCE

at the

MASSACHUSETTS INSTITUTE OF TECHNOLOGY

February 1985

© Frederick J. Pineo 1985

The author hereby grants to M.I.T. permission to reproduce and to distribute copies of this thesis document in whole or in part.

Signature redacted

Signature of Author

Department of Mechanical Engineering
January 19, 1985

Signature redacted

Certified by

J. Karl Hedrick
Thesis Supervisor

Signature redacted

Accepted by

Ain A. Sonin
Chairman, Departmental Committee on Graduate Students

MASSACHUSETTS INSTITUTE
OF TECHNOLOGY

MAR 22 1985

LIBRARIES ARCHIVES



77 Massachusetts Avenue
Cambridge, MA 02139
<http://libraries.mit.edu/ask>

DISCLAIMER NOTICE

Due to the condition of the original material, there are unavoidable flaws in this reproduction. We have made every effort possible to provide you with the best copy available.

Thank you.

Some pages in the original document contain text that is illegible.

ADAPTIVE UPDATE METHOD FOR EMBEDDED REAL-TIME

JET ENGINE MODELS

by

Frederick John Pineo

Submitted to the Department of Mechanical Engineering
on January 18, 1985 in partial fulfillment of the
requirements for the Degree of Master of Science
in Mechanical Engineering

ABSTRACT

Real-time jet engine models that are compact enough to be programmed along with the control laws in the digital engine control (embedded) have recently come into use. As with all models, there are the inevitable modelling errors that limit the capability to discern failures and/or to monitor the health of the engine components. A technique to adapt the model to reflect the particular engine that the control is mated to is a useful way to improve the fidelity of the model. This would allow the model to change as the engine quality changes. Several techniques were explored for the adaptation, and that selected was a modification to the extended Kalman filter. The filter gains are pre-computed at a representative condition and applied to the non-linear engine model. The results show that the adapted model tracks an analytical truth model of the engine in steady state and dynamic modes, and that it can be used for engine condition monitoring, analytical redundancy and possibly synthetic control.

Thesis Supervisor: Dr. J. Karl Hedrick

Title: Professor of Mechanical Engineering

TABLE OF CONTENTS

	<u>Page</u>
ABSTRACT	2
ACKNOWLEDGEMENTS	4
LIST OF FIGURES	5
LIST OF TABLES	6
LIST OF SYMBOLS	7
 CHAPTER	
1. INTRODUCTION	9
Evolution of Real Time Models	10
Benefits of an Adaptive Algorithm	11
Outline of This Study	12
2. ENGINE MODEL	14
Jet Engine Description	14
Model Requirements	17
Detailed Model Description	18
3. ADAPTIVE ALGORITHM DEVELOPMENT	39
Parameter Set Selection	40
Gain Matrix Methodology	48
Inverse Jacobian Gain Matrix	49
Recursive Least Squares Derived Gain Matrix	53
Constant Gain Extended Kalman Filter	57
Extended Kalman Filter	63
Robustness Issues	65
Singular Values	66
Robustness Analysis	68
4. NUMERICAL RESULTS	72
Static Performance	72
Dynamic Tracking	79
5. PROCESSOR REQUIREMENTS	107
Required Processor Time-Current Computer	107
Practical Issues of the Embedded Model	108
6. SUMMARY AND CONCLUSIONS	110
REFERENCES	113
APPENDIX: DATA FOR PARAMETER SET SELECTION	115

ACKNOWLEDGEMENTS

I gratefully acknowledge the guidance of my advisor, J. Karl Hedrick, whose advice and direction during the past six months was instrumental in keeping my work on track and in focus. I also thank the General Electric Company for financial support to perform the work, and Mike French and Mike Idelchik at GE for technical support. Finally, I thank my wife, Jean, for moral support during the many hours spent.

LIST OF FIGURES

		<u>Page</u>
2.1-1	Engine Schematic and Station Descriptions	15
2.3-1	Compressor Characteristics	20
2.3-2	Flow Chart for Real Time Model	33
2.3-3	Heat Soak Representation	37
2.3-4	Thermocouple Compensation	38
3.1-1	Flight Envelope Check-Out Points	44
3.2.1-1	Pole Plot-Scaled Inverse Jacobian Feed-Back Matrix	54
3.3.2-1	Singular Values for Kalman Filter	70
4.2-1 thru 4	Baseline Accel-Dynamic Simulation	80-83
4.2-5 thru 9	Scaled Inverse Jacobian Gain Update of Parameters	85-89
4.2-10 thru 14	Least Squares Derived Gain Update of Parameters	91-95
4.2-15 thru 19	Constant Gain Extended Kalman Filter Update of Parameters	96-100
4.2-20 thru 24	Extended Kalman Filter Update of Parameters	101-105
4.2-25	Summary of Update Methods' Errors	106
A-1	Flow Path for Variable Set Selection	136

LIST OF TABLES

		<u>Page</u>
3.1-1	Engine Variables	41
3.1-2	Sets of Parameters	45
3.1-3	Sensor Errors	47
3.1-4	Engine-to-Engine Variations	47
3.2.4-1	Summary of Continuous Extended Kalman Filter	63
3.2.2-1	Eigenvalues of F100 Engine Model	69
4.1-1	Baseline Performance of the Model	73
4.1-2	Modelling Error Statistics	74
4.1-3	Improvements by Model Adaptation	74
4.1-4	Effects of Engine to Engine Variations	76
4.1-5	Effects of Sensor Errors	77
5.1-1	Processor Time	108
A-1 thru A-12	Results for Sets 1-12	117-128
A-13	Envelope Survey of Parameter Sets	129
A-14 thru A-17	Effects of Sensor Errors	132-135
A-18	RSS of Sensor Error Sensitivities	136
A-19 thru A-21	Effects of Engine to Engine Variations	137-139
A-22	Final Summary	140

LIST OF SYMBOLS

<u>A</u> , <u>B</u> , <u>C</u> , <u>D</u> ; <u>F</u> , <u>G</u> , <u>H</u>	State space representation matrices
A8	Exhaust nozzle area
A	Area
C_p	Specific heat
<u>e</u>	Vector of output errors
FAR	Fuel to air ratio
FF41	Turbine nozzle flow function
FG	Gross thrust
FN	Net thrust
h	Film coefficient
HPC	Compressor horsepower
HPF	Fan horsepower
HPHPT	High pressure turbine horsepower
HPLPT	Low pressure turbine horsepower
<u>J</u>	Jacobian matrix
<u>K</u>	Kalman gain matrix
m	Mass
N_1	Fan rotor speed
N_2	Compressor rotor speed
P	Total pressure
Ps	Static pressure
<u>Q</u> , <u>R</u>	Kalman filter weighting matrices
<u>r</u>	Vector of parameters
T	Total temperatures
<u>u</u>	Vector of inputs
UBHP	Unbalanced torque in high pressure spool
UBLP	Unbalanced torque in low pressure spool
W	Flow
W_F	Fuel flow
W--R	Corrected flow
<u>x</u>	Vector of states

XJHP	HP rotor inertia
XJLP	LP rotor inertia
\mathbf{y}	Vector of outputs
δ	Pressure correction P/14.7 psi
η	Efficiency
θ	Temperature correction T/518.7 °R
τ	Time constant
σ	Singular value

Subscripts

c	Compressor
f	Fan
t	Turbine
2t	LP turbine

Superscripts

Λ	Estimate
-----------	----------

1. INTRODUCTION

The advent of advanced microelectronic circuitry has led to the application of digital engine control to recent turbofan engines. Increased demands on control law complexity to wring out the optimum performance have made hydromechanical controls too heavy, complex, and costly, and also less reliable due to their complexity. Microcircuitry can replace the hardware in the hydromechanical control, and increase performance and reliability with a decrease in weight. Several programs have demonstrated the usefulness of digital controls. The Navy-sponsored Full Authority Digital Electronic Control (FADEC) program (Ref. 1) demonstrated control systems for advanced variable cycle engines. The NASA U.S. Air Force Digital Electronic Engine Control (DEEC) program (Ref. 2) has demonstrated performance improvements on the Pratt and Whitney F100 engine. The NASA Cooperative Control Program (Ref. 3) on the YF-12C triple sonic aircraft was successful in demonstrating integrated inlet/autopilot/auto throttle systems.

The control laws for advanced applications will require many highly reliable sensors. There are two principle solutions to reliability. The first is hardware redundancy, where all or some sensors are duplicated. There is the obvious weight penalty here. The second is analytical redundancy, which uses a reference model of the engine to provide estimates. It is dependent upon the accuracy of the model. This thesis concerns the use and adaptive update of a current model of an advanced afterburning turbofan engine produced at the General Electric Company

Aircraft Engine Business Group in Lynn, Massachusetts. The model is embedded in the digital control and processes in real time during engine operation.

1.1 Evolution of Real Time Models

Models of jet engines can be classified into two types: those that operate in real time, and those that do not. The first category include all models whose equation set processing time is less than or equal to the update time of the model. The second are typically high accuracy models that try to capture all possible effects occurring in the engine cycle. The distinction between the two depend on model complexity and the particular processor. As processors have matured in recent years, the amount of complexity has grown proportionately. A recent survey of jet engine models provides insight into the development (Ref. 4). The highlights are presented here.

The reference classifies the modelling approaches into three categories. These are Parameter Synthesis (PS), Pseudolinear (PL), and Simplified Component (SC). The first method utilizes tabulations of sensed variables as a function of each other. There are no explicit dynamics. This method was used to demonstrate hard failure detection and replacement on a J-85 single spool turbojet engine (Ref. 5). It was also used on a TF-30 two spool afterburning turbofan engine around the flight envelope (Ref. 6). The second method, pseudolinear, has been used on several occasions. It consists of a dynamic linear state space structure, with individual coefficients in the equations varying as a function of the state. One application was on a Pratt and Whitney F100 two spool

afterburning turbofan engine (Ref. 7). This provided an analytical judge for the fan turbine inlet temperature. The final type, the simplified component, is the subject of this investigation.

The simplified components model is based upon highly detailed non-linear engine simulations. Detail is selectively removed in order to achieve real time capability while maintaining accuracy. The model contains information about each component of the engine, and thus is modular in nature. The physics of each process are represented in order to achieve accuracy, along with appropriate dynamics. Simplified component approaches have been used in at least three works. Spang and Corley (Ref. 8) used it for the Quiet Clean, Short Haul, Experimental Engine (QCSEE), French employed the technique for a variable cycle engine (Ref. 9), and Pisano et al. modeled a T700 turboshaft engine using it in Ref. 10. The history of real time models shows that complexity was added as microprocessors developed, and the latest models are highly non-linear representations of the engine cycle.

1.2 Benefits of an Adaptive Algorithm

The potential benefits of analytical redundancy are straightforward. There is the weight savings due to the elimination of physically redundant sensors, and the cost savings. Additionally, analytical redundancy can potentially distinguish between soft (drift and small in range) failures and hard failures (large out-of-range). However, since all models have errors, the magnitude of failure detection is limited to the modelling accuracy. Thus, an algorithm that adapts the model to the particular

engine can reduce the window for detection, plus provide additional benefits.

A good adaptive algorithm, in essence, becomes a self teaching control, and can provide the following benefits. First, it can provide engine condition monitoring (ECM) capability. The detection of component characteristic drifts with engine operating time as the engine deteriorates or gets dirty has a significant impact on maintenance procedures. For example, high pressure turbine efficiency typically decreases due to rubs or other effects, and detection of this fact for a poor engine would easily identify the cause and replacement action. Second, the adaptation capability would be extremely useful to minimize modelling errors in consideration of engine to engine variations. The model could adapt its internal component characterizations to match those of the particular engine that the controller is on. Third, the adaptation would increase accuracy of the estimates of sensed variables, due to the capabilities mentioned above. Finally, with a highly accurate model, the estimates of non-measurable variables could be used for synthetic control. For example, high pressure turbine inlet temperature is important for performance and hot parts life, but currently its measurement is impossible. If a good synthesis of it were possible, the engine could be controlled to it providing increased performance and better hot parts life management. It is for the above reasons that this work was undertaken.

1.3 Outline of This Study

The first task is to describe the component level real time model that is used in the study. Chapter 2 gives a fairly detailed description of the

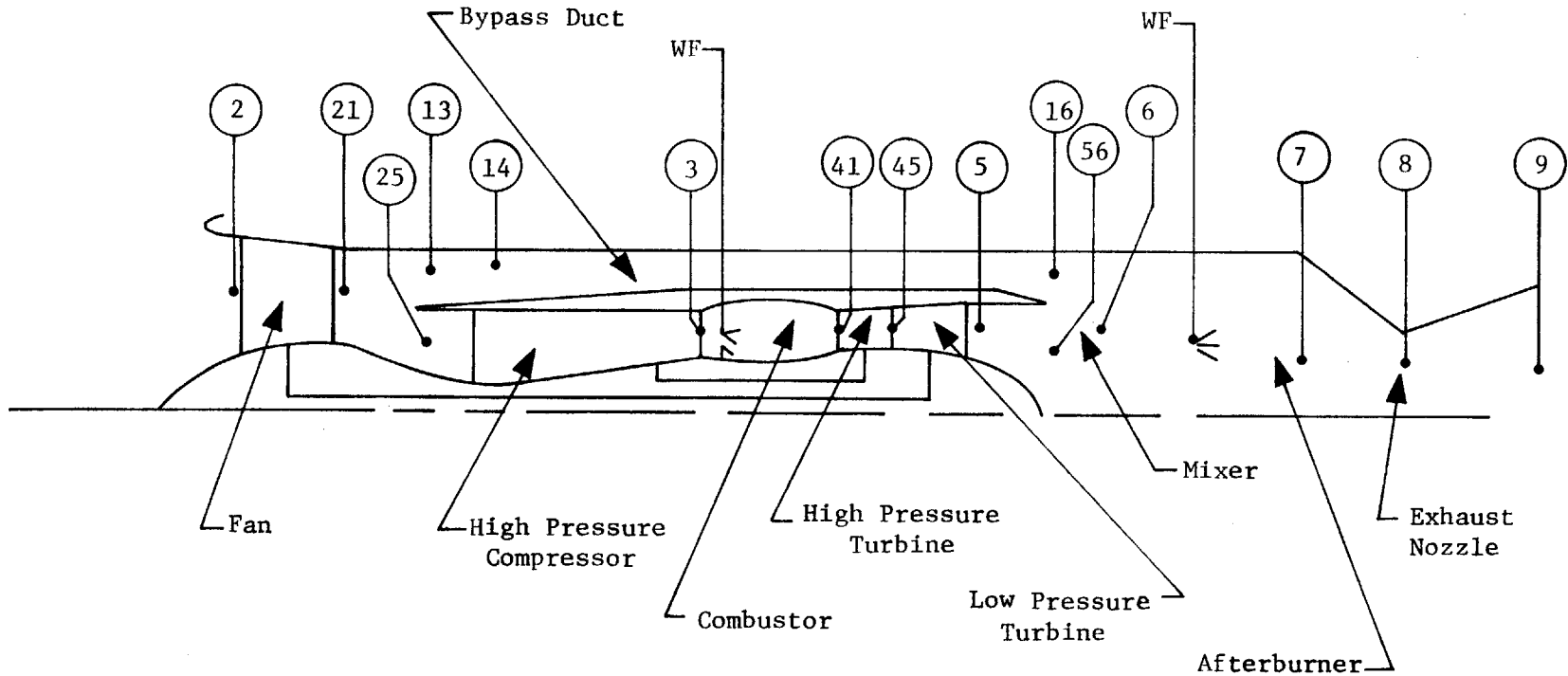
model and its operation. The model is typical in that each component in the engine system is described. Chapter 3 deals with the adaptive algorithm development. Part 3.1 describes the selection of parameters used to adapt the model. Part 3.2 describes the dynamic methodology used to employ the parameters. Part 3.3 discusses robustness issues of the update method. Numerical results are shown in Chapter 4. A discussion of microprocessor technology is included in Chapter 5. Finally, conclusions and recommendations are presented in Chapter 6.

2. ENGINE MODEL

The engine model used in this study was developed at the General Electric Company in Lynn, Massachusetts, and is described in Reference 9. Many of the details of that description are presented here, in order to give a clear picture of the work performed. Some changes to the model that occurred after its initial release are also described in the pages that follow. The model is contained in General Electric Transient Program No. 82086D per Reference 11.

2.1 Jet Engine Description

Before addressing the model details, a brief description of the actual engine that it represents is necessary. The subject engine is a modern, low-bypass turbofan engine with an afterburner for thrust augmentation. The components, from inlet to exhaust are shown in Figure 2.1-1. The fan, or low pressure compressor provides initial supercharge to the high pressure compressor (HPC). Part of the compressed air exiting the fan is bypassed around the high pressure spool in the bypass duct, and is mixed with the core stream at the mixing plane. The highly compressed air from the HPC is mixed with fuel and burned in the combustor, providing sufficient energy to drive the fan and compressor. The hot gases from the combustor are expanded in the high pressure turbine, which is on the same shaft as the HPC, producing the horsepower required to drive the HPC plus all parasitic horsepower such as in the accessory gearbox and for airframe power extraction. The hot gases are further expanded in the low pressure



ENGINE SCHEMATIC AND STATION DESCRIPTIONS

FIGURE 2.1-1

turbine (LPT) which drives the fan on their common shaft. After the LPT, the gases are mixed with the bypass air, and entered into the augmentor section. Here, additional fuel may be injected to provide additional thrust. Finally, the hot gases are expanded in the variable exhaust nozzle, and the expansion provides thrust to propel the jet aircraft.

The jet engine cycle described is a highly non-linear process. It is further complicated by the following factors: it operates over a wide range of flight conditions (altitude and mach number combinations); it operates over a wide range of power settings; and has a high throttle response capability. As evidence of the last statement, the engine can accelerate from flight idle to maximum power in five seconds, which is a fifty-fold increase in thrust.

It is common to describe the points in the process by numbered stations. The station designations for each component are shown in Figure 2.1-1, and amplified here. Inlet to the fan is station 2, and exit is station 21. Because of the hub to tip work split, the inlet to the bypass duct is a different condition than the inlet to the high pressure compressor. Thus, station 13 designates the inlet to the bypass duct, and station 25 designates the entrance to the HPC. Exit from the HPC is station 3, and exit from the combustor is station 41. The high pressure turbine and low pressure turbine are considered close-coupled, so the common designation between them is station 45. Exit from the LP turbine is station 56, which is just before the mixed station 6. The bypass duct exit is station 16, which is axially the same as 56, but in the bypass stream before mixing. Afterburner fuel flow is introduced as station 61, and fully mixed and

burned by station 7, the inlet to the exhaust nozzle. The nozzle throat is station 8, and nozzle exit station is 9.

2.2 Model Requirements

There are many levels of modelling sophistication for the turbofan engine cycle, and there exists the classic trade of complexity versus accuracy. The requirement imposed by having the model contained in the engine's digital control imposes a heavy penalty on complexity, but if the model is to be used for a number of control purposes, there may be an equally heavy penalty on inaccuracy.

The modelling requirements are composed of those dictated by engine operation and those dictated by the digital engine control. Regardless of model structure the model must be operational from ground idle (lowest power setting) to maximum afterburner; for altitudes from sea-level to 60,000 ft, and for flight mach numbers to 1.6. In this case, operational means stable model characteristics with modelling errors no greater than five percent on engine measured variables. For this application, the engine measured variables are fan rotor speed (N_1), compressor rotor speed (N_2), compressor discharge static pressure (PS3C), and low pressure turbine total temperature (T5). The type of processor in the digital engine control will dictate the size and nature of the equation set used to describe the engine. The processor used in this case imposed the following requirements. First, all equations describing the process characteristics are expressed as polynomial equations no greater than third order. Second, there are no tables or table look-up involved. Third, in order to operate in real time, all equations are evaluated in an overall update time of .01

seconds. Fourth, no iteration is permitted between time steps. Finally, only integer exponents are allowed, plus square roots.

It may be noted that the choice of processor has a strong influence on model structure. As stated previously, the processor for this application required polynomials. Other machine languages may be far more efficient with table look-up routines. Also, as the state of the art advances, model complexity can advance beyond the present model. Alternatively, the advances may permit the extended Kalman filter to become practical as necessary. All previous attempts at the full Kalman filter equations have faced the computational burden of updating the covariance equations in real time, but have concluded that the burden is too much (Refs. 8, 10). Further analysis of current and future processor technology is reserved for Chapter 5.

2.3 Detailed Model Description

The description of the model is borrowed heavily from Reference 9. In many places, the description is further amplified. The overall perspective for this model is a component by component description of the jet engine aero-thermodynamic cycle with sufficient complexity to provide accuracy and sufficient simplicity to meet the real time processing requirements. The first phase of the description involves the original model, and the second adds detail of the latest incorporations to increase model accuracy. It should be noted that many of the later additions violate some of the rules stated in Section 2.2. The main reason for these violations is that advances in microprocessors since 1981 have made the violations a minor

computational issue. The model is described by component from inlet to exhaust.

The first component in the engine is the fan, or low pressure compressor. It takes the shaft energy provided by the low pressure turbine, and through the blade aerodynamics, converts it to pressure energy. The fan operates over a wide range of pressure ratio and flow in order to control thrust. The operational characteristics of the fan are generically represented by a four-dimensional fan map as in Figure 2.3-1A. The figure shows the highly non-linear relationships between airflow, speed, pressure ratio, and efficiency. The x-axis is corrected fan airflow, where the correction parametrically collapses performance over a variety of inlet conditions. The definition of corrected airflow is

$$W1R = \frac{W1 \times \sqrt{T2/518.67}}{P2/14.696} = \frac{W1 \sqrt{\theta_2}}{\delta_2} \quad 2.3-(1)$$

The y axis is fan pressure ratio. Also shown are the corrected speed lines and lines of constant efficiency, called efficiency islands. Thus at a given corrected speed and corrected flow, there is a defined pressure ratio at a given efficiency. Finally, the stall or surge line is shown.

The map characteristics are compressed and linearized by transforming it as a function of exit corrected flow in place in inlet corrected flow. The new map is shown in Figure 2.3-1B. Thus define exit corrected flow

$$W21R = \frac{W21 \sqrt{T25/518.67}}{P21/14.696} = \frac{W21 \sqrt{\theta_{25}}}{\delta_{25}} \quad 2.3-(2)$$

Then
$$P21/P2 = f(W21R, N_1 / \sqrt{\theta_2}) \quad 2.3-(3)$$

COMPRESSOR CHARACTERISTICS

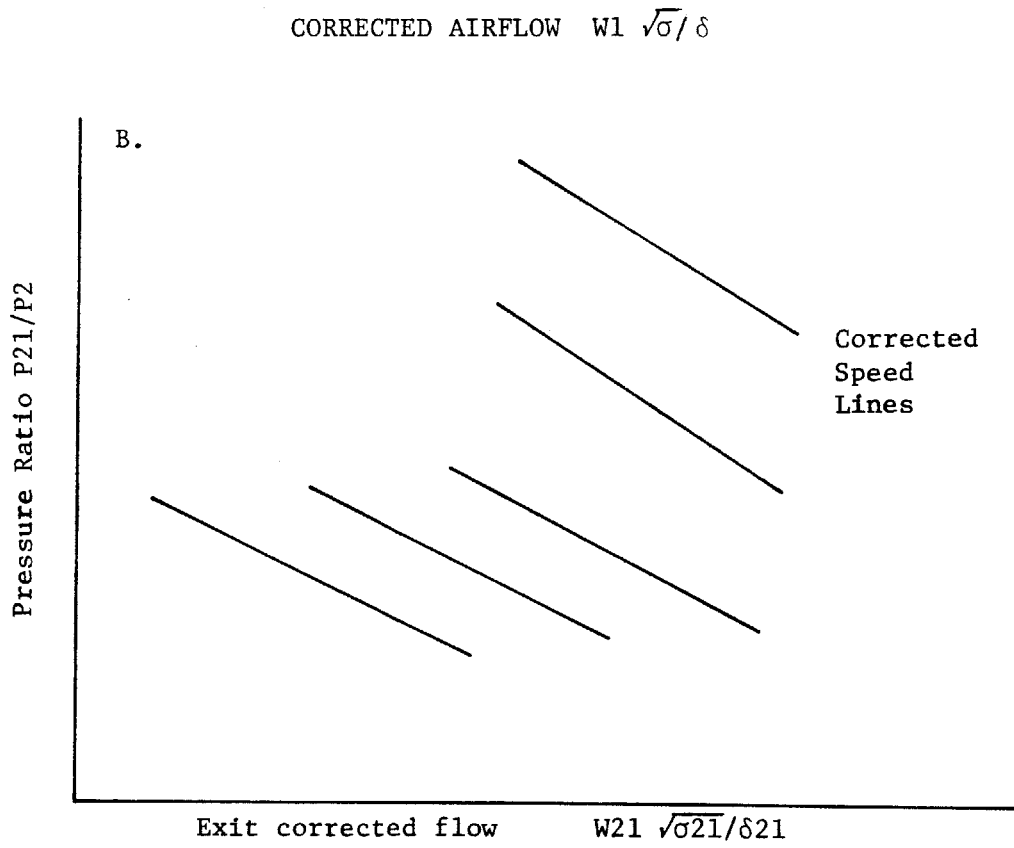
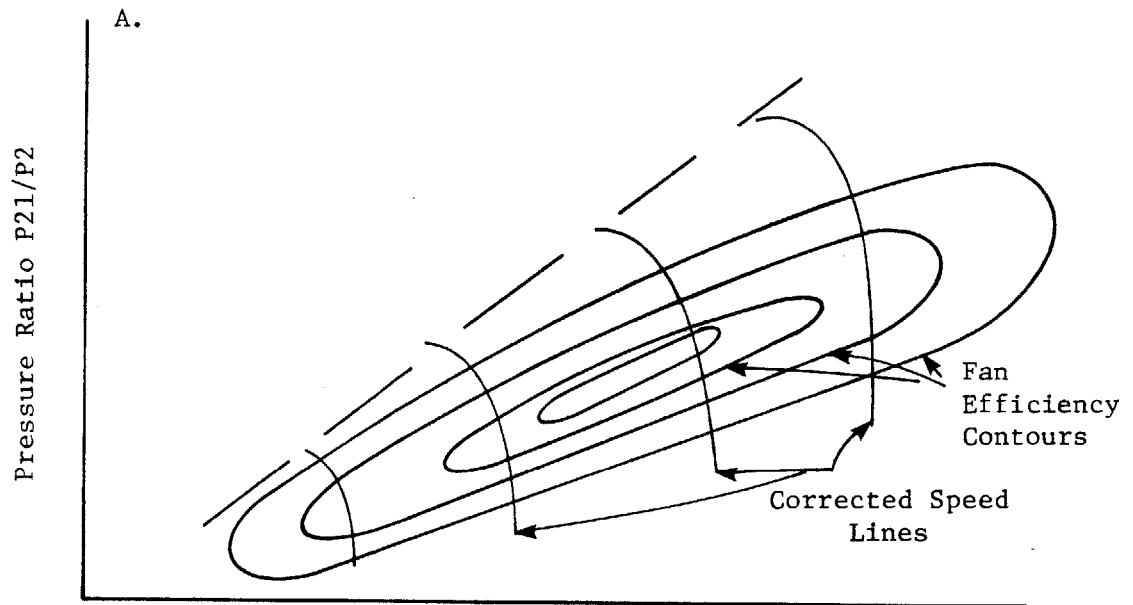


FIGURE 2.3-1

Now, the temperature ratio must be calculated in order to calculate fan work. For adiabatic compression, temperature ratio is a function of pressure ratio and efficiency.

$$\frac{T_{21}}{T_2} - 1 = \left(\frac{P_{21}}{P_2} - 1\right) \left(\frac{\gamma-1}{\gamma}\right) / \eta_f \quad 2.3-(4)$$

If the fan characteristic is simplified, fan efficiency is most strongly a function of corrected speed. Thus, the final functional relationship used in the model is

$$T_{21}/T_2 = f(P_{21}/P_2, N_1/\sqrt{\theta_2}) \quad 2.3-(5)$$

Then fan inlet airflow is a function of exit corrected airflow pressure ratio and temperature ratio. Since $W_{21} = W_1$, then

$$W_1 = \frac{W_{21R} \times (P_{21}/14.696)}{\sqrt{T_{21}/518.67}} \quad 2.3-(6)$$

And fan horsepower is calculated

$$HPF = f(W_1, T_{21}, T_2) \quad (2.3-(7))$$

The calculation of airflow may seem backward here, but whether it is based on inlet or exit flow, there is the necessity to iterate the flow to match continuity requirements. The iteration is done in time rather than by multiple passes, as is described in the iteration and integration logic

section. The above functional relationships consist of polynomials and segmented linear functions with a total of 54 arithmetic and logical operations to represent the fan from choke to stall for speeds from 30% to 100%.

The intercompressor duct downstream of the fan splits the flow between the bypass duct and the core compressor. The inlet states to the high pressure compressor are treated as fixed fractions of the states at the exit from the fan.

$$P_{25} = C \times P_{21} \quad 2.3-(8)$$

$$T_{25} = C \times T_{21} \quad 2.3-(9)$$

The high pressure compressor is modelled similarly to the fan. Exit corrected airflow was used to compress and linearize the flow-speed-pressure ratio characteristic. Thus

$$W_{3R} = \frac{W_3 \times \sqrt{T_3/518.67}}{P_3/14.696} \quad 2.3-(10)$$

$$P_3/P_{25} = f(W_{3R}, N_2/\sqrt{\theta_{25}}) \quad 2.3-(11)$$

$$T_3/T_{25} = f(P_3/P_{25}, N_2/\sqrt{\theta_{25}}) \quad 2.3-(12)$$

$$W_3 = f(W_{3R}, T_3, P_3) \quad 2.3-(13)$$

Compressor horsepower is calculated from flow and temperature rise.

However, the parasitic bleeds that are used to cool the high pressure and low pressure turbine components must be accounted for. These parasitics are modelled as a constant fraction of inlet airflow.

$$W_{25} = C \times W_3 \quad 2.3-(14)$$

$$HPC = f(W_3, T_3, T_{25}) \quad 2.3-(15)$$

One final parameter is calculated because it is a sensed variable: compressor discharge static pressure. Here it is represented as a constant fraction of the total pressure P_3 . The implication is that the mach number at the exit of the compressor is relatively constant. The above modelling required 55 operations to represent the compressor for speeds from 75% to 100% (the normal operational range) for loading from full acceleration to full deceleration.

The air from the HPC is diffused, entered into the main combustor, mixed with fuel and the fuel air mixture is burned. There is a pressure drop caused by aerodynamic losses, and a temperature rise due to the burning of the fuel air mixture. The pressure drop is an aerodynamic function, and is represented as a simple function of corrected airflow.

$$P_{41} = P_3 \times f(W_{3R}) \quad 2.3-(16)$$

The temperature rise is a function of the fuel-air ratio and the combustor inlet temperature, T_3 .

$$T41 = T3 + f(\text{FAR41}, T3) \quad 2.3-(17)$$

It is necessary to calculate both airflow and mass flow for the turbine nozzle flow function check. Again, the parasitics are a fraction of total core airflow:

$$\text{WA41} = C \times \text{W25} \quad 2.3-(18)$$

$$\text{W41} = \text{WA41} + \text{WFM}/3600 \quad 2.3-(19)$$

Note that WFM, the main burner fuel flow, is conventionally expressed in pounds per hour. The fuel-air ratio is then

$$\text{FAR41} = (\text{WFM}/3600)/\text{WA41} \quad 2.3-(20)$$

These functional relationships required only 14 steps to describe the process.

The next step in the model is representing the bypass duct to insure proper back pressure on the fan and the LP turbine. Note here that due to the required static pressure balance between the core stream and the bypass stream at the mixing plane, the correct representation in the model will insure accuracy. The purpose of bypassing a fraction of the airflow is to increase overall cycle efficiency, while maintaining a high level of thrust. In a pure turbojet cycle there is high thrust, but also high specific fuel consumption. For a turbofan cycle, with a high bypass ratio, the thermodynamic cycle is more efficient but produces less thrust with the

same airflow. Thus, the subject engine has the high thrust properties of the turbojet cycle, with the better SFC properties of the turbofan.

The duct inlet temperature and pressure must be calculated consistently with the amount of energy exiting from the fan. For the pressure energy, the following must hold:

$$P_{13} \times W_{13} + P_{25} \times W_{25} = P_{21} \times W_{21} \quad 2.3-(21)$$

However, the properties at station 14, which is downstream of the splitter and includes a loss from 13 to 14, is of interest. Thus we calculate ($W_{14} = W_{13}$)

$$P_{14} = C \times P_{13} = C \left(\frac{P_{21} \times W_{21} - P_{25} \times W_{25}}{W_{14}} \right) \quad 2.3-(22)$$

The thermal energy balance requires that the following equation holds true:

$$T_{14} \times W_{14} = T_{21} \times W_{21} - T_{25} \times W_{25} \quad 2.3(23)$$

or

$$T_{14} = (T_{21} \times W_{21} - T_{25} \times W_{25})/W_{14} \quad 2.3-(24)$$

There is an input of heat into the bypass stream from the core engine casing in the hot section. This thermal energy is modeled as a simple convective heat transfer.

$$T16 = T14 + f(T3, T25, W14) \quad 2.3-(25)$$

There is also a pressure loss from inlet to exit of the bypass duct due to normal aerodynamics and irregularities in the core casings. The loss is calculated based on "pseudo" mach numbers, which are closely related to the square of the actual mach numbers.

$$P16 = P14 \times (1 - f(W16, T16, P14)) \quad 2.3-(26)$$

It is necessary to calculate the static pressure at station 16 in order to preserve the static pressure balance at the mixing plane. It is a straightforward compressible flow relation, that is simplified for the computational speed required.

$$PS16 = P16 \times f(W16, P16, T16, AE16) \quad 2.3-(27)$$

The high pressure turbine consists of a choked nozzle to direct the hot gases onto the turbine blades, and the turbine wheel, which is on a common shaft with the high pressure compressor. The nozzle is choked throughout the normal operating range in order to control the HPC back pressure, and to prevent aerodynamic fluctuations downstream of the turbine from effecting the compressor. The nozzle model is simple:

$$W41 \times \sqrt{T41}/P4 = C \quad 2.3-(28)$$

or the error in nozzle continuity is

$$EFF41 = C - W41 \times \sqrt{T41}/P4 \quad 2.3-(29)$$

This error will be used in the iteration scheme described later.

Turbine work and horsepower are directly related to pressure ratio. The design of the two turbines and their close coupling produces the following convenient relationship:

$$P45/P4 = f(PS16/P4) \quad 2.3-(30)$$

Turbine horsepower is then

$$HPHPT = C \times W41 \times T41 f(P45/P4) \quad 2.3-(31)$$

Since the HPC horsepower was previously computed, the unbalanced power in the shaft can be obtained.

$$UBHP = (HPHPT/(HPC + f(WFM, WFR))) - 1 \quad 2.3-(32)$$

The function in the relation is an approximation of the parasitic horsepower in the HP spool required to drive the main fuel pump, the afterburner fuel pump, the exhaust nozzle actuators, and accounts for bearing losses.

The low pressure turbine further expands the hot gases to extract energy to drive the fan. Also, some cooling flows extracted from the HP compressor are re-introduced into the core stream. Downstream of the

turbine wheel are swirl, strut and diffusion losses that are included in this calculation.

The flow through the turbine is that of the high pressure turbine plus parasitic flows that are a fraction of W25.

$$W45 = W41 + C \times W25 \quad 2.3-(33)$$

The low pressure turbine nozzle is not hard-choked, so the flow function is a function of pressure ratio:

$$W45 \times \sqrt{T45/P45} = f(PS16/P45) \quad 2.3-(34)$$

Expressed more conveniently, since T45 is desired:

$$T45 = (P45 \times f(PS16/P45)/W45)^2 \quad 2.3-(35)$$

Then turbine work may be calculated

$$HPLPT = C \times W45 \times f(T45) \times f(PS16/P45, N_1, T45) \quad 2.3-(36)$$

Since the fan horsepower was previously calculated, the unbalance in the low pressure spool is found.

$$UBHP2T = (HPLPT/(HPF + C)) - 1 \quad 2.3-(37)$$

The constant accounts for bearing losses and windage.

The temperature control sensor is mounted downstream of the rotor, and the sensed temperature is defined by turbine pressure ratio.

$$T5 = T56 = T45 \times f(PS16/P45) \quad 2.3-(38)$$

The discharge pressure includes the previously mentioned swirl losses, diffusion losses, and strut losses. These are functions of mass flow, which is calculated from W45 and cooling flows.

$$W56 = W45 + C \times W25 \quad 2.3-(39)$$

$$P56 = PS16 \times f(W56 \sqrt{T56}/PS16, N_1/T45) \quad 2.3-(40)$$

After exiting from the LP turbine, the hot core gases are combined with the bypass stream air, and after mixing flow into the afterburner. Flow continuity demands that the total flow is the sum of the two streams

$$W6 = W56 + W16 \quad 2.3-(41)$$

The energy balance results in

$$T6 \times W6 = T16 \times W16 + T56 \times W56 \quad 2.3-(42)$$

A bias is included in the final form

$$T6 = C \times (T16 \times W16 + T56 \times W56)/W6 \quad 2.3-(43)$$

The pressure at station 6 includes any pumping gain resulting from the mixing of two streams at different pressures. There are losses downstream of the mixing plane. When non-afterburning, the loss is simply the friction and diffusion losses in the tail pipe. When afterburning, there is additional loss due to heat addition. The pumping and tail pipe losses are combined:

$$P_{61} = P_{56} \times (1 - f(W_6 \sqrt{T_6}/P_{56}, N_1/\sqrt{\theta_2})) \quad 2.3-(43)$$

For non-afterburning, the losses to the nozzle entrance are accounted for, thus

$$P_7 = P_{61} \quad 2.3-(44)$$

$$T_7 = T_6 \quad 2.3-(45)$$

The introduction and burning of fuel in the afterburner provides substantial temperature rise for thrust augmentation. The reason can be seen by examining the gross thrust function

$$FG/(W_8 \sqrt{T_8}) = f(P_8/P_{amb}) \quad 2.3-(46)$$

Thus

$$FG = C \times W_8 \times \sqrt{T_8} \times f(P_8) \quad 2.3-(47)$$

As T_8 increases, the gross thrust will. Then temperature rise is a function of fuel air ratio:

$$T_8 = T_6 + f(WFM, WFR, W_6) \quad 2.3-(48)$$

The pressure loss is a function of airflow and temperature rise (or ratio).

$$P_{8W} = P_{61} \times (1 - f(W_6 \sqrt{T_6}/P_{56}, T_7/T_6)) \quad 2.3-(49)$$

The gases are accelerated to sonic velocity in the exhaust nozzle, and expanded to ambient conditions in the divergent portion of the nozzle. The nozzle operates choked by design, and there is some leakage. The nozzle throat flow coefficient is calculated to provide a good calculation of back pressure on the engine. The flow coefficient is represented as

$$CF_8 = f(P_8/P_{amb}, A_8, P_8 - P_{amb}) \quad 2.3-(50)$$

The throat area is corrected for inward nozzle deflection at low pressure ratios. Note here that the nozzle position is part of a feedback loop to the control, and thus the control senses area.

Nozzle flow is computed from the following equation, where C accounts for leakage, and WFR is afterburner fuel flow.

$$W_8 = W_6 \times (1-C) + WFR \quad 2.3-(51)$$

Since the nozzle is choked, and all the variables are calculated, there is a second continuity check. From the choked nozzle

$$\frac{W8\sqrt{T8}}{P8 \times A8 \times CF8} = \text{const.} \quad 2.3-(52)$$

or

$$P8C = \frac{C \times W8\sqrt{T8}}{A8 \times CF8} \quad 2.3-(53)$$

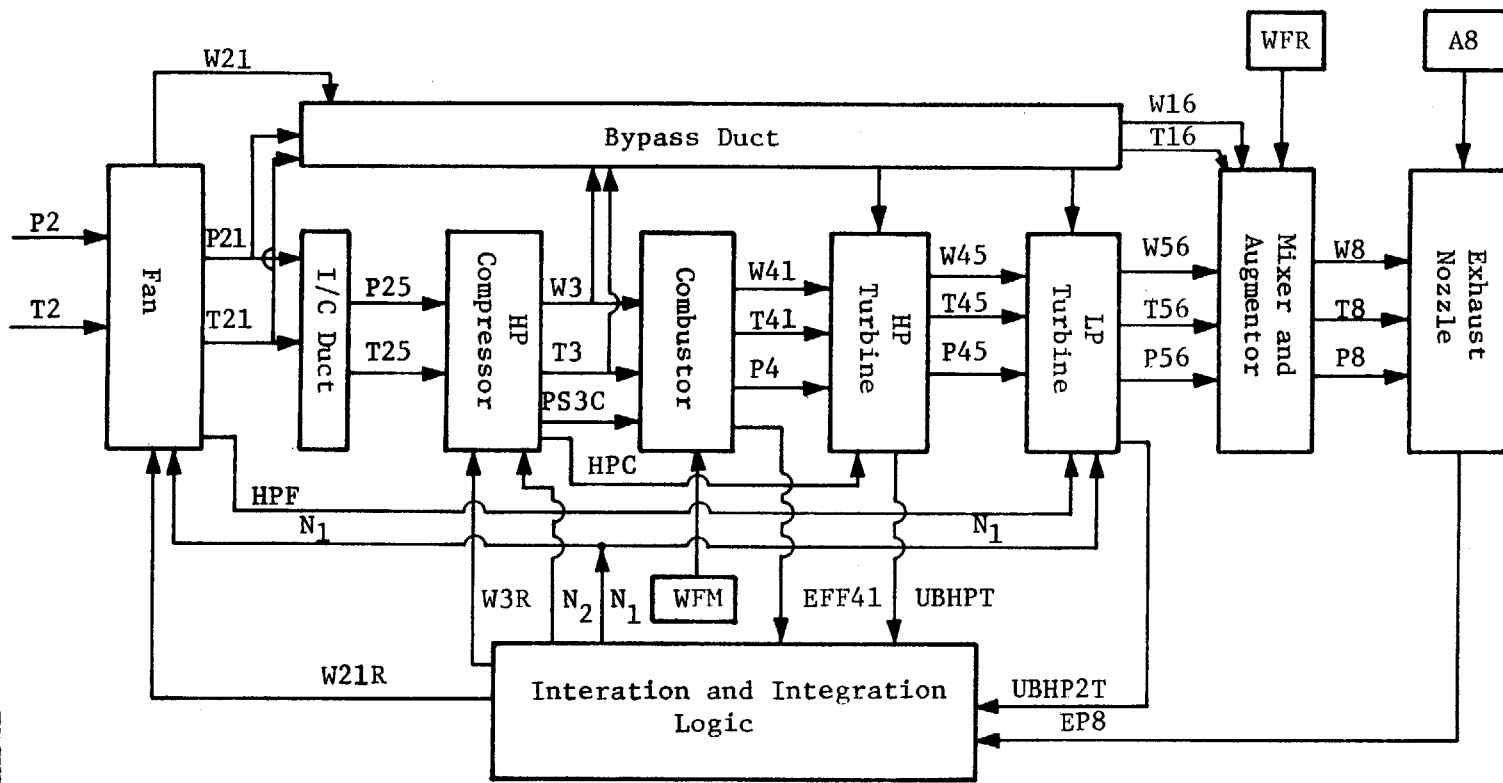
Thus, a second error is formed by comparing the choked P8, P8C, to that calculated from known losses, P8W, EQN 2.3-(49)

$$EP8 = (P8W - P8C)/P8C \quad 2.3-(54)$$

A summary of the flow of information from inlet to exhaust is shown in Figure 2.3-(2). It is seen that the critical parameters for each component are calculated and passed on to the next component. Now the integration and iteration routine is discussed.

On the very first pass through the equation set, the initial values of the rotor speeds N_1 and N_2 are guessed, as are the two exit flow functions W21R and W3R. On subsequent passes, the unbalanced torques and the continuity errors force the changes in these terms. Thus, for the fan rotor, the following equation gives the new rotor speed.

$$N_1(t + .01) = N_1(t) + C \times UBHP2T/XJLP/N_1 \quad 2.3-(55)$$



MODEL LOGIC

FIGURE 2.3-2

This equation is a simple time step interaction of the speed rate of change.

$$\frac{dN_1}{dt} = C \times UBHPZT/XJLP/N_1 \quad 2.3-(56)$$

Similarly for the high pressure spool

$$N_2(t + .01) = N_2(t) + C \times UBHP/XJHP/N_2 \quad 2.3-(57)$$

The two continuity errors are forced to zero by the time step iteration of the errors. Thus

$$W21R(t + .01) = W21R(t) + C \times EFF41 + C \times EP8 \quad 2.3-(58)$$

$$W3R(t + .01) = W3R(t) + C \times EFF41 + C \times EP8 \quad 2.3-(59)$$

The gains on these two loops are high enough to decouple them from the rotor integrations. Therefore, in each time step, there may be a small error in the continuity errors, but they are quickly forced to be small by the iteration logic. It is also noted that within each time step there is no iteration. This completes the description from the reference, and now some of the detail added since the reference was published are added.

Three additional major effects were added to the above model. These are off-schedule variable geometry effects, the effects on non-adiabatic compression and expansion (also known as heat soak), and additional

modelling to represent the transient response of the turbine discharge rakes. The first will effect the amount of flow and a given compressor speed. The second effects the transient responses of the components, and the third is to give a fair comparison between the model prediction of the sensor output and the actual output.

Both the fan and high pressure compressor have variable inlet guide vanes and stator vanes to better mach airflow and speed at off design conditions. The main effects are that when the variable geometry is closed relative to a scheduled position, the flow and efficiency will be lower. This effect is especially true during transients, where the inertia of the VG system causes it to lag the scheduled value. Thus, for better transient matching between the model and engine, the off-angle effects are included. If the difference between actual and scheduled is termed DVGL for the fan and DVGH for the compressor, then the following relationships apply. For the fan, the effect on corrected flow is a function of corrected speed and DVGL, as is the effect on efficiency. In the model, efficiency is not a direct parameter, so the off-angle effect changes temperature ratio at pressure ratio. For the high pressure compressor the effects are a function of corrected core speed and DVGH.

The heat soak modelling is added to better match the transient response of the model to the actual engine. Heat soak in the engine is a reflection of the non-adiabatic processes occurring in the engine. This is especially true in the turbine, where the temperature gradient from the hot gas to metal is as much as 1000°F. The approach used is a lumped parameter estimate of the heat storage in each component. The alternative to this type of modelling is an elaborate bookkeeping of all parts exposed to the

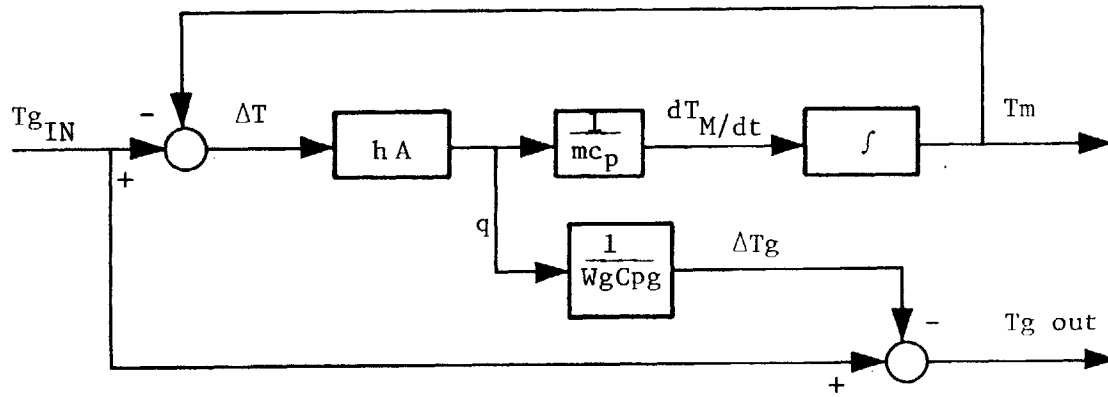
gas path. The lumped parameter model was generated by analyzing data and comparing it to adiabatic models. The general form is derived from simple heat transfer. The following equations briefly describe the modelling.

For the metal absorbing heat from the gas stream

$$MC_p \frac{dT_m}{dt} = hA(T_g - T_m) = Wg C_{pg} (T_{g_{in}} - T_{g_{out}}) \quad 2.3-(60)$$

Figure 2.3-(3) expresses these equations in block diagram form. The input to the system is the adiabatic temperature as calculated in the real time model. The output includes the non-adiabatic effects of heat soak.

The final addition is to realistically model the temperature sensor dynamics. This temperature sensor consists of eight two sensor probes located as equally spaced circumferential locations. The sensors have to be rugged enough to withstand the long operational life of the engines; and are therefore slow in response time due to the mass. One representation is a lag with a variable time constant. From convective heat transfer theory, the time constant will be proportional to Reynolds number raised to some exponent. The representation is shown in the figure 2.3-(4). The current main fuel control uses a lead/lag compensation scheme with a variable lead and a fixed lag. The variable lead is an attempt to model the sensor dynamics, and the lag is for stability. The overall modeling used for this study is shown in figure 2.3-(3). This concludes the description of the real time model.



Simplify to the following

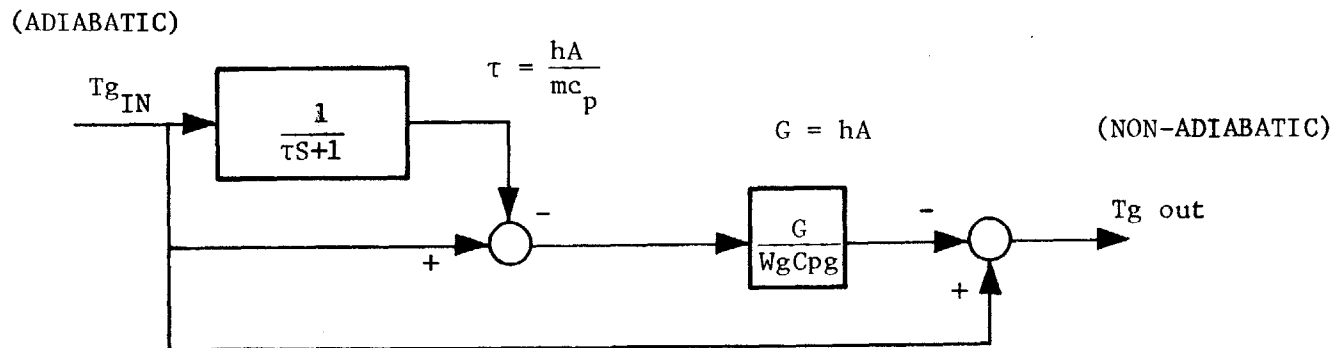


FIGURE 2.3-3

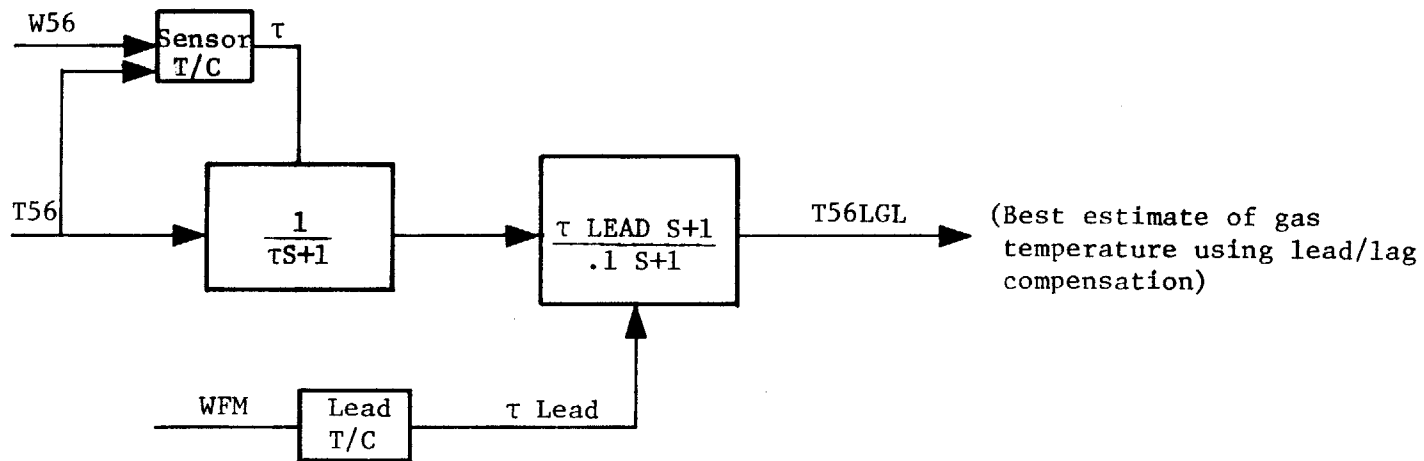
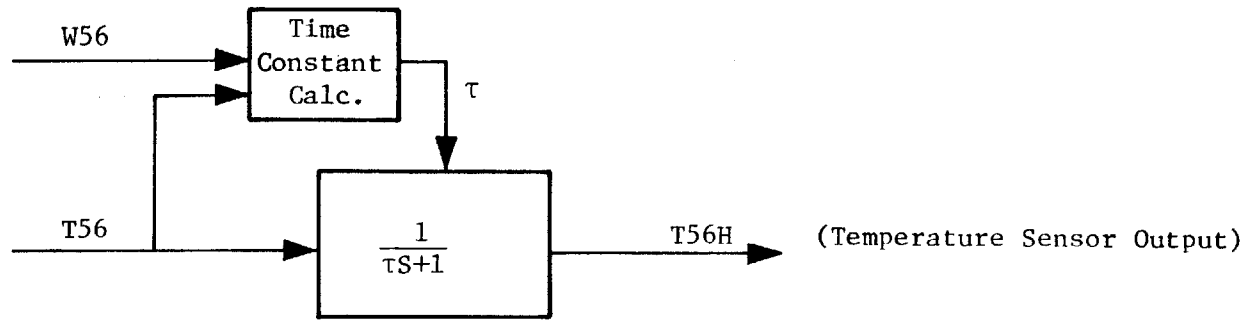


FIGURE 2.3-4

3. ADAPTIVE ALGORITHM DEVELOPMENT

It was previously stated that the goal of the study is to define a sensible methodology to force the model to "track" the engine outputs. The first fact that lead to the selected method was the obvious realization that all models have errors. One traditional approach to correct for modelling errors has been to use the Kalman filter equations to update the model. The second fact considered was that even if the model was exactly correct for one engine in the population of those produced, it would be in error for many other engines. Thirdly, for those engines that the model matched exactly when new, as the engine running time accumulates, the engine deteriorates, and the modelling errors would grow. Finally, the method selected should be able to correct small modeling errors without corrupting the model. Model corruption means that it would take a large and unrealistic change in a model variable to force the model to track the engine. The method should be able to adapt the model for engine to engine variations. And further, it should be able to adapt the model as the particular engine deteriorates. The last item has significant implications. If, for example, the method involved changing a component efficiency as engine run time accumulated, one could reliably predict that that particular component was deteriorating and should be replaced. This capability will enhance engine condition monitoring (ECM) and provide advanced diagnostics for overhaul shops. In summary, the method should be capable of changing component performance in a logical manner in order to track the engine, and a sensible set of component characteristics must be determined.

3.1 Parameter Set Selection

The engine sensors produce four outputs to "track," and thus the size of the variable set may be up to four in number. The criteria for selecting the set of parameters are the following. First, each parameter should be dominant in matching one sensed variable. This will result in a quasi-diagonal manipulation, and should prevent two variables from "fighting" each other to match a sensor. Second, the change in the parameters to match the engine outputs around the flight envelope should be relatively small. This requirement is related to corruption of the model. Third, the change in parameters should be small when considering engine to engine variations in component performance. Similarly the parameters selected must be insensitive to errors in the measured variables. For example, the main fuel control uses the metering valve position to indicate fuel flow. When considering the variations from metering valve to metering valve, broad spec fuels, fuel density variations and the like, the relationship between metering value position and fuel mass flow rate may vary by as much as 5%. Similarly, the exhaust nozzle area feedback signal may be in error by as much as 4%. Finally, the synthesis of important parameters such as turbine inlet temperature should be insensitive to all of the above problems.

The questions to be answered are the number of parameters to adjust and the type of parameters to adjust. The first idea is that by varying four parameters, there is more flexibility, but perhaps if only three are matched, the errors in the fourth are small. The second concerns itself with whether only engine performance parameters alone are selected, or should biases be imposed on the control inputs to account for errors in

measuring fuel flow. The specific questions to be addressed are: should 3 or 4 engine sensors be tracked; what combination of engine parameters and sensor biases be used; and are the parameter changes required to match engine performance acceptably small. These questions are answered based solely on static performance of the model. The dynamic considerations are attacked in section 3.2.

The first step is to identify potential performance parameters that can be changed to correct for modelling errors. A logical starting place is engine to engine variations that exist in the production population. These variables are listed in the table below.

TABLE 3.1-1 ENGINE VARIABLES

η_f	Fan Efficiency
WIR	Fan Corrected Flow @ Corrected Speed
η_c	High Pressure Compressor Efficiency
W25R	HPC Corrected Flow @ Corrected Speed
η_B	Combustor Efficiency
η_t	HP Turbine Efficiency
FF41	Turbine Nozzle Area Flow Function
η_{2t}	LP Turbine Efficiency
Wc	Percentage Cooling Flow

In addition to these variables, two control variables may require biases to account for inaccuracy. These are the fuel flow, W_f , and exhaust nozzle area A8. The two could be in error by as much as 5% and 4% respectively.

Static derivatives are taken with respect to each variable to determine the effect of each variable on engine sensed parameters. Since the engine is a two degree of freedom system, two inputs are held constant while

taking derivatives. For the nine engine variables, the fuel flow and exhaust nozzle area were held constant. For example, a one point change in turbine efficiency (one point equals 1% change) at constant fuel flow and nozzle area resulted in -14 RPM on the low pressure shaft, +65 RPM on the high pressure shaft, +0.5 PSI on compressor discharge static pressure, and -2° in turbine exit temperature. Several parameters were eliminated upon examination of the derivatives. The effects of a change in high pressure compressor efficiency are indistinguishable from those of high pressure turbine efficiency for the variables measured. The two can be isolated with a measurement of HPC discharge temperature, which is unavailable for the subject engine. Therefore, eliminate compressor efficiency. Burner efficiency only effects specific fuel consumption strongly, therefore eliminate it. The percentage cooling flow is similarly weak, so it too is deleted from the list. Now six engine variables remain, and further work is required to assess the selection.

Sets of variables and control biases are made, and the weeding out process begins by determining the magnitude of changes required to force the model to track the engine. This exercise requires the establishment of a "truth model" to base the model against. The truth model could be actual engine data from one particular engine, or it could be data generated by a highly detailed description contained in a mammoth computer simulation. The latter is used in this case. It is an internal General Electric model of the subject engine, which is a very large scale dynamic simulation including very complex component performance representations including vitiation and dissociation effects. It is incapable of operating in real time. For example, the description of fan performance requires over 50

equations and hundreds of arithmetic and logical operations. This model describes the so-called nominal engine behavior. Thus the comparison is established between the real time model and the nominal engine at important flight conditions around the flight envelope. At a given flight condition there will exist differences between the real time model and the truth model in fan rotor speed, N_1 high pressure rotor speed, N_2 , compressor discharge static pressure, PS3C, and turbine exit temperature T56. In order to eliminate the errors, four variables in the model are changed to match them. For example, employ changes in fan efficiency, turbine efficiency, fan speed-flow (WIR) and compressor speed flow (W25R) to account for differences in N_1 , N_2 , PS3C, and T56. If it takes +1 point in fan efficiency, -.5 PTS in turbine efficiency and +0.3% in flows to eliminate the differences, then one may say that the modelling errors are equivalent to component mis-representations of this magnitude. Alternatively stated, the real time model has a nominal implied delta η_F of zero points, but an actual delta of one point is necessary. Thus, through the following discussion, the parameters involved are deltas from a nominal value of zero. It may be noted the component efficiencies are not directly calculated in the real time model. There is no equation which states that η_F is 84%, for example. They are implied in the equation of temperature ratio at a pressure ratio.

The combinations are selected to produce diagonal dominance in the derivative matrix. Twelve possible sets are explored. Four sets are for matching all four measured engine outputs. Eight sets are for matching only three outputs. The sets are summarized in Table 3.1-2. The table shows the combinations of engine variables and sensor biases, along with

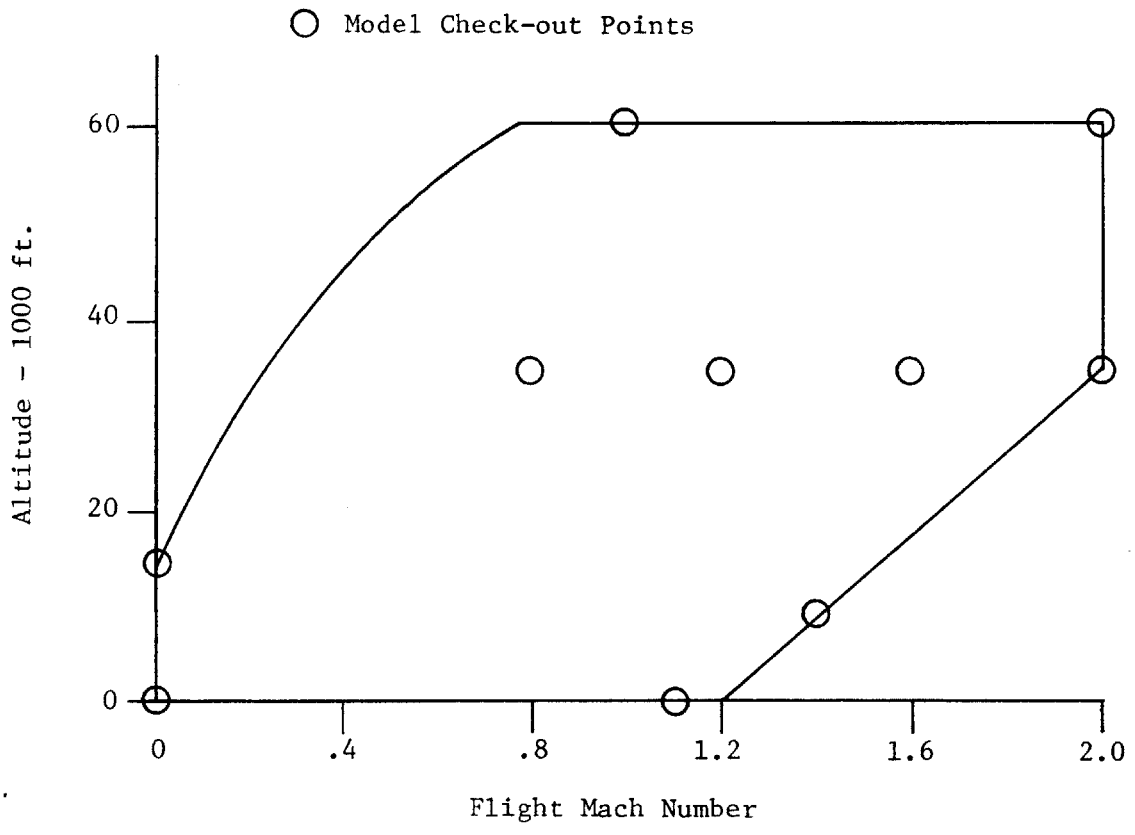


FIGURE 3.1-1

the sensor outputs to be tracked. The first four sets track all four outputs, the second four sets track all except PS3C, and the last four track all outputs except N_2 .

TABLE 3.1-2 SETS OF PARAMETERS

All Parameters are Deltas from a Nominal Value of Zero

Set Number	Engine Variables	Sensor Biases	Matched Sensors
1	WIR, η_t , FF41, η_F	--	N_1 , N_2 , PS3C, T56
2	WIR, η_t , , η_F	WF	N_1 , N_2 , PS3C, T56
3	η_t , FF41, η_F	A8	N_1 , N_2 , PS3C, T56
4	η_t , , η_F	A8, WF	N_1 , N_2 , PS3C, T56
5	WIR, η_t , η_F	--	N_1 , N_2 , T56
6	WIR, η_t	WF	N_1 , N_2 , T56
7	η_t , η_F	A8	N_1 , N_2 , T56
8	η_t	A8, WF	N_1 , N_2 , T56
9	WIR, FF41, η_t	--	N_1 , PS3C, T56
10	WIR, , η_t	WF	N_1 , PS3C, T56
11	FF41, η_t	A8	N_1 , PS3C, T56
12	, η_t	A8, WF	N_1 , PS3C, T56

These sets were tested for tracking around the flight envelope. The points in the flight envelope are depicted in Figure 3.1-1. As can be seen, the model was checked out at all extremes of flight conditions. The results were judged upon the size of parameter changes, and the ability to synthesize turbine inlet temperature T41. The findings are shown in Appendix 1, which contains the detailed results. Two thrust levels were

explored. The first is intermediate rated power (IRP) which is the highest thrust without afterburner, and the second is maximum afterburner, which is the greatest possible thrust setting.

The following conclusions are made based upon an examination of the results of this segment of the study. Those sets that bias A8 provide marginal improvement in T41 synthesis when compared to those that do not. Also, in many cases the bias became greater than 10% which is unacceptable. Note here that A8 is "known" from the large scale model, and should not require a bias. Finally, at low power settings, as changes have a low influence, especially at 400 square inches. The conclusion is to eliminate A8 as a potential variable. This step eliminates two of the four variable sets and four of the three variable sets. For the remaining four variable sets, the T41 synthesis is virtually identical, but the variations on fuel flow are small compared to those on turbine nozzle area. Thus this set, number 1, is eliminated. The remaining sets of 3 variables matching N_2 are comparable and are not eliminated at this point. Set number 9 is eliminated for the same reason as number 1 above. In summary, sets numbers 2, 5, 6, and 10 remain.

These four remaining sets are further judged by their performance in consideration of possible sensor errors. The known sensor errors for the following sensors are tabulated below. These errors are judged to be random and uncorrelated, and therefore, to assess the effects, the root-sum-square (RSS) technique is employed (see Appendix 1 for the detailed results of this analysis). The effects of these sensor errors were studied at sea level static conditions and at 60000 Ft/mach no = 1. The conclusions eliminate two sets. Set number 5 is eliminated because of

large sensitivities of fan efficiency and fan airflow. Also, the synthesis of PS3C is poor. Set number 6 is eliminated due to a large sensitivity on fan airflow. This leaves sets 2 and 10.

TABLE 3.1-3 SENSOR ERRORS

Fan Speed	N_1	0.5% Full Scale (14000 RPM)
Core Speed	N_2	0.5% Full Scale (17000 RPM)
Static Pressure	PS3C	0.25% Full Scale (450 PSIA)
Temperature	T5	16°
Fuel Flow	W_F	5% of Point
Nozzle Area	A8	4% of Point

The final selection criteria was to subject the two remaining sets to random engine to engine variations, and check the effect on the synthesis of T41. The engine to engine variations arise out of manufacturing tolerances and buildup procedures. The General Electric Design Practice suggests the following as good assumptions on these variations.

TABLE 3.1-4 ENGINE TO ENGINE VARIATIONS

Fan Efficiency	η_f	±0.6 PTS
Fan Speed-Flow	W1R	±1.0%
Compressor Efficiency	η_c	±0.7 PTS
Compressor Speed-Flow	W25R	±1.0%
Turbine Efficiency	η_t	±0.8 PTS
Turbine Flow Function	FF41	±1.0%
LP Turbine Efficiency	η_{2t}	±1.0 PTS
LP Turbine Flow Function	FF45	±1.0%
Cooling Flow		±0.4%

The final conclusion is to use the 4 variable set due to smaller sensitivities to engine to engine variations. See Appendix 1. It is also more flexible due to the additional parameter. Now the work can proceed to the dynamics of the update.

3.2 Gain Matrix Methodology

The task at hand is to develop the means to update the model in a dynamic sense that insures stability of the model while updating. The dynamics of update should be relatively fast for two reasons. First, model errors at low power will, in general, be different than model errors at high power. Since the response time of the engine is about 4 seconds, the update scheme should be about this fast. Second, if the model is to be used for dynamic control, then it should be actually faster than the engine response time in order to successfully track transients. The problem, in essence, becomes a multidimensional control problem, where the model should follow the reference of the engine sensors in real time. The criteria for judging the success of the dynamic update method are the success in tracking the engine, the minimization of additional processor time, and the minimization of additional through-put (variable names) to be carried along.

Four methods with increasing levels of complexity are explored. The first uses the inverted Jacobian Matrix as a gain matrix on the errors. It is scaled as a function of power setting to insure stability. The second is a method inspired by recursive least squares which penalizes both errors between the engine and model and changes in the model parameters. The third is the so-called constant gain extended Kalman filter (Ref. 8, 10,

12). The final is the extended Kalman filter. Each method is developed in this section, and the results are shown in Section 4.

3.2.1 Inverse Jacobian Gain Matrix

The following method is deemed the simplest possible method of updating the parameters in order to track the engine. Start with some definitions. Let the vector \underline{r} be the vector of changes in model parameters.

$$\underline{r}^t \triangleq [\Delta W_l R, \Delta \eta_t, \Delta W_f, \Delta \eta_f] \quad 3.2.1-(1)$$

Let the vector \underline{Y} be the vector of engine outputs.

$$\underline{Y}^t \triangleq [N_1, N_2, PS3C, T5] \quad 3.2.1-(2)$$

Then the Jacobian is defined as the derivative of \underline{Y} with respect to \underline{r}

$$\underline{J} \triangleq \frac{d\underline{Y}^t}{d\underline{r}} ; J_{ij} = \left. \frac{dY_i}{dr_j} \right| (\Delta Y_i = 0_j \quad i \neq j) \quad 3.2.1-(3)$$

and therefore

$$\Delta \underline{Y} = \underline{J} \times \Delta \underline{r} \quad 3.2.1-(4)$$

Now, we define a vector \underline{e} as the vector of output errors between the model and the engine. To eliminate this error in the linear case, solve for $\Delta \underline{r}$ that eliminates \underline{e}

$$\underline{e} = \underline{Y}_r - \underline{Y} \quad 3.2.1-(5)$$

$$\Delta \underline{r} = \underline{J}^{-1} \underline{e}$$

Since the engine and model are non-linear, iteration is necessary. This iteration is handled by performing a time step integration of the vector $\Delta \underline{r}$. Thus

$$\underline{r}(t + .01) = \underline{r}(t) + \alpha \times (\underline{J}^{-1} \times \underline{e}) \times .01 \quad 3.2.1-(6)$$

In the equation, alpha is a constant to scale the Jacobian to insure stability.

This method ignores the dynamics of the model and engine. This fact can be seen by examining the meaning of the Jacobian for this case, which is the relation between \underline{r} and \underline{Y} steady state. Take a simple two degree of freedom representation, and write out the dynamic relations to show \underline{X} and \underline{Y} as functions of \underline{r} .

$$\begin{bmatrix} \dot{x}_1 \\ \dot{x}_2 \end{bmatrix} = \begin{bmatrix} a_{11} & a_{12} \\ a_{21} & a_{22} \end{bmatrix} \begin{bmatrix} x_1 \\ x_2 \end{bmatrix} + \begin{bmatrix} b_1 \\ b_2 \end{bmatrix} r \quad 3.2.1-(7)$$

$$Y = \begin{bmatrix} c_1 & c_2 \end{bmatrix} \begin{bmatrix} x_1 \\ x_2 \end{bmatrix}$$

Then the transfer function from u to x in Laplace form is

$$\begin{aligned} X(s) &= (sI - A)^{-1} Br(s) \\ &= \frac{\begin{bmatrix} a_1 s + b_1' \\ a_2 s + b_2' \end{bmatrix} r(s)}{a_3 s^2 + b_3 s + c_3} \quad 3.2.1-(8) \end{aligned}$$

And the output is

$$Y(s) = c x (s) = \frac{c^1 s + d^1}{a_3 s^2 + b_3 s + c_3} x r(s) \quad 3.2.1-(9)$$

Then the Jacobian, defined for this case by $(dy/dr)_{ss}$ is the transfer function at time equals infinity.

$$\left[\frac{c^1 s + d^1}{a_3 s^2 + b_3 s + c_3} \right] \Bigg|_{t=\infty} = \frac{d^1}{c_3} \quad 3.2.1-(10)$$

It can be seen that the Jacobian ignores the dynamic terms in the transfer function.

Stability of the update scheme was explored by performing a state space analysis of the dynamics at a high power condition. The model contains two states, N_1 and N_2 , plus the four dynamic variables become states. The state space representation is derived in two steps. First, a reference state and input condition are determined at sea level static (SLS) IRP. The following are defined

States $\underline{x} \triangleq \begin{bmatrix} \delta N_1 \\ \delta N_2 \end{bmatrix} =$ Perturbations from nominal

Outputs $\underline{Y} \triangleq \begin{bmatrix} \delta N_1 \\ \delta N_2 \\ \delta PS3C \\ \delta T5 \end{bmatrix} =$ Perturbations from nominal

Inputs

$$\underline{u} \triangleq \begin{bmatrix} \delta W_f \\ \delta A8 \end{bmatrix} = \text{PERTURBATIONS FROM NOMINAL}$$

Then

$$\begin{aligned} \dot{\underline{x}} &= \underline{A} \underline{x} + \underline{B} \underline{u} \\ \underline{Y} &= \underline{C} \underline{x} + \underline{D} \underline{u} \end{aligned} \quad 3.2.1-(11)$$

is the state space representation. Now impose the condition that $\underline{u} = 0$.

Equation 3.2.1-(11) becomes

$$\begin{aligned} \dot{\underline{x}} &= \underline{A} \underline{x} \\ \underline{Y} &= \underline{C} \underline{x} \end{aligned} \quad 3.2.1-(12)$$

These equations are applicable to the nominal value of the parameter vector \underline{r} , which is zero. Now allow \underline{r} to vary, and form a new representation.

$$\begin{aligned} \dot{\underline{x}} &= \underline{A} \underline{x} + \underline{B}' \underline{r} \\ \underline{Y} &= \underline{C} \underline{x} + \underline{D}' \underline{r} \end{aligned} \quad 3.2.1-(13)$$

The update equation is

$$\begin{aligned} \dot{\underline{r}} &= \alpha \underline{x} \underline{J}^{-1} \underline{e} \\ \dot{\underline{r}} &= \alpha \underline{J}^{-1} \underline{x} (\underline{Y}_{eng} - \underline{C} \underline{x} - \underline{D}' \underline{r}) \end{aligned} \quad 3.2.1-(14)$$

The new closed loop update method (for a fixed engine reference) is

$$\begin{bmatrix} \dot{\underline{x}} \\ \dot{\underline{r}} \end{bmatrix} = \begin{bmatrix} \underline{A} & \underline{B}' \\ -\alpha \underline{J}^{-1} \underline{C} & -\alpha \underline{J}^{-1} \underline{D}' \end{bmatrix} \begin{bmatrix} \underline{x} \\ \underline{r} \end{bmatrix} + \begin{bmatrix} 0 \\ \alpha \underline{J}^{-1} \underline{Y}_{eng} \end{bmatrix} \quad 3.2.1-(15)$$

or

$$\underline{X}' = \underline{A}'\underline{X}' + B'Y_{-eng} \quad 3.2.1-(16)$$

The closed loop eigenvalues of the A' matrix determine stability. A multi-dimensional "root locus" for varying values of α are shown in Figure 3.2.1-(1). A value for α of 2 was chosen at high power and .74 for low power. The reason for the low value is that the Jacobian reflects static relationships and must be reduced for stable dynamics. The results are shown in Section 4.

3.2.2 Recursive Least Squares Derived Gain Matrix

This next method is analyzed because of the ability to penalize large changes in the parameters and, in effect, prevent corruption of the model. The previous method will move the variables with no consideration of their magnitude. Recursive Least Squares is used as a tool for model validation when large amounts of data are available. The goal is to process the data sequentially and carry the information from one pass to the next. This avoids the complications of carrying large matrices that Classical Least Squares employs.

The adaptation of Recursive Least Squares to this problem is shown in the equations that follow. Start with a performance index J_p , and use a linear model between the vector \underline{r} and the error \underline{e} . The performance index penalizes errors as well as changes in parameters. The subscripts refer to the indicated time step.

$$J_{pi} \triangleq \underline{e}_i^T R_1 \underline{e}_i + (\underline{r}_i - \underline{r}_{i-1})^T R_2 (\underline{r}_i - \underline{r}_{i-1}) \quad 3.2.2-(1)$$

POLE PLOT
 SCALED INVERSE JACOBIAN F/B MATRIX

$$\underline{r}_{i+1} = \underline{r}_i + \alpha J^{-1} \underline{e}$$

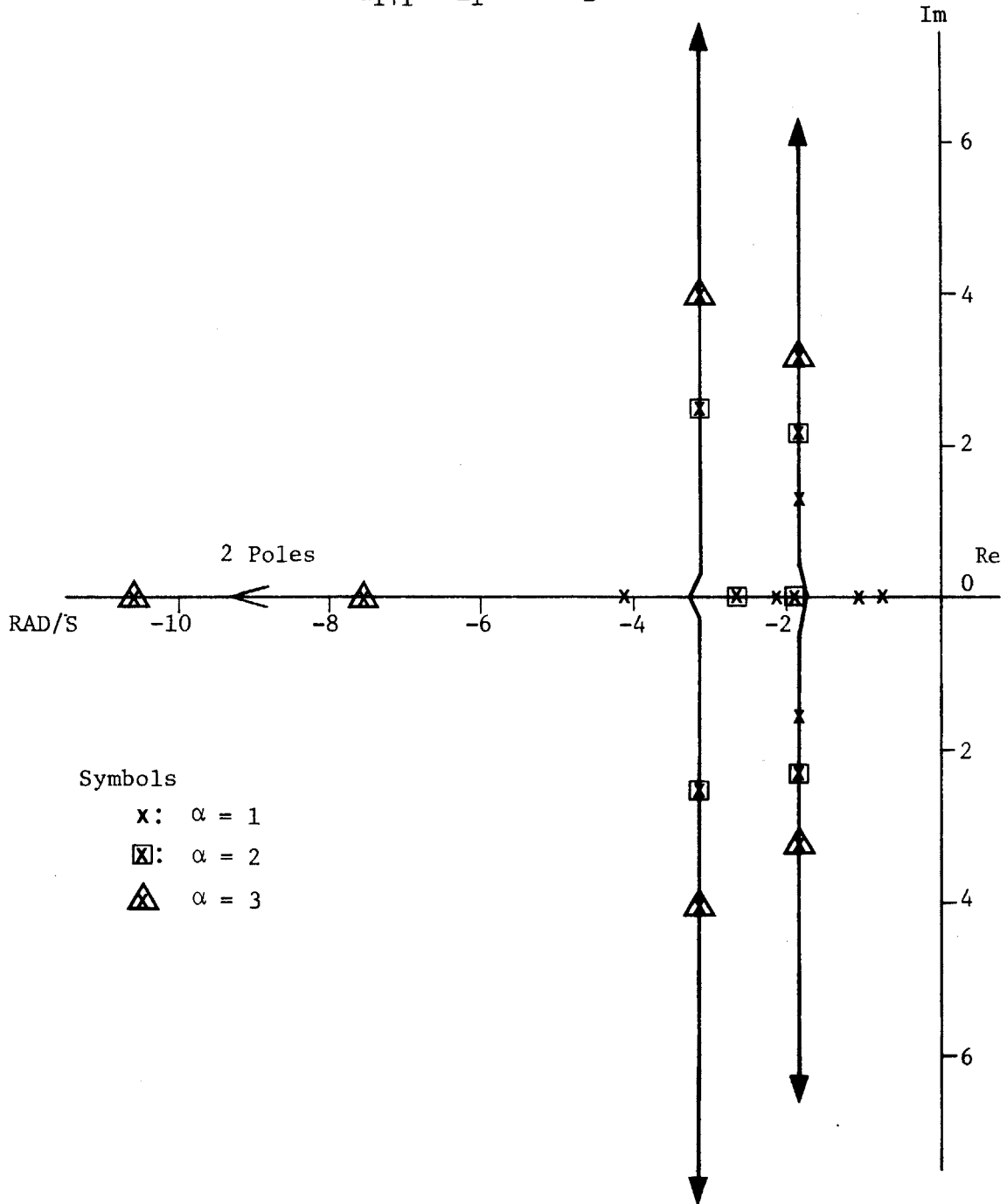


FIGURE 3.2.1-1

Assume the relationship between \underline{e} and \underline{r} is linear using the Jacobian, J

$$\underline{e}_i(\underline{r}_i) \triangleq Jx(\underline{r}_i - \underline{r}_{i-1}) + \underline{e}_{i-1} \quad 3.2.2-(2)$$

where

$$J \triangleq \frac{d\underline{e}_i}{d\underline{r}_j} = \text{JACOBIAN}$$

For simplification let \underline{R}_1 in the performance index be set to \underline{I} , and let \underline{R}_2 be αI such that we are penalizing accuracy and parameters relatively through α .

We seek to minimize the performance index with respect to \underline{r}_i . Thus, take the partial derivative and equate it to zero.

$$\frac{d^J p_i}{d\underline{r}_i} = \frac{d}{d\underline{r}_i} \left\{ \underline{e}_i^T \underline{e}_i + \alpha(\underline{r}_i - \underline{r}_{i-1})^T (\underline{r}_i - \underline{r}_{i-1}) \right\} = 0$$

$$2 \frac{d\underline{e}_i^T}{d\underline{r}_i} \underline{e}_i + 2 \alpha I (\underline{r}_i - \underline{r}_{i-1}) = 0 \quad 3.2.2-(3)$$

We wish to solve for a relation that updates \underline{r}_i from \underline{r}_{i-1} , thus solve for $\underline{r}_i - \underline{r}_{i-1}$ and note the definition of J .

$$\alpha I (\underline{r}_i - \underline{r}_{i-1}) = -J \underline{e}_i$$

Employ equation 3.2.2-(2) for the definition of \underline{e}_i .

$$\alpha \underline{I} (r_i - r_{i-1}) = -\underline{J} (\underline{J} (r_i - r_{i-1})) + e_{i-1} \quad 3.2.2-(4)$$

Thus $(\underline{J}^2 + \alpha \underline{I}) (r_i - r_{i-1}) = -\underline{J} e_{i-1}$

or $r_i - r_{i-1} = -(\underline{J}^2 + \alpha \underline{I})^{-1} \underline{J} e_{i-1} \quad 3.2.2-(5)$

$$= \underline{K} e_{i-1}$$

$$\underline{r}_i = \underline{r}_{i-1} + \underline{K} e_{i-1} ; \underline{K} = -[\underline{J}^2 + \alpha \underline{I}]^{-1} \underline{J} \quad 3.2.2-(6)$$

Therefore, in the linear case we have the above calculation of \underline{K} in each time step, to update the parameters \underline{r} .

The non-linear case requires the derivation of the Jacobian in each pass. However, for ease of the computational burden, the following simplification can be made. The Jacobian can be preprogrammed as a function of corrected fan speed. The reasons for this effect are two-fold. First, corrected fan speed is indicative of the thermodynamic processes for the fan shaft, and thus the derivatives for variables related to the fan shaft, act consistently with corrected fan speed. Second, there is a tight relationship between corrected fan speed and corrected core speed. Therefore all parameters related to the core can be related to fan speed. With this information, use the following logic as the update gain matrix. Let α now be a vector penalizing the diagonal elements of R_2 individually.

Let the Jacobian in each time step be a function of the corrected fan speed

$$\text{JACOBIAN} \triangleq \underline{J}_i = \underline{J}_i (N_1/\sqrt{\theta_2}) = J (N_1/\sqrt{\theta_2})_i$$

Then define the gain matrix K_i

$$\underline{K}_i \triangleq [\underline{J}_i^2 + \alpha \underline{I}]^{-1} \underline{J} \quad 3.2.2-(7)$$

Finally update the parameter vector \underline{r} once per time step

$$\underline{r}(t + .01) = \underline{r}(t) + \underline{K}_i e(t)$$

In order to control the size of the $\underline{\Delta r}$, let α_i be a function of r_i such that at high r_i , the $\underline{\Delta r}_i$ is small due to a large penalty from α .

$$\alpha_i = \gamma r_i$$

In other words, as r_i increases, the penalty on $\underline{\Delta r}_i$ increases.

In the actual iteration scheme, the inverse in equation 3.2.2-(7) is not taken, in order to save computational time. The results are shown in Section 4.

3.2.3 Constant Gain Extended Kalman Filter

The following method is based on the well-known Kalman-Bucy Theory (Ref. 13) with significant modifications. In the basic form, the Kalman

filter is a minimum variance, unbiased state estimator for the continuous linear system described by the following equations.

$$\dot{\underline{x}}(t) = \underline{F}(t) \underline{x}(t) + \underline{G}(t) \underline{U}(t) + \underline{W}(t) \quad W(t) \sim N(0, Q(t))$$

$$\underline{Y}(t) = \underline{H}(t) \underline{x}(t) + \underline{V}(t) \quad V(t) \sim N(0, R(t))$$

where

$\underline{x}(t)$ is the state vector

$\underline{U}(t)$ is the input vector

$\underline{W}(t)$ is the process noise-Gaussian with zero mean and covariance $Q(t)$

$\underline{Y}(t)$ is the output vector

$\underline{V}(t)$ is the measurement noise-Gaussian with zero mean and covariance $R(t)$

The best estimate of X , given by \hat{x} is

$$\dot{\hat{x}} = F(t) \hat{x}(t) + K(t) [Y(t) - H(t) \hat{x}(t)] \quad 3.2.3-(1)$$

where $K(t)$ is the Kalman gain matrix.

The theory is further detailed in Section 3.2.4 which explores the full equation set for the extended Kalman filter. Suffice to say here that a significant computer burden may be relieved by precomputing a gain matrix based on a time invariant linear model of the non-linear engine. This approach has been suggested in several works (ref. 12, 13) and executed in several others (Ref. 8, 10). Therefore the method is explored here, but with the addition of the \underline{r} parameters included as states.

In the previous section, a state space representation of the engine was derived for a high power condition. Reviewing that derivation, the perturbations around the nominal point results in a representation

$$\begin{aligned}\dot{\underline{x}} &= \underline{A} \underline{x} + \underline{B} \underline{u} \\ \underline{Y} &= \underline{C} \underline{x} + \underline{D} \underline{u}\end{aligned}\tag{3.2.3-2}$$

Let the control perturbations be zero, and introducing the parameter vector \underline{r} results in

$$\begin{aligned}\dot{\underline{x}} &= \underline{A} \underline{x} + \underline{B}' \underline{r} \\ \underline{Y} &= \underline{C} \underline{x} + \underline{D}' \underline{r}\end{aligned}\tag{3.2.3-3}$$

Now, make the four variables in \underline{K} states, whose nominal trajectory is zero.

$$\dot{\underline{r}} = 0$$

An alternative method is the so-called adaptive control reference model approach as outlined in Ref 14.

Therefore, form a new system

$$\begin{aligned}\begin{bmatrix} \dot{\underline{x}} \\ \dot{\underline{r}} \end{bmatrix} &= \begin{bmatrix} \underline{A} & \underline{B}' \\ \underline{o} & \underline{o} \end{bmatrix} \begin{bmatrix} \underline{x} \\ \underline{r} \end{bmatrix} + \begin{bmatrix} \underline{B} \\ \underline{o} \end{bmatrix} \delta_u ; \quad \delta u = 0 \\ \underline{Y} &= \begin{bmatrix} \underline{C} & \underline{D}' \end{bmatrix} \begin{bmatrix} \underline{x} \\ \underline{r} \end{bmatrix}\end{aligned}$$

3.2.3-(4)

Finally a Kalman filter may be employed. Let

$$\underline{\dot{x}}' = \underline{A}' \underline{x}' + \underline{r}$$

The equations become

$$\begin{aligned} \underline{\dot{x}}' &= \underline{A}' \underline{x}' \\ \underline{Y} &= \underline{C}' \underline{x}' \end{aligned} \tag{3.2.3-5}$$

And the Kalman filter becomes

$$\begin{aligned} \hat{\underline{x}}' &= \underline{A}' \hat{\underline{x}}' + \underline{K} (\underline{Y} - \hat{\underline{Y}}) \\ \hat{\underline{Y}} &= \underline{C}' \hat{\underline{x}}' \end{aligned} \tag{3.2.3-6}$$

The above equations apply for the linear time invariant case. Now introduce the non-linearities.

$$\begin{aligned} \hat{\underline{x}}' &= \underline{f} (\hat{\underline{x}}, t) \hat{\underline{x}} + \underline{K} (Y - \hat{Y}) \\ \hat{Y} &= \underline{h} (\hat{\underline{x}}, t) \hat{\underline{x}} \end{aligned} \tag{3.2.3-7}$$

Here the f and h functions represent the non-linear real time model, which is being used as the state estimator.

If the K matrix is derived at one condition, and allowed to be constant, then we have the constant gain extended Kalman filter. Thus, the method is to specify the Q and R matrices, and determine the steady state gain, K_{∞} .

$$K_{\infty} = P_{\infty} H^T R_{\infty}^{-1} \tag{3.2.3-8}$$

In order to calculate the filter gains, the Q and R matrices must be specified, and the steady state Ricatti equation solved. The filter gain is computed from

$$K = PH^T R^{-1}$$

Where $0 = FP + PF^T + Q - PH^T R^{-1} HP$ 3.2.3-(9)

The guidance for specifying the Q and R matrices are from Ref. 10. The Q matrix is a measure of process noise, which for this case implies modelling error. It is assumed to be diagonal. For the elements corresponding to N_1 and N_2 , the terms were selected as representing the standard deviation equal to 1% of maximum value. The remaining terms, corresponding to the \underline{r} parameters, were chosen to be 3% based on the results of the envelope survey in Section 3.1. The R matrix (sensor noise) was chosen to be similarly diagonal, with the elements corresponding to the known errors in measurement. The errors are previously detailed in Table 3.1-3.

A check on the open loop and closed loop eigen values is shown. For the open loop case, the poles are at -6.4, -3.2 and four zeros for the \underline{r} parameters. The closed loop poles are at -2.46, -5.01, $-5.75 \pm 4.79j$, and $-6.82 \pm 5.45j$. The filter should be adequately fast. The implementation and results are shown in Section 4. The resulting K matrix is

$$K = \begin{bmatrix} 8.18 & 0.54 & 1.18 & 0.763 \\ 0.67 & 6.99 & 9.24 & 1.920 \\ -0.098 & -.024 & 0.807 & -.1288 \\ 0.009 & .128 & 0.196 & -.111 \\ 0.034 & .014 & 0.764 & .2868 \\ 0.109 & -.036 & 0.475 & -.1967 \end{bmatrix}$$

The details of the specific derivation are shown below. The linearized model at sea level static IRP is shown in the equations below.

States: $\underline{x}' = [N_1, N_2, \Delta WLR, \Delta \eta_t, \Delta Wf, \Delta \eta_f]^T$

Outputs: $\underline{y}' = [N_1, N_2, PS3C, T5]^T$

Equations: $\dot{\underline{x}}' = \underline{F} \underline{x}'$

$\underline{y}' = \underline{H} \underline{x}'$

Definitions: $\underline{F} = \left. \frac{dx_i}{dx_j} \right|_{(\Delta x_i = 0, i = j)}$

$\underline{H} = \left. \frac{dx_i}{dx_j} \right|_{(\Delta x_i = 0, i \neq j)}$

Detailed matrices:

$$\underline{F} = \begin{bmatrix} -5.5 & 3.17 & -325 & -62 & 100 & 377 \\ 0.63 & -4.08 & -44 & 363 & 113 & -105 \\ 0 & 0 & 0 & 0 & 0 & 0 \\ 0 & 0 & 0 & 0 & 0 & 0 \\ 0 & 0 & 0 & 0 & 0 & 0 \\ 0 & 0 & 0 & 0 & 0 & 0 \end{bmatrix}$$

$$\underline{H} = \begin{bmatrix} 1 & 0 & 0 & 0 & 0 & 0 \\ 0 & 1 & 0 & 0 & 0 & 0 \\ .005 & .025 & 1.63 & 0 & 1.04 & .82 \\ .023 & -.055 & -4 & -5 & 0 & -7 \end{bmatrix}$$

These matrices were determined using the full non-real time computer model.

3.2.4 Extended Kalman Filter

The extended Kalman filter is explored to give a reference in performance for the "best" update algorithm. The following material is taken heavily from Reference 13.

The continuous extended Kalman filter equations are summarized in Table 3.2.4-1. Shown are the system model and measurement model, the assumptions about initial conditions, the state estimate, the error covariance and the gain equations. The execution of all the implied bases requires considerable processor time. General simplifications may be made, while still retaining the attractive features of the filter.

TABLE 3.2.4-1 SUMMARY OF CONTINUOUS EXTENDED KALMAN FILTER

(Ref. 13)

System Model	$\dot{\underline{x}}(t) = \underline{F}(\underline{x}(t), t) + \underline{W}(t); \underline{W}(t) \sim N(0, Q(t))$
Measurement Model	$\underline{Z}(t) = \underline{h}(\underline{x}(t); t) + \underline{V}(t); \underline{V}(t) \sim N(0, R(t))$
Initial Conditions	$\underline{x}(0) \sim N(\hat{\underline{x}}(0), P_0)$
Other Assumptions	$\underline{E}[\underline{W}(t) \underline{V}^T(\tau)] = 0$ all t and τ
State Estimate	$\dot{\hat{\underline{x}}} = \underline{F}(\hat{\underline{x}}(t), t) + \underline{K}(t) [\underline{Z}(t) - \underline{h}(\hat{\underline{x}}(t), t)]$
Error Covariance	$\dot{\underline{P}}(t) = \underline{F} \times \underline{P}(t) + \underline{P}(t) \times \underline{F}^T + \underline{Q}(t) - \underline{P}(t) \underline{H}^T \underline{R}^{-1}(t) \underline{H} \underline{P}(t)$
Gain Equation	$\underline{K}(t) = \underline{P}(t) + \underline{H}^T \underline{R}^{-1}(t)$
Definitions	$\underline{F} = \frac{d\underline{F}(\underline{x}(t), t)}{d\underline{x}(t)} \quad \left \quad \underline{x}(t) = \hat{\underline{x}}(t)$ $\underline{H} = \frac{d\underline{h}(\underline{x}(t), t)}{d\underline{x}(t)} \quad \left \quad \underline{x}(t) = \hat{\underline{x}}(t)$

The following simplifications should not detract from the filter algorithm, and are in essence, assumptions about the engine behavior and sensor behavior. First, the Q and R matrices are assumed independent of time and the state. The Q matrix is a measure of process noise or modelling error. Although the model tends to be more accurate (relative to the truth mode) at high power, this would lead to additional complication with marginal results. The R matrix is a measure of sensor noise. For the two speed signals, the noise is fairly independent of rotor speed. The PS3C signal accuracy is essentially a percentage of full scale error, and thus is independent of level. The same holds for the T56 signal. Thus the time dependence on Q and R may be eliminated. The second major simplification deals with the F and H matrices. As in Section 3.2.2, these will be treated as functions of corrected fan speed (of the model) only. Thus they are functions of one state, and the relationships may be preprogrammed.

The details of the extended Kalman filter result in the following logic. Apply the above definitions:

$$\begin{aligned} \underline{F}(\hat{x}(t), t) &= F(\hat{N}_1/\sqrt{\theta_2}) \\ \underline{H}(\hat{x}(t), t) &= H(\hat{N}_1/\sqrt{\theta_2}) \\ Q(t) &= Q \\ R(t) &= R \end{aligned} \tag{3.2.4-1}$$

The initial condition assumptions are straightforward. For $\hat{x}(0)$, use the value to which the model converges at time zero. For the initial covariance, assume that the initial conditions error standard deviation is equal to the Q matrix.

The sequential processing tasks are then:

For time equal zero

$$\underline{K}(o) = \underline{P}(o) \underline{H}^T (\hat{N}_1/\sqrt{\theta_2}) \underline{R}^{-1} \quad 3.2.4-(2)$$

$$\dot{\hat{x}}(o) = \dot{\hat{x}}(o)_{RTM} + \underline{K}(o) [Z(o) - Z(o)_{RTM}] \quad 3.2.4-(3)$$

$$\begin{aligned} \dot{\underline{P}}(o) = & \underline{P}(o) \underline{F}(o) + \underline{F}^T(o) \underline{P}(o) + \underline{Q} \\ & - \underline{P}(o) \underline{H}^T(o) \underline{R}^{-1} \underline{H}(o) \underline{P}(o) \end{aligned} \quad 3.2.4-(4)$$

For subsequent time steps

$$\underline{K}(t) = \underline{P}(t) \underline{H}^T (\hat{N}_1/\sqrt{\theta}) \underline{R}^{-1} \quad 3.2.4-(5)$$

$$\dot{\hat{x}}(t) = \dot{\hat{x}}(t)_{RTM} + \underline{K}(t) [Z(t) - Z(t)_{RTM}] \quad 3.2.4-(6)$$

$$\begin{aligned} \dot{\underline{P}}(t) = & \underline{P}(t) \underline{F} (N_1/\sqrt{\theta}) + \underline{F}^T (N_1/\sqrt{\theta}) \underline{P} + \underline{Q} \\ & - \underline{P}(t) \underline{H}^T (N_1/\sqrt{\theta}) \underline{R}^{-1} \underline{H} (N_1/\sqrt{\theta}) \underline{P}(t) \end{aligned} \quad 3.2.4-(7)$$

$$\underline{P}(t + .01) = \underline{P}(t) + \dot{\underline{P}}(t) \times .01 \quad 3.2.4-(8)$$

$$\hat{x}(t + .01) = \hat{x}(t) + \dot{\hat{x}}(t) \times .01 \quad 3.2.4-(9)$$

The last two are the simple time step integration of the time derivatives.

3.3 Robustness Issues

The robustness of the update can be judged in several ways, and the analysis depends upon the update method used. As seen in the Results

Section, and in the Conclusions Section, the selected update method is the Constant Gain Extended Kalman Filter. Therefore, the robustness analysis is done for this method. A Bode plot of the singular values of the Kalman filter judges the robustness of the update. The following information reviews singular value theory from Ref. 15.

3.3.1 Singular Values

The singular values of the transfer function matrix indicate whether the response of the system at a given frequency is "large" or "small." They are equivalent to the gain at a frequency for the single input-single output system, and may be plotted similarly on a Bode plot to determine the multi-variable frequency response of any MIMO system.

Start by defining the complex conjugate transpose of a matrix F which equals F^H .

$$F = \begin{bmatrix} 2 + 3 \\ 3 - j \end{bmatrix}, \quad F^H = [2 - 3j, 3 + j]$$

Now define the spectral norm:

$$\|F\|_2 = \max_{z \neq 0} \frac{\|Fz\|_2}{\|z\|_2} \quad 3.3.1-(1)$$

Then

$$\|F\|_2 = \max_i \sqrt{\lambda_i \{F^H F\}} \quad 3.3.1-(2)$$

Where λ_i are the eigenvalues of $F^H F$ which are real, non-negative.

Now, define the singular values of F :

$$\sigma_1(F) = \lambda_1 \sqrt{(F^H F)} \geq 0 \quad 3.3.1-(3)$$

Then the maximum singular value is

$$\sigma_{\text{MAX}}(F) = \text{MAX}_i [\sigma_i(F)] = ||F||_2 \quad 3.3.1-(4)$$

From equation 3.3.1-(2). Also the minimum singular value is

$$\sigma_{\text{MIN}}(F) = 1 / ||F^{-1}||_2 \quad 3.3.1-(5)$$

Now apply these definitions and relations to control theory, as from Ref.

16. Consider a mimo system with input $\underline{u}(s)$, output $\underline{Y}(s)$, and transfer function matrix $\underline{G}(s)$. These are related below, in typical fashion.

$$\underline{Y}(s) = \underline{G}(s) \times \underline{u}(s) \quad 3.3.1-(6)$$

Take the complex conjugate transpose, and divide both sides by $||\underline{u}||_2$

$$\frac{||\underline{Y}(s)||_2}{||\underline{u}(s)||_2} = \frac{||\underline{G}(s) \underline{u}(s)||_2}{||\underline{u}(s)||_2} \quad 3.3.1-(7)$$

The magnitude of the RHS of this equation depends on the vector $\underline{U}(s)$. The largest magnitude that the LHS of this equation can attain is calculated from the singular values of $G(s)$:

$$\max_{\underline{u}(s) \neq 0} \frac{\|G(s) \underline{u}(s)\|_2}{\|\underline{u}(s)\|_2} = \sigma_{\text{MAX}}(G(s)) = \sqrt{\lambda_{\text{MAX}} G^H G} \quad 3.3.1-(8)$$

The same holds for minimum values.

Thus $G(j\omega)$ is small when its maximum singular value is small, and $G(j\omega)$ is large when the minimum singular value is large. It is seen that a plot of the singular values versus frequency yields the sensitivity as a function of the input frequency, as in the SISO case. Thus, at low frequency, a large minimum singular value is desired, and at high frequency, a small maximum singular value is desired.

3.3.2 Robustness Analysis

The assessment of robustness depends on the BODE plot of the singular values of the closed loop constant gain Kalman filter. The singular values of the filter algorithm are evaluated at SLS IRP power setting. The linearized approximation from Section 3.2.3 is used to evaluate the closed loop singular values. Recall that, for the linear Kalman filter, the following equations apply:

$$\begin{array}{ll} \text{Filter} & \hat{\underline{x}} = F\hat{\underline{x}} + K(Z - \hat{Z}) \\ \text{Output} & \hat{Z} = H\hat{\underline{x}} \end{array} \quad 3.3.2-(1)$$

Reducing yields $\dot{\hat{x}} = (F - KH) \hat{x} + KZ$ 3.3.2-(2)

The singular values of the closed loop matrix (F-KH) determine robustness.

A controls design package determines the minimum singular value and maximum singular value as a function of frequency for the closed loop system. Figure 3.2.3-1 depicts the two singular values plotted against frequency in radians/second. The typical high "gain" at low frequency is exhibited along with the decreasing "gain" at high frequency. The 0.0 dB points are at 1.5 rad/s for the minimum singular value at 13 rad/s for the maximum singular value, and both fall off at about 20 dB per decade. Now these characteristics must be judged against the unmodeled dynamics of the engine and high frequency sensor noise.

The unmodelled dynamics include the gas volume dynamics within the engine, and the sensor dynamics. The first type by referring to a study of the Pratt & Whitney F100 Turbo-Fan engine from Ref. 17. That engine is similar to the subject engine: it is a two spool, low-bypass augmented engine, but of a higher thrust class due to its size. However, the dynamics will be similar. A sixteen state model of that engine shows eigenvalues ranging from -0.66 to -573.4 radians/second. The table below shows them in detail.

TABLE 3.3.2-1 EIGENVALUES OF F100 ENGINE MODEL

1)	-0.66	11)	-39.71
2)	-1.964	12)	-47.52
3)	-2.732	13)	-49.38
4,5)	-6.102 ± 2.259j	14)	-58.26
6,7)	-18.62 ± 5.253j	15)	-177.7
8)	-19.45	16)	-573.4
9,10)	-20.66 ± 0.921j		

31-DEC-84
13:24
MAG
OPEN
GAIN=1.0
PH
PL

CL DISPLAY:
WHAT NEXT?

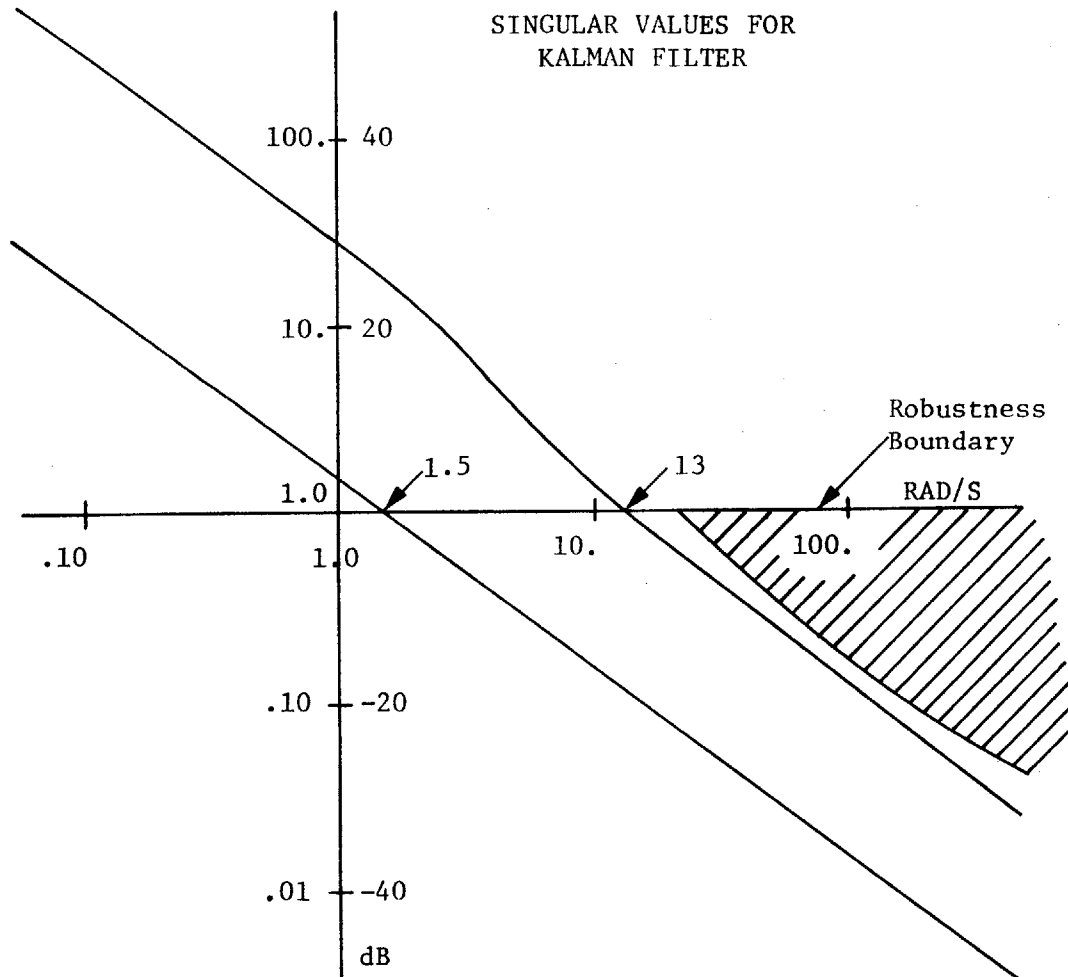


FIGURE 3.3.2-1

The first two relate to the "slow" heat storage in the hot section turbines, the next three include rotor dynamics and the volume dynamics in the afterburner. The remainder are temperatures and pressures that relate to the fast volume dynamics of the engine. Therefore, the principle concern are the filter response for the higher frequencies, which are unmodeled. Before continuing, it should be noted again that the subject engine is smaller in size and therefore, all gas dynamics will be faster than this F100 engine, and tend to push the poles that are of the order -20 to -25 or faster based on airflow and volume ratios.

The magnitude of the effects of gas volume dynamics must be less than about 8 dB at 25 rad/sec in order to have a robust filter. This is the only frequency of concern, and further investigation may be required. The higher frequency unmodelled dynamics are considered not to be of major concern, due to the slope of the maximum singular value characteristic.

The sensor dynamics can be ignored if the frequency is high (as the noise typically is). Another method to design in robustness to sensor noise is to allow the filter to update the model only for residuals that are greater than the known range of sensor errors. Thus, for the N_1 sensor, the update would be "turned off" if the difference in N_1 was less than 0.5% of full scale.

In summary for this section, the constant gain Kalman filter algorithm is robust against unmodelled dynamics based on the known high frequency dynamics typical of low bypass turbofan engines, and against sensor noise due to not updating within the bounds of known sensor noise.

4. NUMERICAL RESULTS

The results of this study are divided into two sections: steady state and dynamic. The static results display the required parameter adjustments that force the model to track the engine on a steady state basis. They also show some of the capabilities of the update in terms of T41 synthesis, condition monitoring and adaptability. These are compared to the model without an update. The dynamic performance compares the four candidate update methodologies against the model without an update.

4.1 Static Performance of the Update

The magnitude of the parameter changes required to match the "truth" model determine the update's ability to detect sensor failures. If the changes are small, then failures are more easily detected, but if they are large, the model cannot detect small (or drift) failures. These results are summarized for three types of tests. The first shows the comparison between the engine model and the nominal "truth" model around the flight envelope. This will show the initial "size" of the four dimensional box that encloses possible nominal modelling error. The second test displays the updating vector's reaction to normal engine to engine variations. The third test shows the method's reaction to sensor errors. The important judging criteria is the synthesis of turbine inlet temperature, T41, compared against the model without an update.

The first step is to establish the baseline performance of the model on a stand alone basis. The model results around the flight envelope are

shown in Table 4.1-1 for comparison to the truth model. The real time model is given the same control inputs (fuel flow and exhaust nozzle area) as the truth model, and the modelling errors on the four outputs plus thrust and T41 are summarized.

TABLE 4.1-1 BASELINE PERFORMANCE OF THE MODEL

ALT	XM	PLA	Sensors				Performance	
			EN ₁ %	EN ₂ %	EP ₃ %	ET ₅ %	ET41 _R ^o	EFN%
0	0	87	+0.9	-0.4	0	+0.0	-1°	+3.3
0	1.1	87	-0.5	+0.1	-3.1	+1.1	+41°	-3.8
10000	1.4	87	-0.5	0.0	-4.2	+2.6	+49°	-8.3
15000	0	87	+2.1	+0.2	+1.4	-0.3	-3°	+3.2
35000	0.8	87	+1.3	+0.2	+2.3	-0.9	-15°	+1.3
35000	1.2	87	+0.9	-0.2	+0.5	+0.3	-1°	+1.3
35000	1.6	87	+0.5	-0.4	-2.1	+1.0	+25°	+0.6
35000	2.0	87	-1.0	-0.2	-4.3	+2.1	+40°	+8.9
60000	1.0	87	+5.6	+2.2	+2.5	-1.2	-9°	+0.7
60000	2.0	87	-1.2	-0.1	-3.7	+2.2	+37°	+11.7
0	0	130	+1.4	-0.4	+0.6	+0.6	+15°	+4.3
0	1.1	130	+0.5	-2.7	+1.3	+1.3	+38°	-5.9
10000	1.4	130	+0.3	-3.9	+1.9	+1.9	+46°	-11.1
15000	0	130	+2.7	+1.0	0.0	0.0	+9°	+3.0
35000	0.8	130	+2.2	+1.9	-0.7	-0.7	-5°	-1.6
35000	1.2	130	-0.5	0	+0.6	+0.6	+14°	-4.3
35000	1.6	130	+0.8	-2.1	+0.8	+0.8	+26°	-6.6
35000	2.0	130	0	-3.9	+1.5	+1.5	+36°	-9.8
60000	1.0	130	+3.6	+3.7	-2.0	-2.0	-41°	+3.3
60000	2.0	130	-0.4	-3.3	+1.5	+1.5	+33°	-6.1

The average errors and standard deviations are summarized in Table 4.1-2. For the two speeds, PS3C, T5, and thrust, the errors are in

percent, whereas for T41 they are in degrees Rankine. The update method should improve the predictions of T41 and thrust by eliminating the four output errors. This information established the basis for judging the effectiveness of the update.

TABLE 4.1-2 MODELLING ERROR STATISTICS

<u>Parameter</u>	<u>Average Error</u>	<u>Standard Deviation</u>
N ₁	0.9%	1.7%
N ₂	0.2%	0.7%
PS3C	-1.0%	2.6%
T5	0.6%	1.2%
T41	+14.5°	23°
F _N	-0.8%	6.1%

The adaptation of the model for the parameter set of interest was discussed in Section 3.1. This set is composed of an adder to fan efficiency, an adder to high pressure turbine efficiency, an adder to fan speed/flow relationship and a bias on the metering value measurement of fuel flow. The results of the envelope survey are shown in the appendix in Table A-2. They are summarized in Table 4.1-3 below.

TABLE 4.1-3 IMPROVEMENTS BY MODEL ADAPTATION

<u>Parameter</u>	<u>Average Error or Delta</u>	<u>Standard Deviation of Error or Delta</u>
T41	-1.0°	13°
F _N	-1.1%	6.4%
Fan Eff.	0.8 PTS	3.7 PTS
HPT Eff.	0.3 PTS	1.6 PTS
Fan Flow	1.9%	2.0%
Fuel Flow	0.2%	0.8%

The table shows the average errors and standard deviations for T41 and thrust. the T41 synthesis is significantly improved while the thrust synthesis is marginally improved. The parameter deltas are "small" except for fan efficiency. Thus around the flight envelope on a "nominal" engine, the expected variations are of the order 4 points on fan efficiency, 2 points on turbine efficiency, 2 percent on airflow, and 1 percent bias on fuel flow. These are the magnitudes of the modelling errors, and impose the smallest four-dimensional box for identifying sensor errors. By this, it is meant that if a sensor were drifting, it would have to cause an efficiency change of greater than four percent before it could be declared a fault. The section on sensor errors further amplifies the point.

The next set of results covers the effects of engine to engine variations as discussed in Section 3.1 and shown in Appendix 1. The expectation here is that the update method can distinguish component quality through the adaptation of component parameters. If, for example, high pressure turbine efficiency decreased by two points, it is desired that the model would move this parameter (and this parameter only) by two points on a relative basis. Thus, the time history of the update set (or vector) would be indicative of engine component health.

The comparison is made by adjusting the truth model for the engine variations, and then matching the resulting N_1 , N_2 , PS3C and T5 at the same fuel flow and exhaust nozzle area. The base point is at seal level static, standard day intermediate rated power setting. Appendix 1 contains the detailed information, which is summarized in Table 4.1-4. The Table presents the base case plus the individual effects as deltas from the base case. In the first variation, by changing fan efficiency of the truth

model by +0.6%, the vector changes model fan efficiency by 0.58%, turbine efficiency by +0.04 points, fan airflow by -0.19 percent and fuel flow bias by -0.09 percent. The method, therefore identifies the change in fan efficiency almost exactly. This result reveals the health monitoring capabilities of the update.

TABLE 4.1-4 EFFECTS OF ENGINE TO ENGINE VARIATION

Change to "Truth" Model	Vector Updates Relative to Base			
	f-Pts	t-PTS	Airflow%	W _f %
BASE	-1.55	0.81	2.03	-0.68
$\eta_f + 0.6$ PTS	+0.58	+0.04	-0.19	-0.09
Airflow +1.0%	+0.04	-0.08	+1.10	-0.08
$\eta_c + 0.7$ PTS	+0.17	+0.53	+0.04	-0.14
Comp. Airflow + 1.0%	+0.89	-0.15	+0.17	-0.05
$\eta_t + -0.8$ PTS	+0.27	+0.73	+0.04	-0.12
FF41 + 1.0%	-0.73	-0.30	-0.84	-0.93
$\eta_{2t} + 1.0$ PTS	+0.46	+0.19	-0.39	-0.18
FF45 + 1.0%	-0.33	+0.42	+0.49	+0.10
Cooling flow +0.4%	-0.30	-0.30	-0.28	-0.27

These results are further analyzed item by item from the table. The second item, fan airflow, is also correctly identified. The third item, compressor efficiency, is not contained in the parameter vector. However its result looks strongly like a turbine efficiency change. This is because the changes in HPC and HPT efficiency are virtually indistinguishable without a measurement of compressor discharge temperature, T3. The fourth item, compressor airflow is identified as a change in fan efficiency. This is an unfortunate result. Perhaps the direction on fan airflow will

distinguish the two in the general case. Next, turbine efficiency is correctly identified. Turbine flow function changes result in a negative change in all parameters, which is good if it is unique to the other possible changes. The remaining variations do not show a distinguishing single characteristic, but perhaps the direction of the vector is unique. In conclusion, for the three component characteristics in the update vector, the adaptation responds in a unique direction, and in the correct direction. The other directions of the vector could be explored further.

Finally, the effects of sensor errors are explored. Table A-14 in the appendix displays the detailed results for IRP and maximum afterburner. The results for the two power settings are the same, and shown in Table 4.1-5. The sensor errors are shown on the left-hand side, and the resulting parameter variations follow on the right.

TABLE 4.1-5 EFFECTS OF SENSOR ERRORS

Sensor Error	$\Delta\eta_f$ PTS	$\Delta\eta_t$ PTS	Δ Airflow, %	ΔW_f , %
BASE	-1.55	0.81	2.03	-0.68
Fuel Flow + 5.0%	+0.01	-0.12	-0.01	-4.74
Nozzle Area + 4.0%	-0.43	-0.43	+2.15	+0.67
N_1 + 0.5%	+0.60	+0.03	-1.24	-0.05
N_2 + 0.5%	-0.80	+0.54	-0.19	-0.15
PS3C + 1.1 PSI	+0.21	0.00	+0.29	+0.32
T5 + 16° R	-0.65	-0.51	-0.22	+1.07

In the first case, the control sensed fuel flow is 5 percent greater than that actually entering the burner. This could be because of a leak, for example, or the metering value position feedback could be in error.

The update correctly removes the bias on fuel flow without significantly effecting the other three variables. The nozzle area sensor error effects all four variables, but fan airflow most strongly. A fan speed error shows up as efficiency and airflow. This result is logical. For detection, the normal variations in airflow dictate the magnitude. Previously, the modelling errors at high power are at most 2 percent on airflow. The magnitude of airflow error bound is calculated by adding the normal model errors (2%) plus the RSS effect of engine to engine variations (1.6%) and the sensor error (2.5%). The last two are RSS'd together because of the random nature. Thus the box in the airflow direction is equal to 5.0% airflow variation. (Take the square root of $(1.6)^2 + (2.5)^2$ and add 2.0%.) Therefore, an N_1 error of 4% ($5.0/1.24$) is detectable in a simple-minded sense. The above calculation is an estimate of the detection capability. There are many other considerations to detection, and the analysis is beyond the scope of this work.

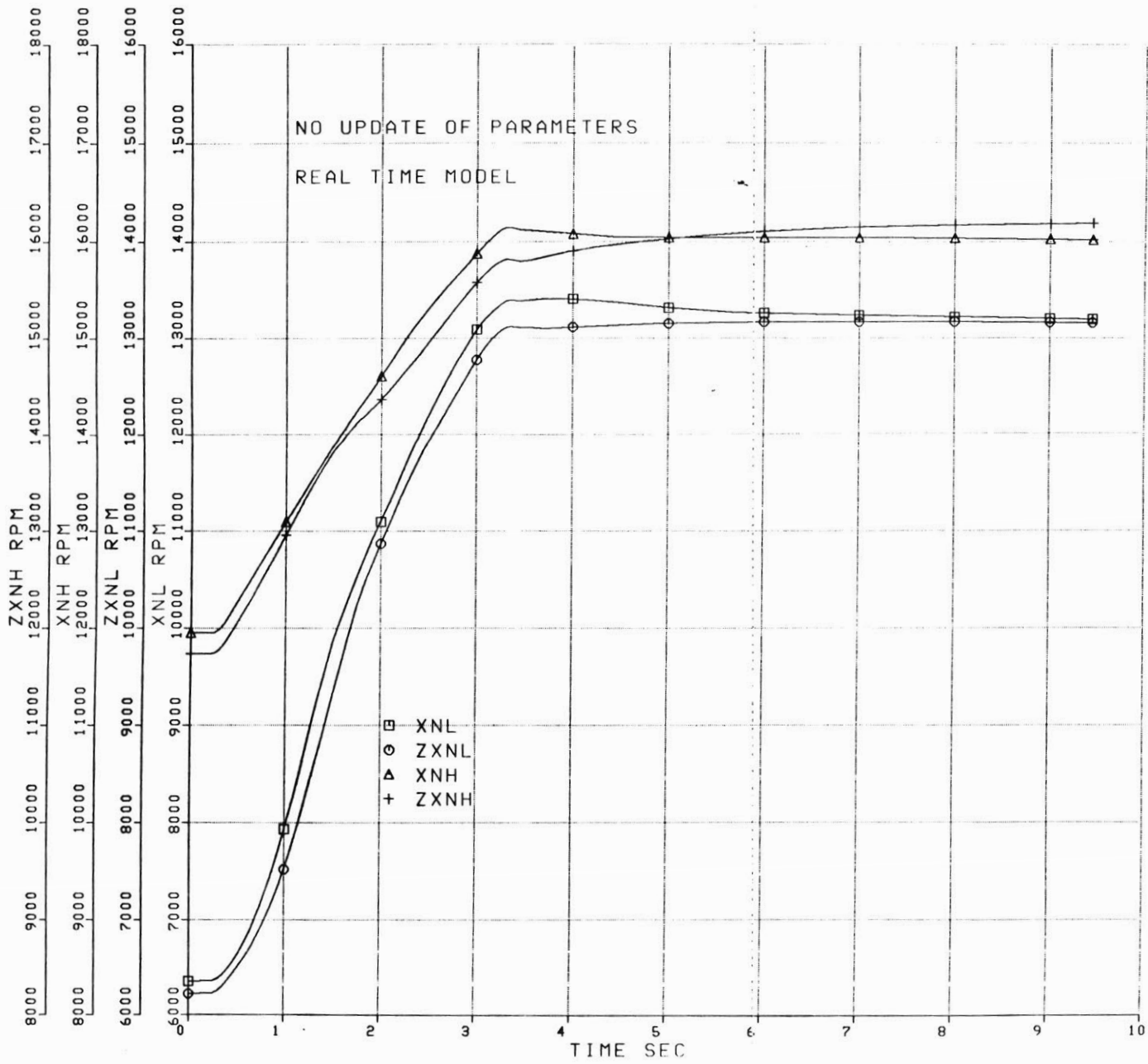
In summary of the static results, the magnitudes of parameter changes have been established for three cases: modelling errors around the flight envelope, engine to engine variations and sensor errors. None are excessively large, permitting possible detection of small in range sensor failures. The engine variation analysis establishes that the adaptation is unique for the three parameters in the update vector, and may be unique for those not included. The sensor error analysis shows positive detection of fuel flow sensor error, and possible failure directions for other failures. This could be done in a further study.

4.2 Dynamic Performance of the Four Strategies

The goal of this analysis is to check the tracking ability of the update methods analyzed in Section 3. The engine transient is an acceleration from flight idle to IRP in about 3 seconds at sea level static, standard day. This is a rapid time response, considering that thrust increases by 40 times the flight idle setting. The truth model is the large scale dynamic simulation which provides the control demanded fuel flow and exhaust nozzle area. These are input to the model, which estimates the four sensed parameters. The errors between the estimates and the truth model outputs are converted to parameter adjustment through a gain matrix, and the parameters are therefore dynamically updated.

A baseline for comparison is established by performing the acceleration without updating the four parameters. Figures 4.2-1 through 4.2-4 show the results. The first figure shows the comparison of the two rotor speeds verses time. The two prefixed by "Z" are the reference speeds from the large scale simulation. The maximum fan speed error is about 6% of point at $t=1.3$ seconds, and the maximum compressor speed is 2% of point at $t=2.0$ seconds. Near the end of the transient, the core speed prediction is drifting away. The second figure shows the comparison of the remaining two sensed variables: PS3C and T558. The PS3C estimate is fair, but the temperature estimate is poor. The error is 8% at $t=.8$ seconds, and about 5.5% at the maximum temperature. The third figures shows the synthesis of T41 and thrust. The former is more important, and the result is an under-prediction of nearly 100° at the peak temperature. This is important, as turbine life is highly influenced by T41. The final figure summarizes the

FIGURE 4.2-1



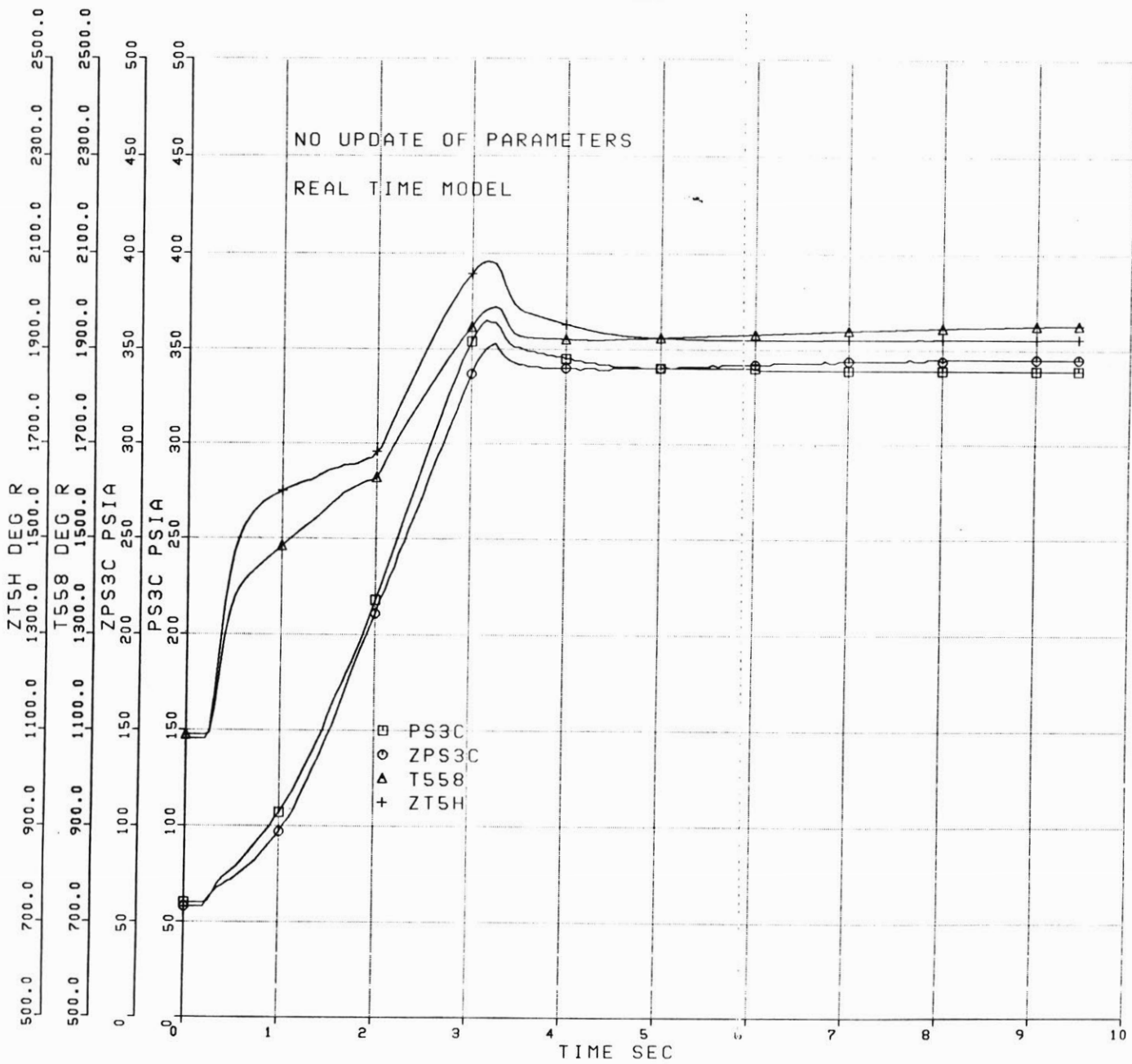


FIGURE 4.2-2

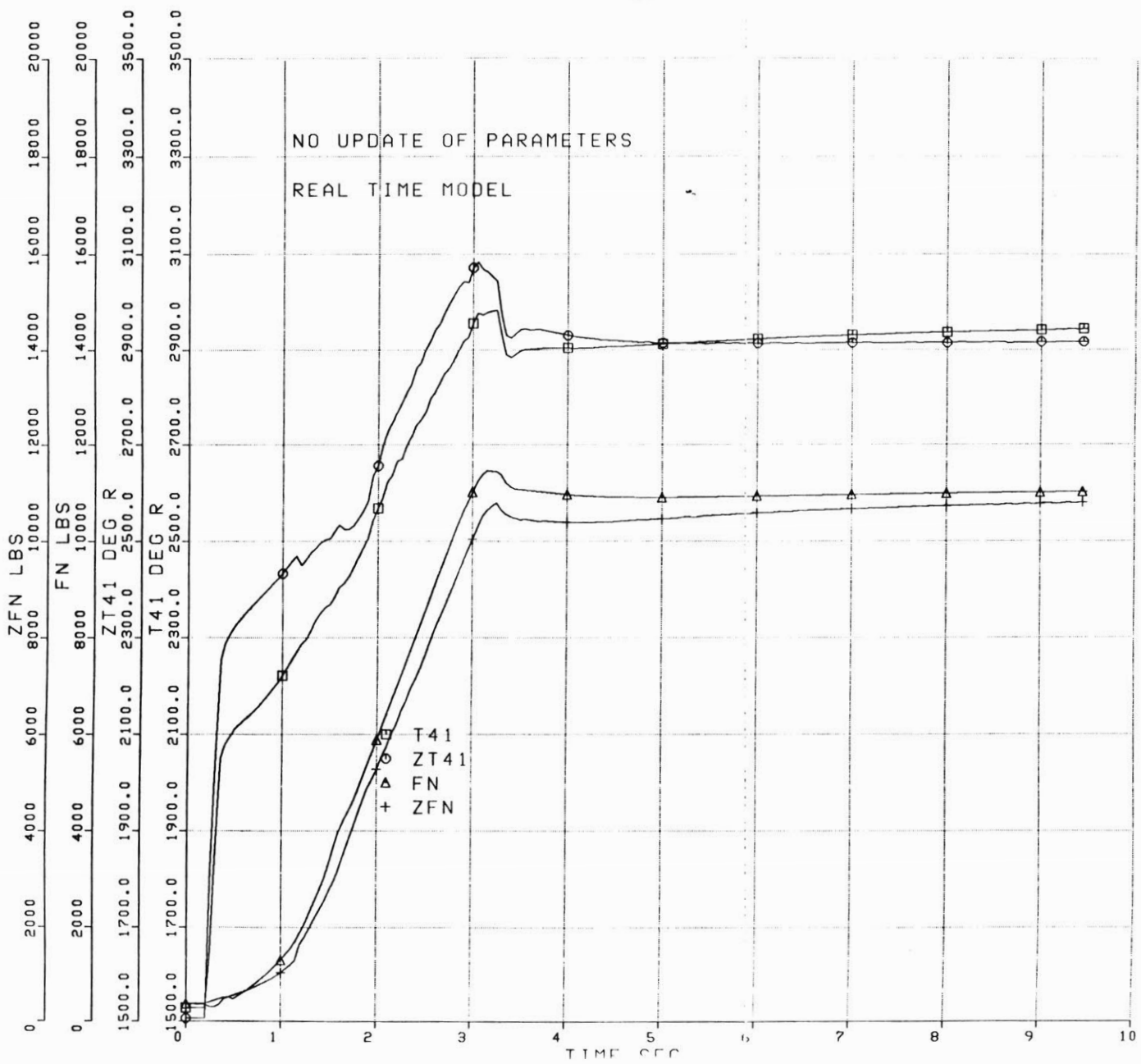


FIGURE 4.2-3

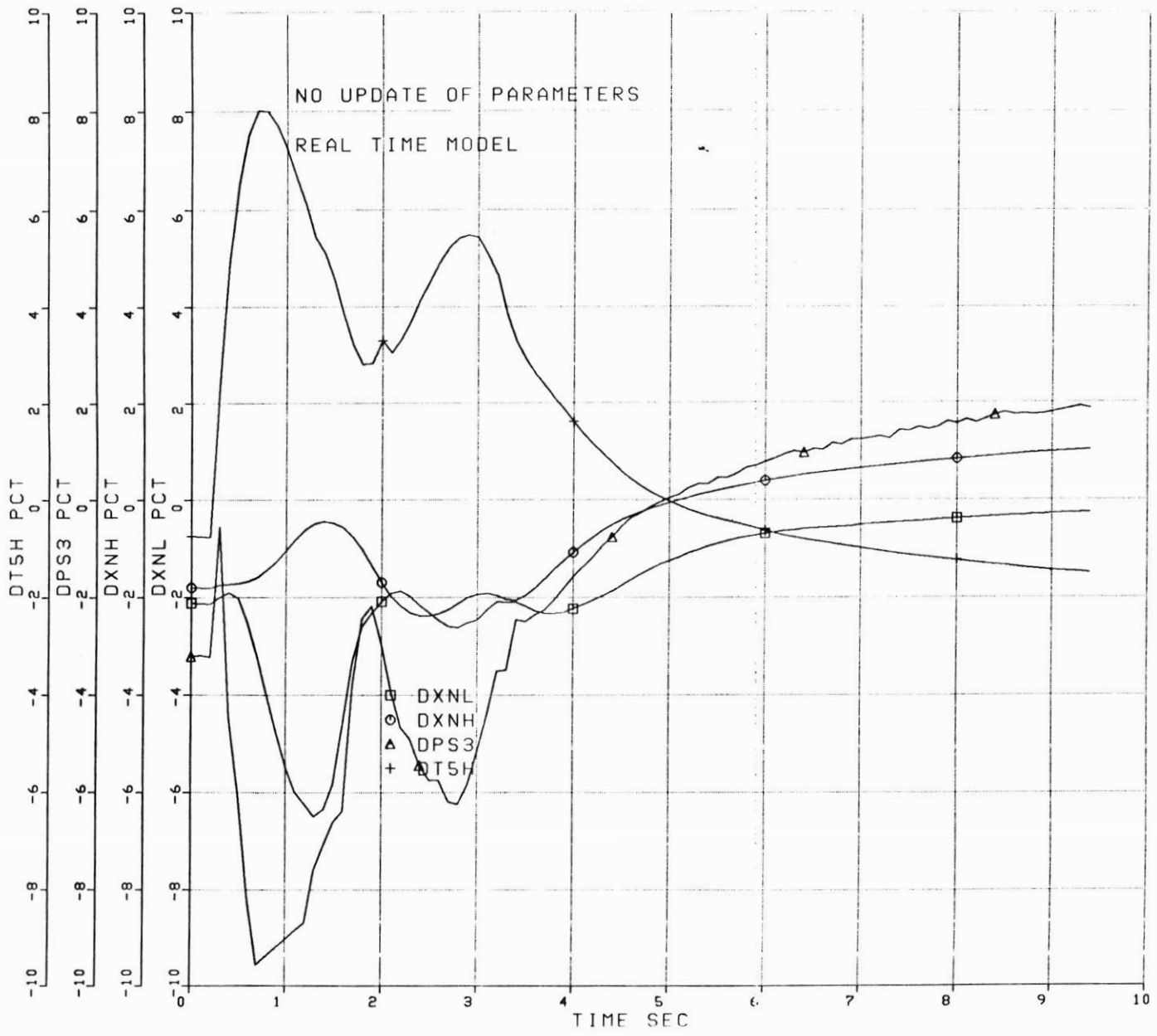


FIGURE 4.2-4

percent errors for the four variables during the transient. These figures establish the baseline comparison with which to judge the improvements.

The next set of figures show the results for the case where the gain matrix multiplying the error vector is the inverse of the Jacobian. Figures 4.2-5 through 4.2-8 relay information similar to the first set. Figure 4.2-5 displays the comparison of the two rotor speeds. The differences between the truth model and the real time model are reduced by correcting the modelling errors. Now the fan speed error is now 3.8% at $t=1.0$ seconds. However, the tracking could be better. The next figure shows the temperature and pressure sensor comparisons. The estimate of PS3C is improved, and the T558 estimate is significantly improved-- especially at the peak over temperature. The T41 synthesis is now off by only 20° , as shown in Figure 4.2-7. The error summary figure (4.2-8) shows significant improvement during the transient, plus the errors are forced to be small at steady state. Finally figure 4.2-9 shows the parameter changes during the accel. Note that at $t=0$, the model is not initialized to the truth model. The modelling errors are significant in the first 3 seconds, resulting in nearly 8 points in the two efficiencies. This result could limit the ability to detect transient faults.

The results for the least squares derived gain matrix are shown in Figures 4.2-10 through 4.2-14. Two results are worth noting with respect to the previous method. First, in Figure 4.2-13, the error in PS3C is not driven to zero. This unfortunate fact is due to the influence of the penalty on individual parameter size. The effect is to cause the gain matrix to change so that it cannot correct the error. (That is, the net result of the gains times the error vector has no influence on PS3C as for

FIGURE 4.2-5

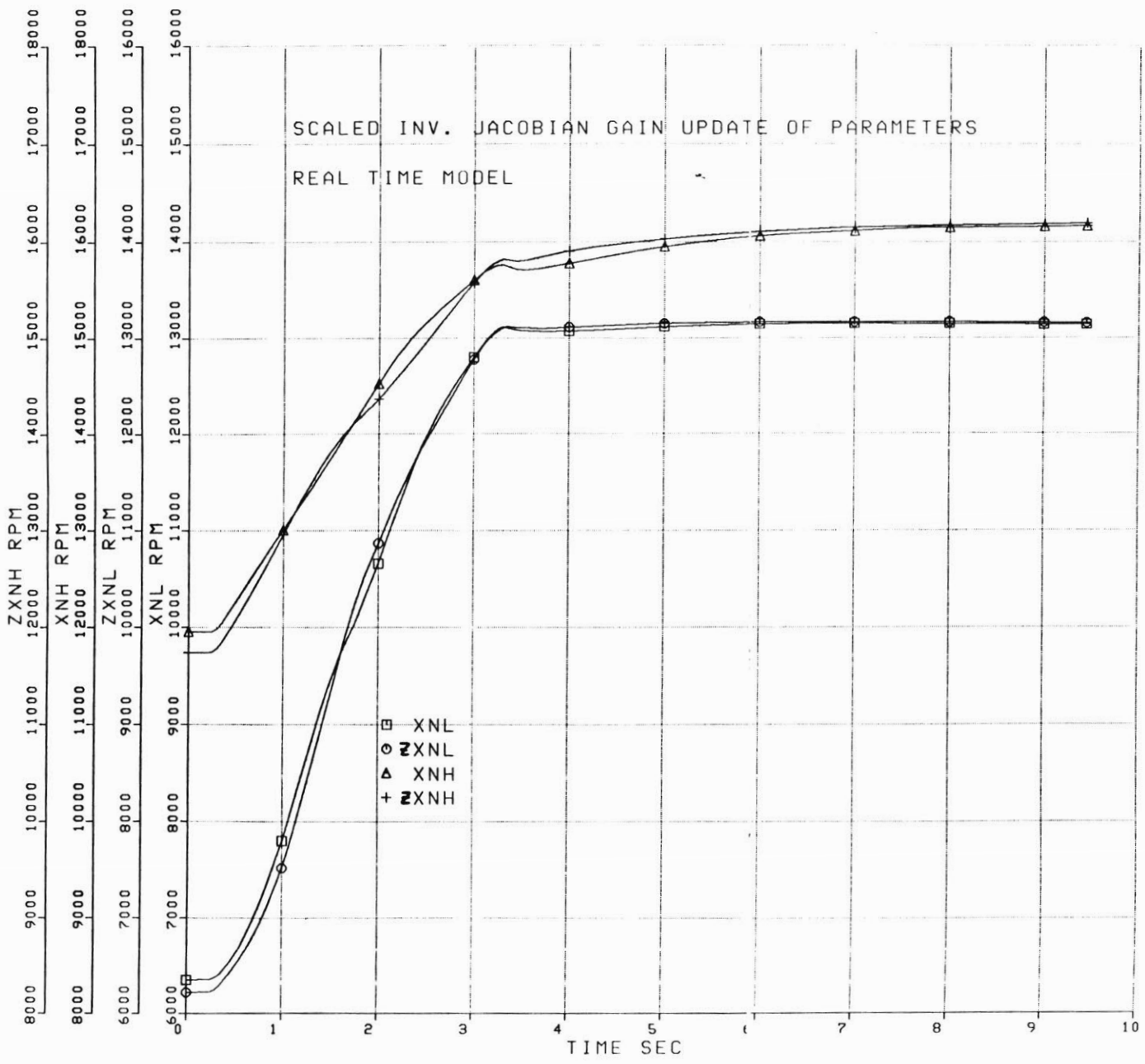
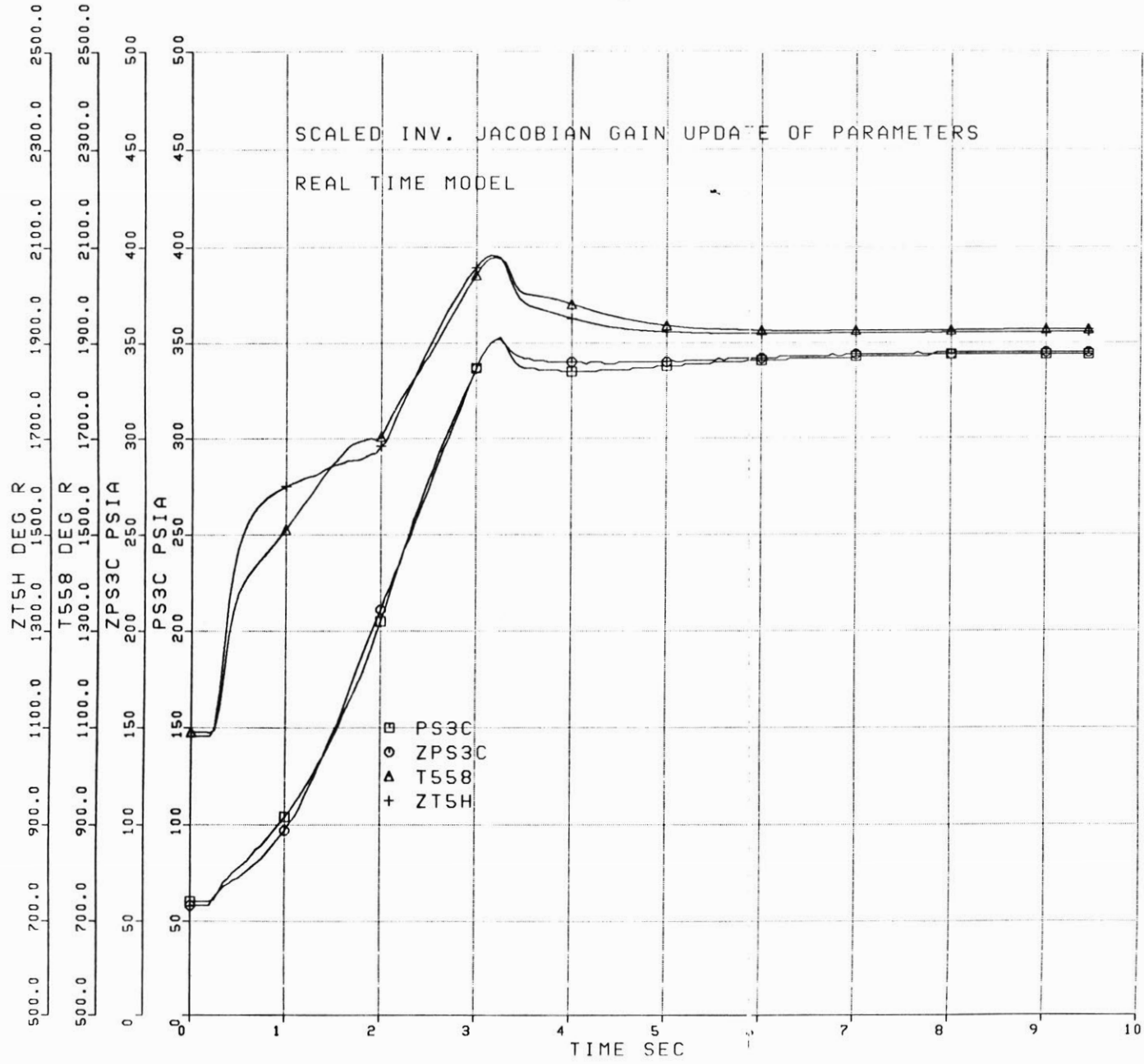


FIGURE 4.2-6



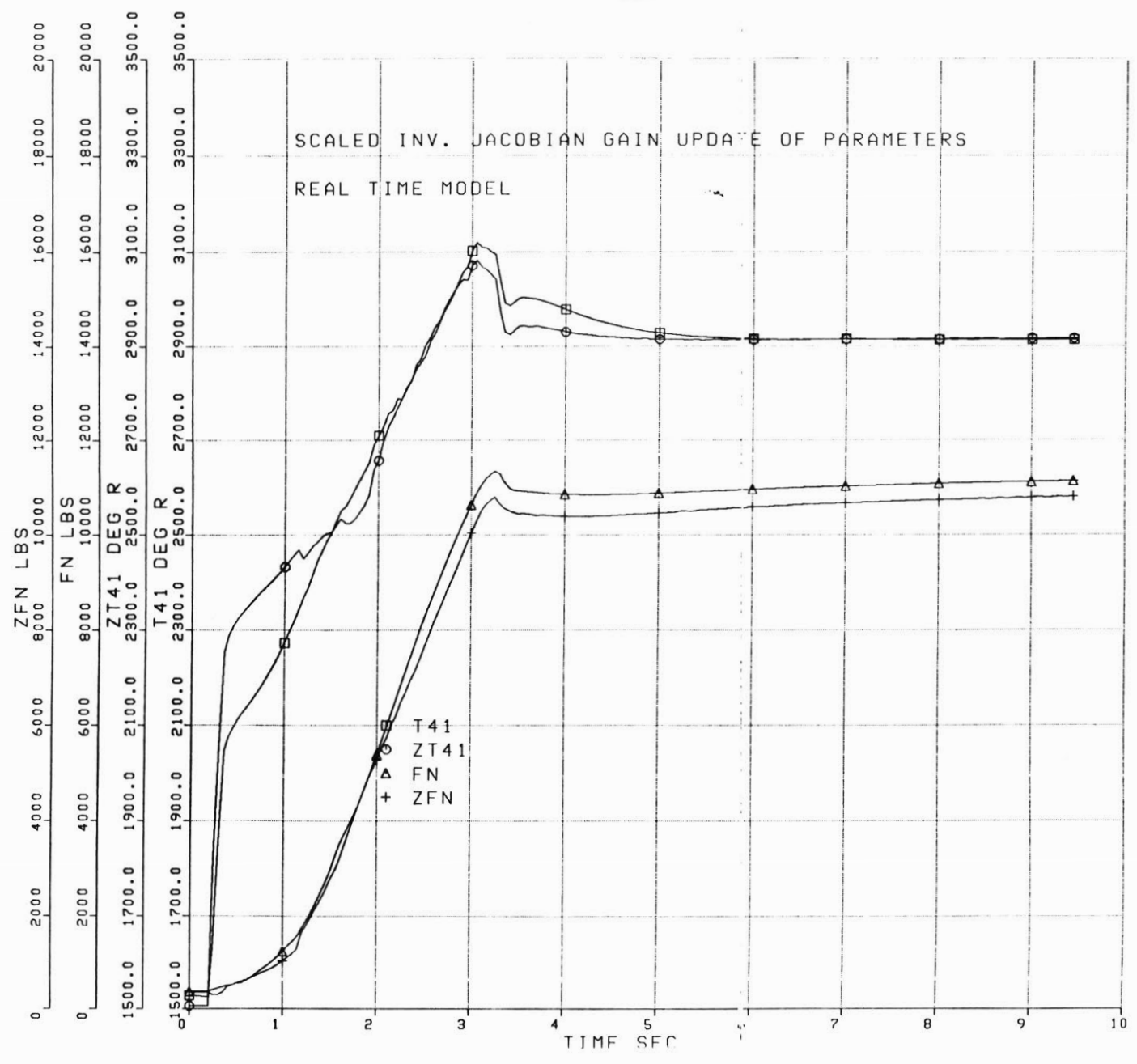


FIGURE 4.2-7

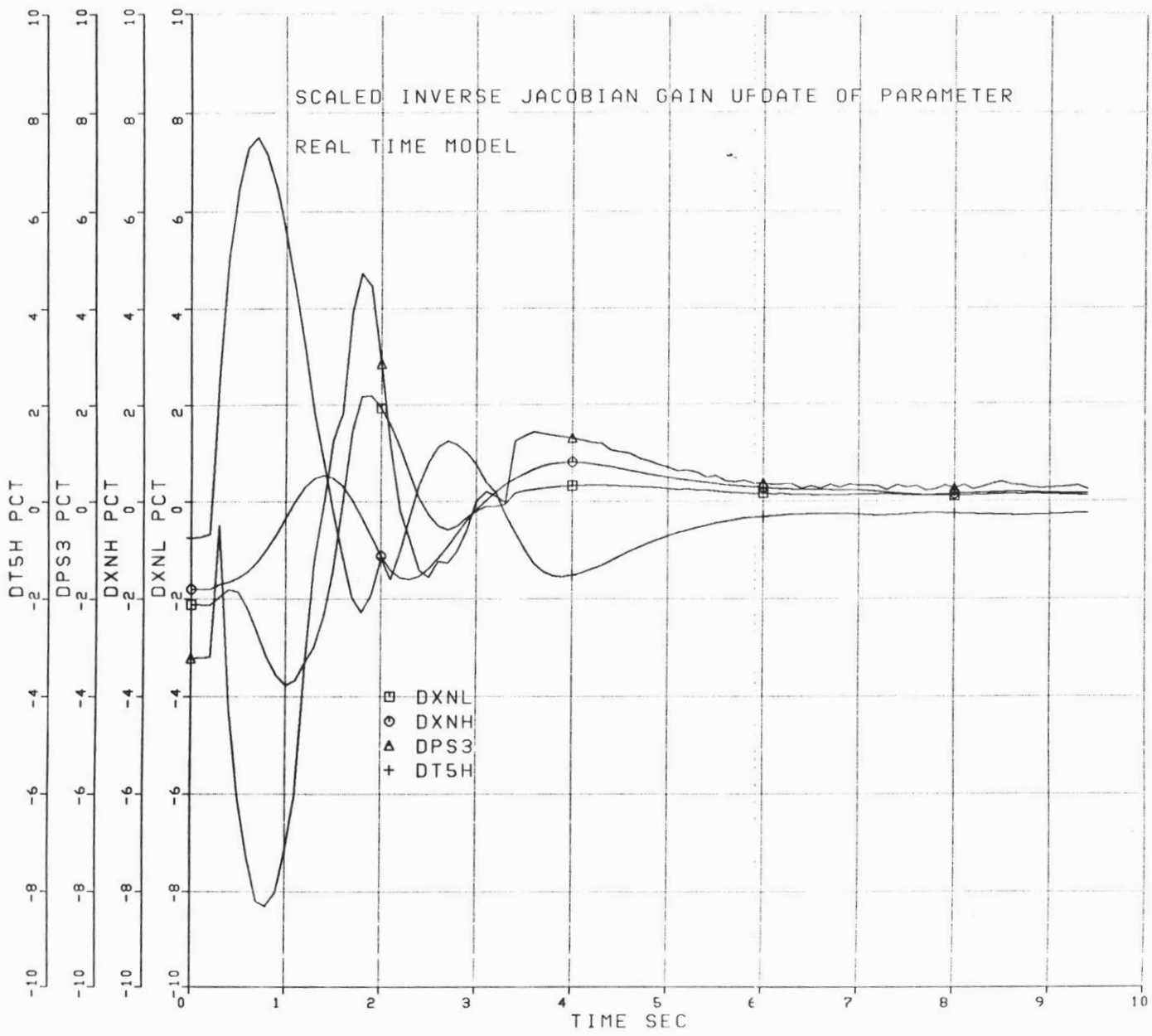
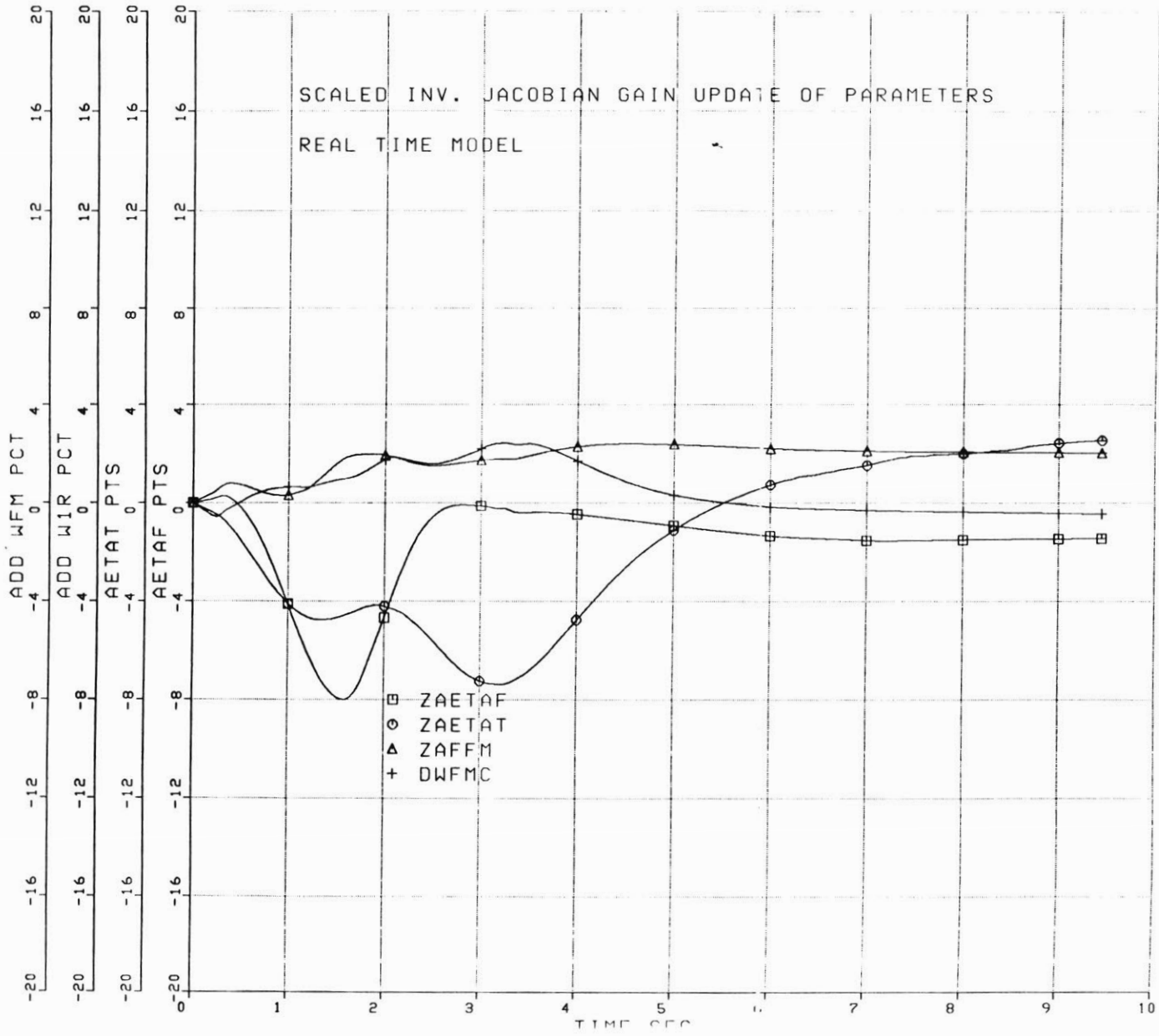


FIGURE 4.2-8

FIGURE 4.2-9



non-controllability). Secondly, in Figure 4.2-14, the fan airflow is changed by almost 11%, which is undesirable. The T41 synthesis, shown in Figure 4.2-12 is about the same as the previous method.

The constant gain Kalman filter shows the typical good tracking ability of the algorithm in Figures 4.2-15 through 4.2-19. The first figure shows a significant result: the rapid initialization of the filter, plus the small tracking deviations. The improvement in PS3C and T558 estimation is shown in the next figure. In the final figure of the set (Figure 4.2-19), the parameter changes are detailed. The stepping effect on the turbine efficiency is the result of the decision not to update if the errors are less than 0.3%.

The final set of figures, 4.2-20 through 4.2-24, show this transient for the extended Kalman filter update of the four parameters. The results are similar to the constant gain version. However, the initialization is slower due to the initial condition on the covariance matrix P. See Figures 4.2-20 and 4.2-21.

Finally Figure 4.2-25 displays a composite of the updates for estimation errors. These lines are the boundaries of the estimates of the four sensed variables. The constant gain extended Kalman filter shows the smallest boundary, with the errors less than 1% at $t=3$ seconds. These twenty-five figures are part of the basis for the final conclusions and recommendations. The choice here is to determine which dynamic method is the best. From these results, the two Kalman filters appear to be the best choice.

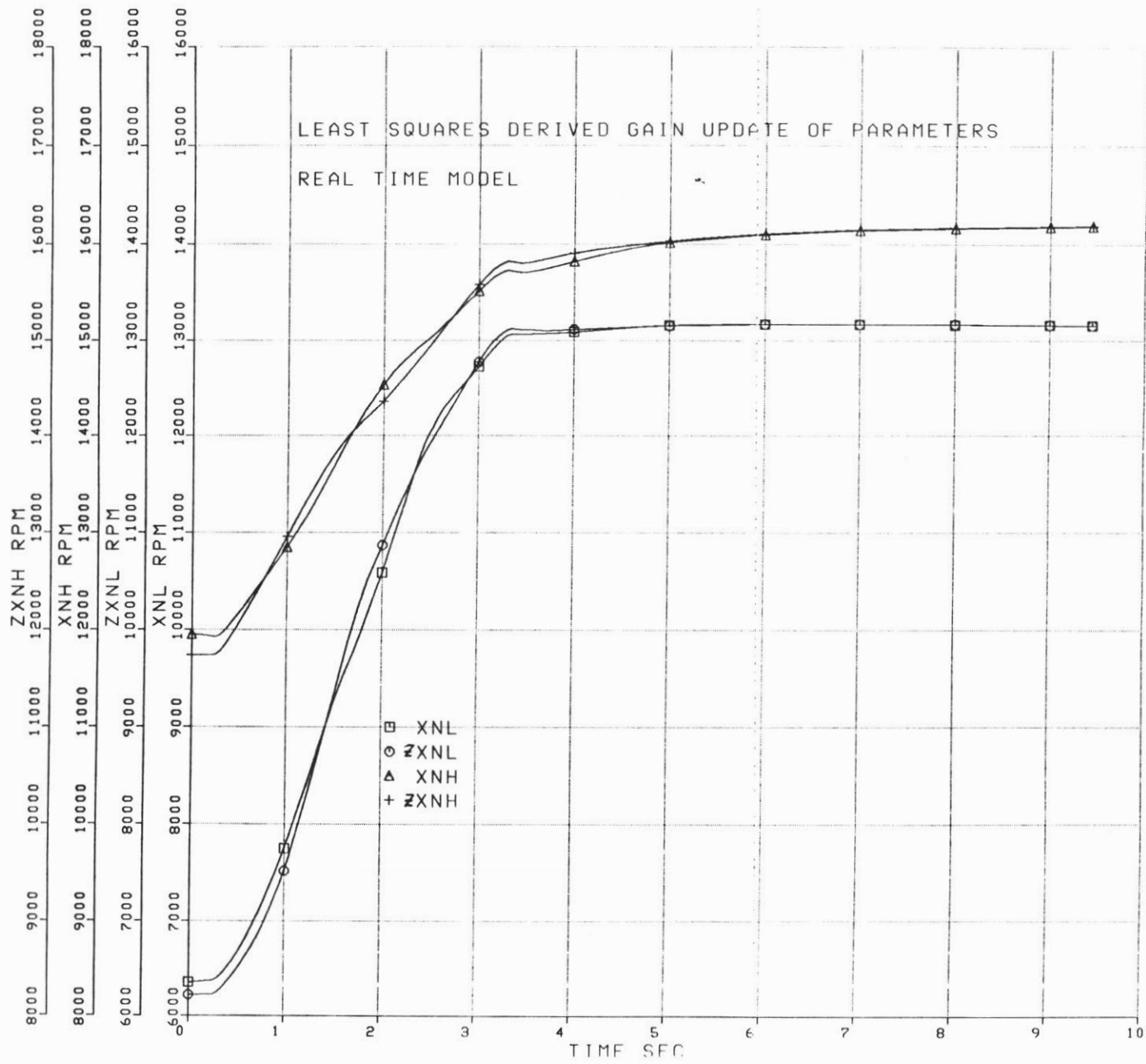


FIGURE 4.2-10

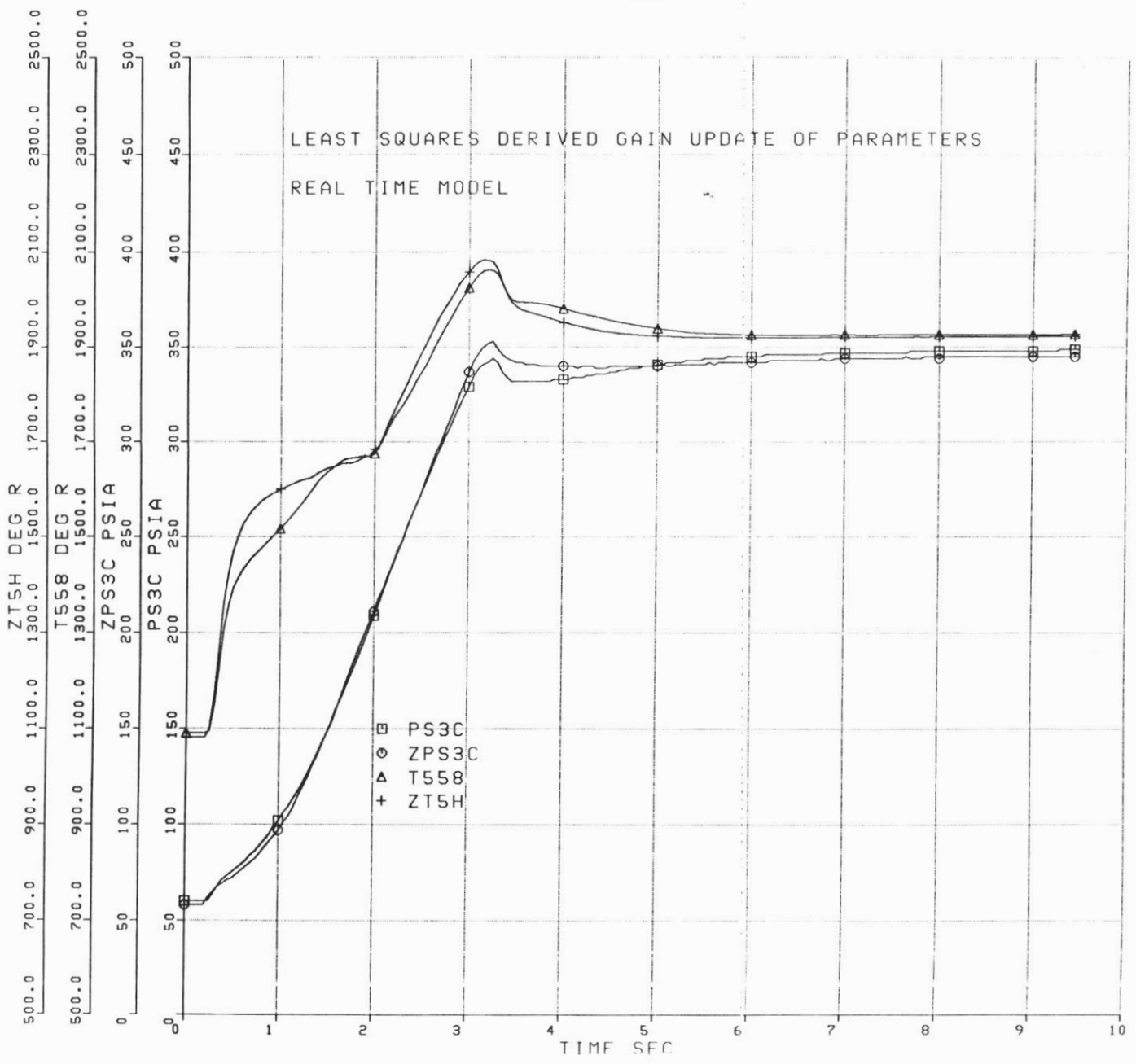
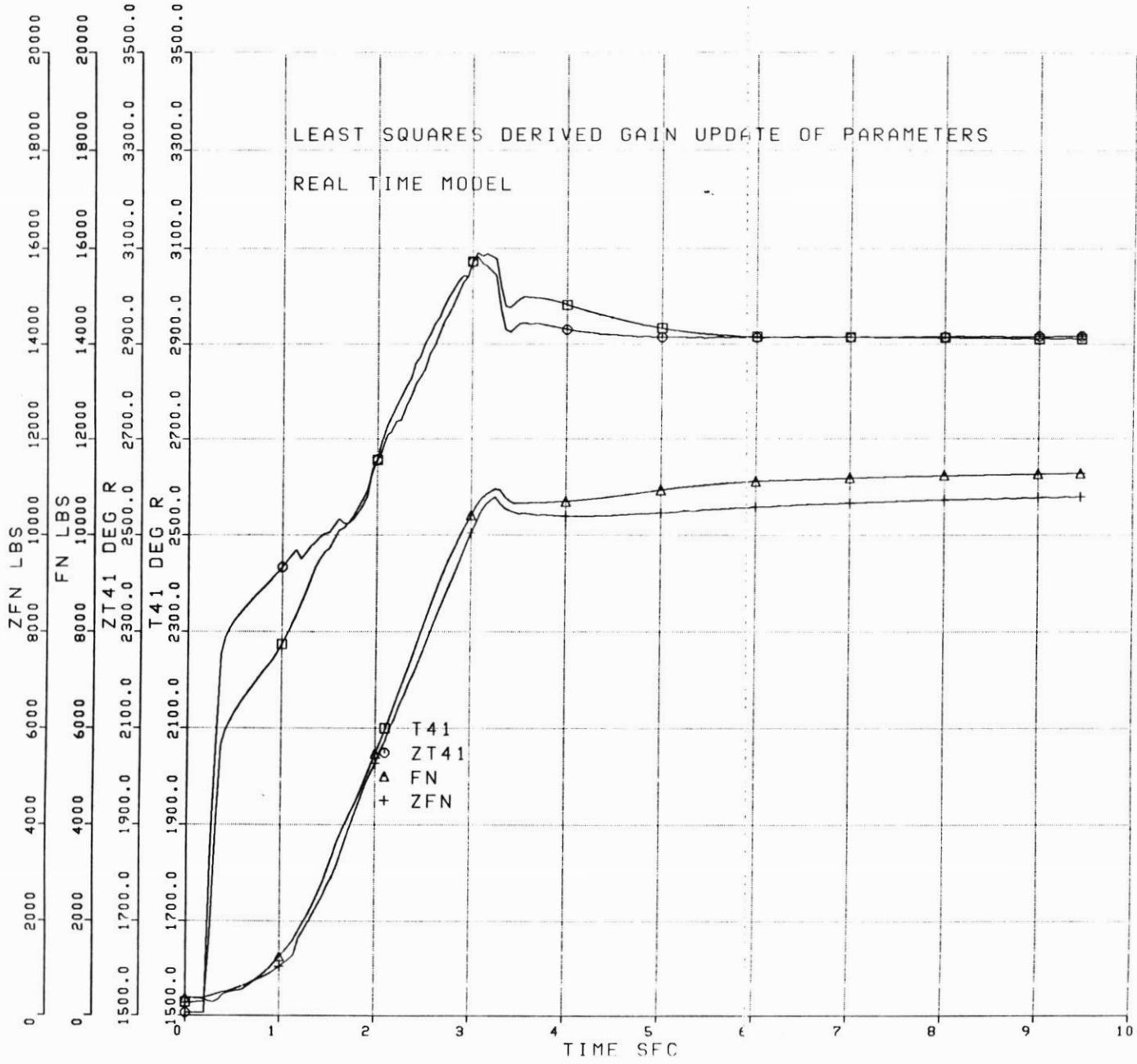


FIGURE 4.2-11

FIGURE 4.2-12



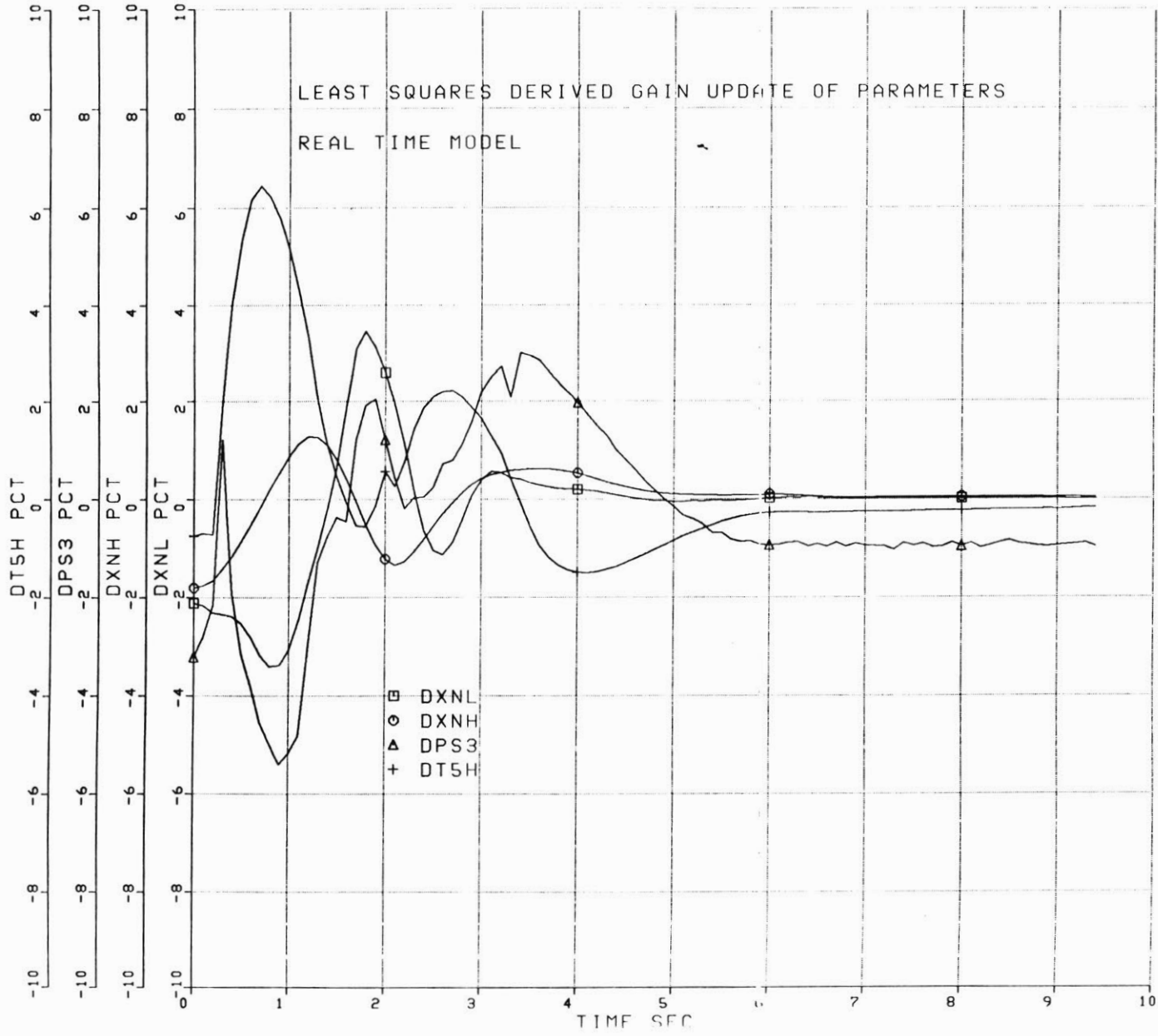
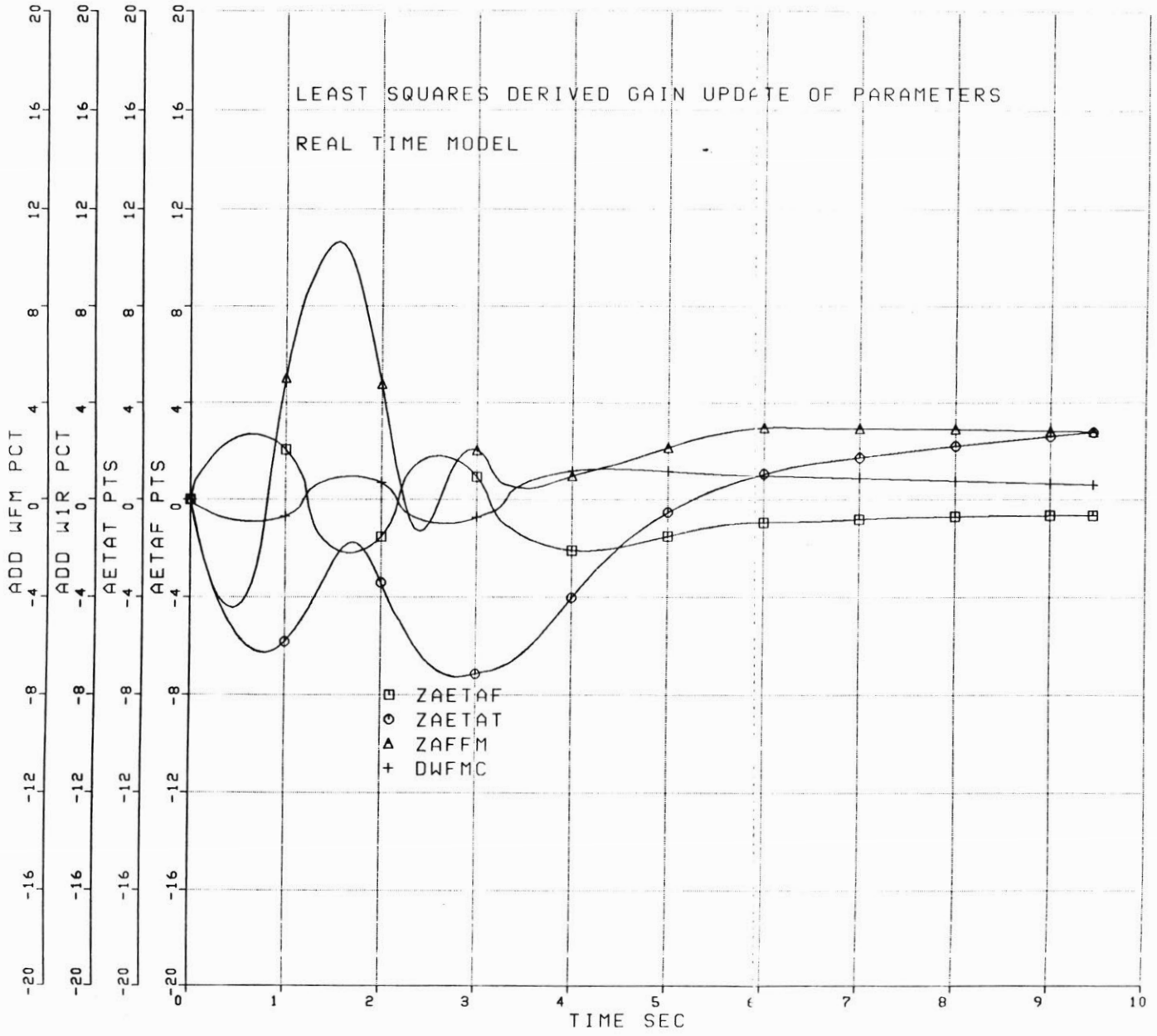


FIGURE 4.2-13

FIGURE 4.2-14



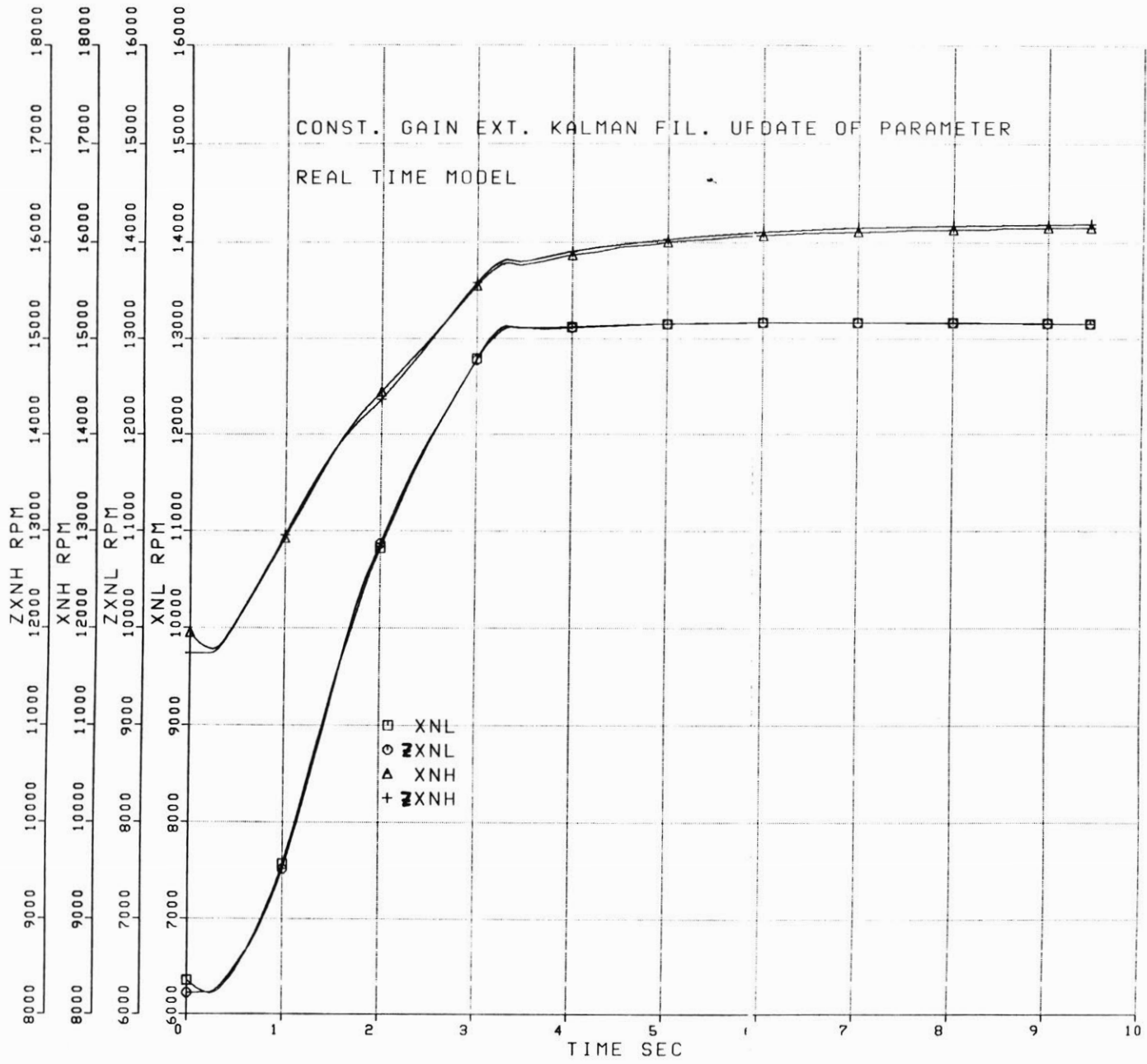


FIGURE 4.2-15

FIGURE 4.2-16

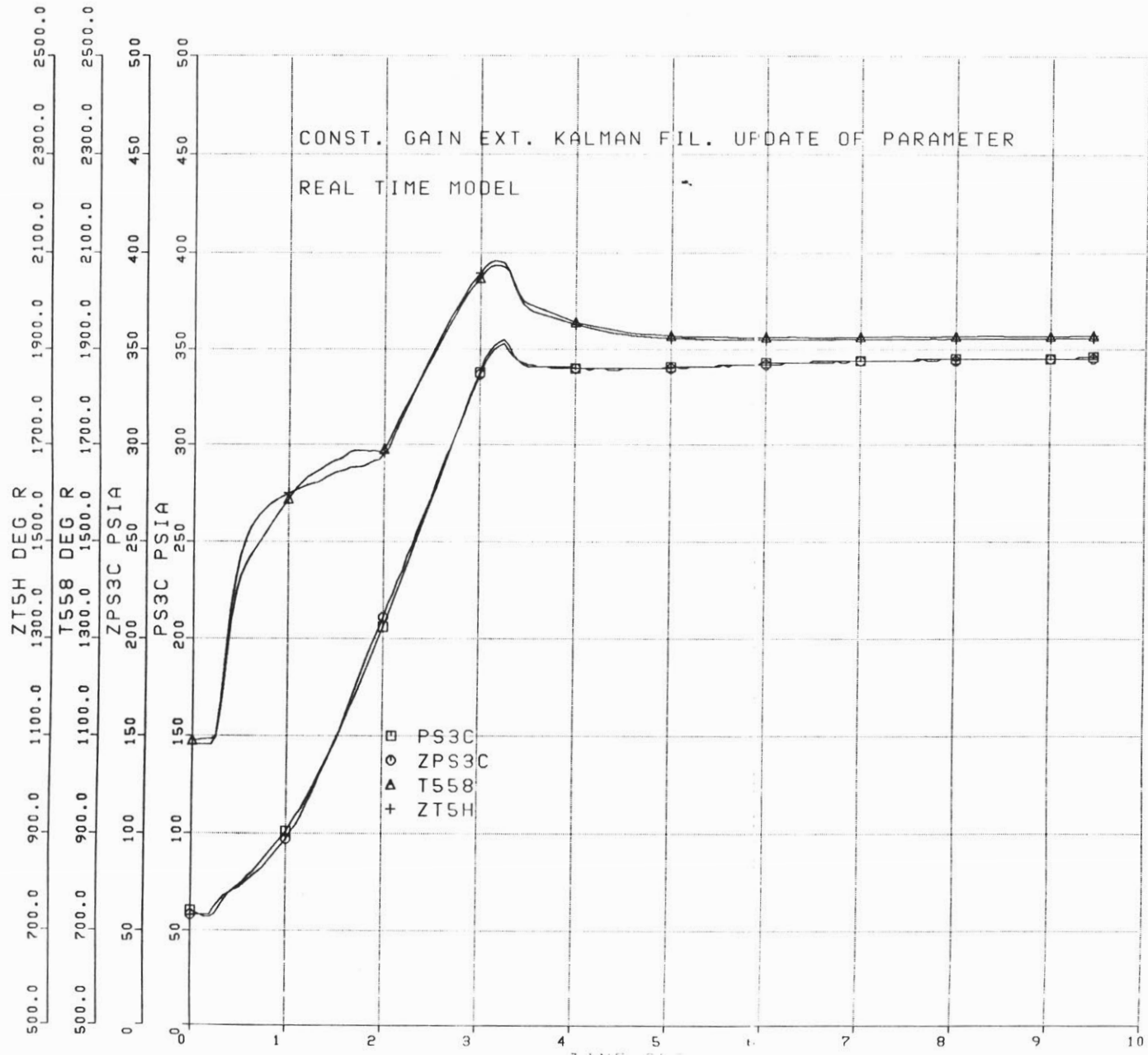
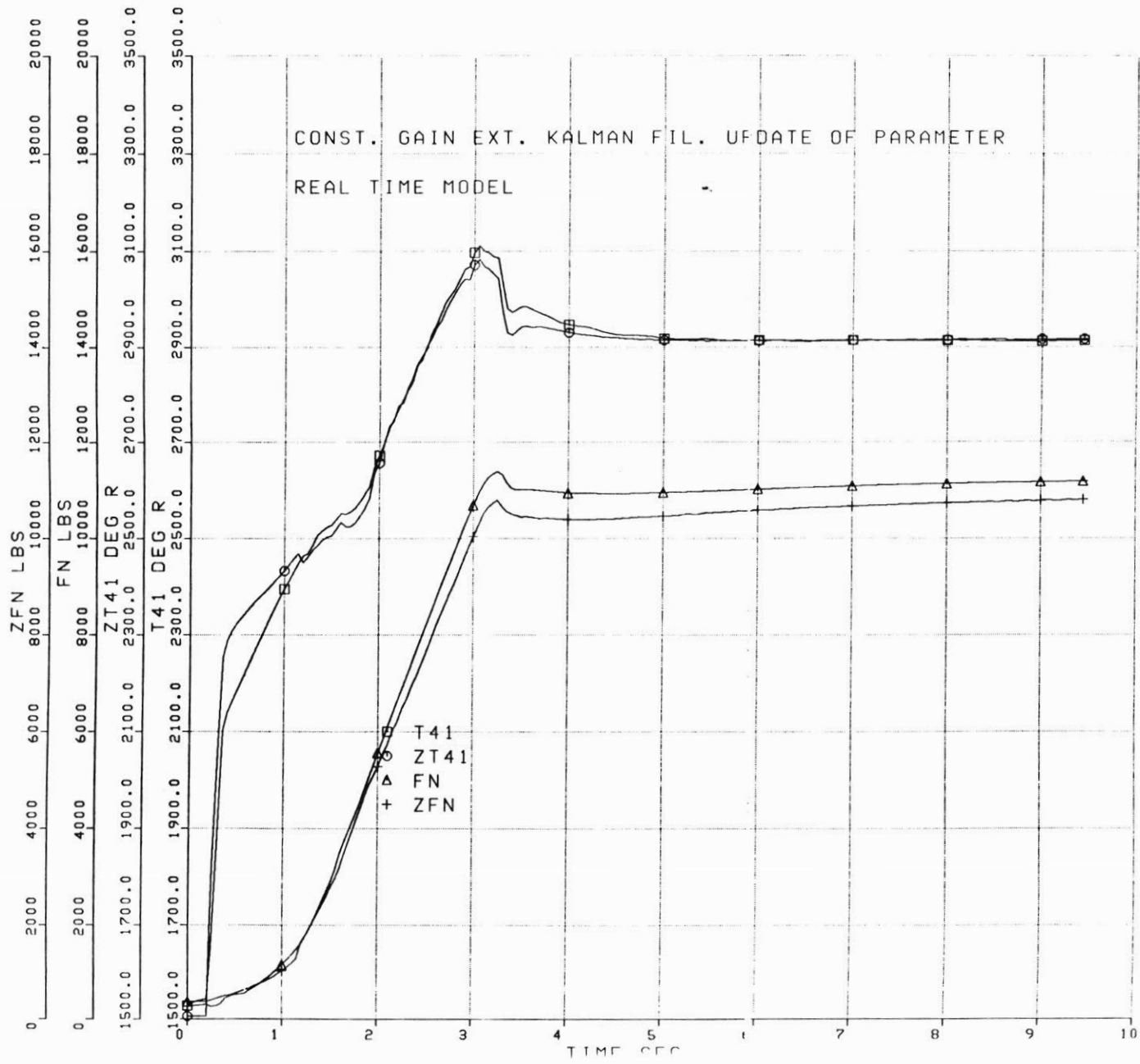


FIGURE 4.2-17



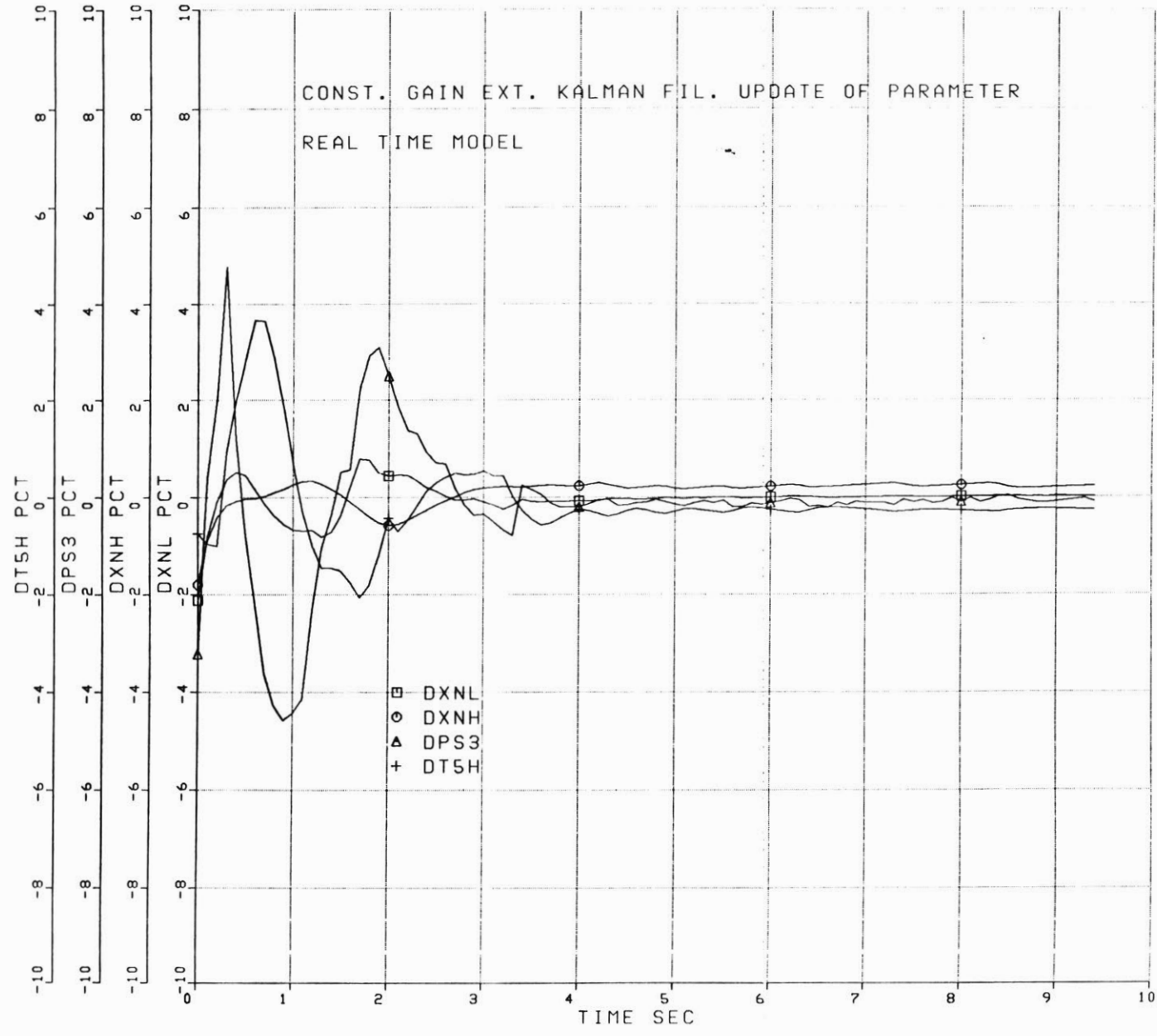


FIGURE 4.2-18

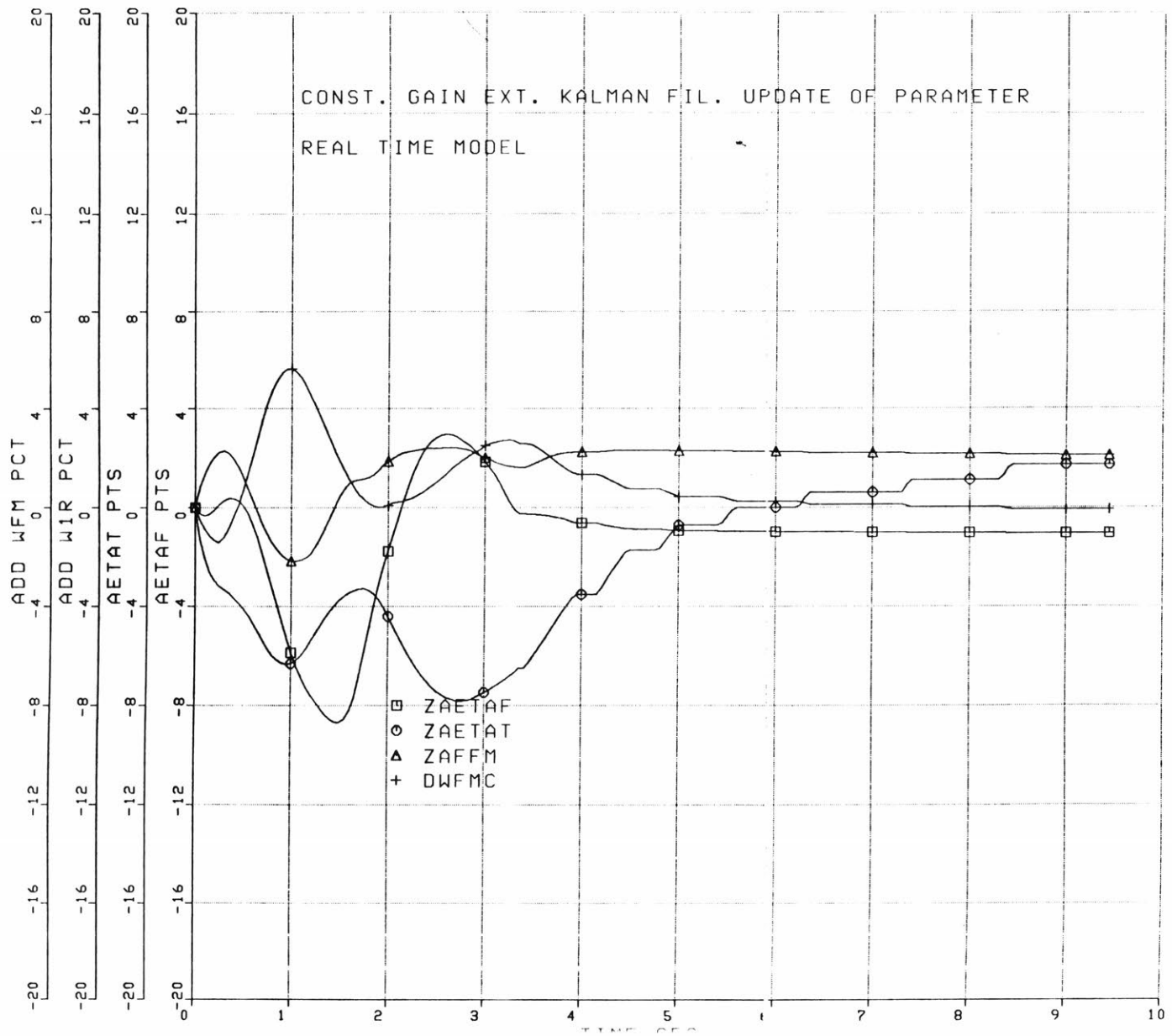


FIGURE 4.2-19

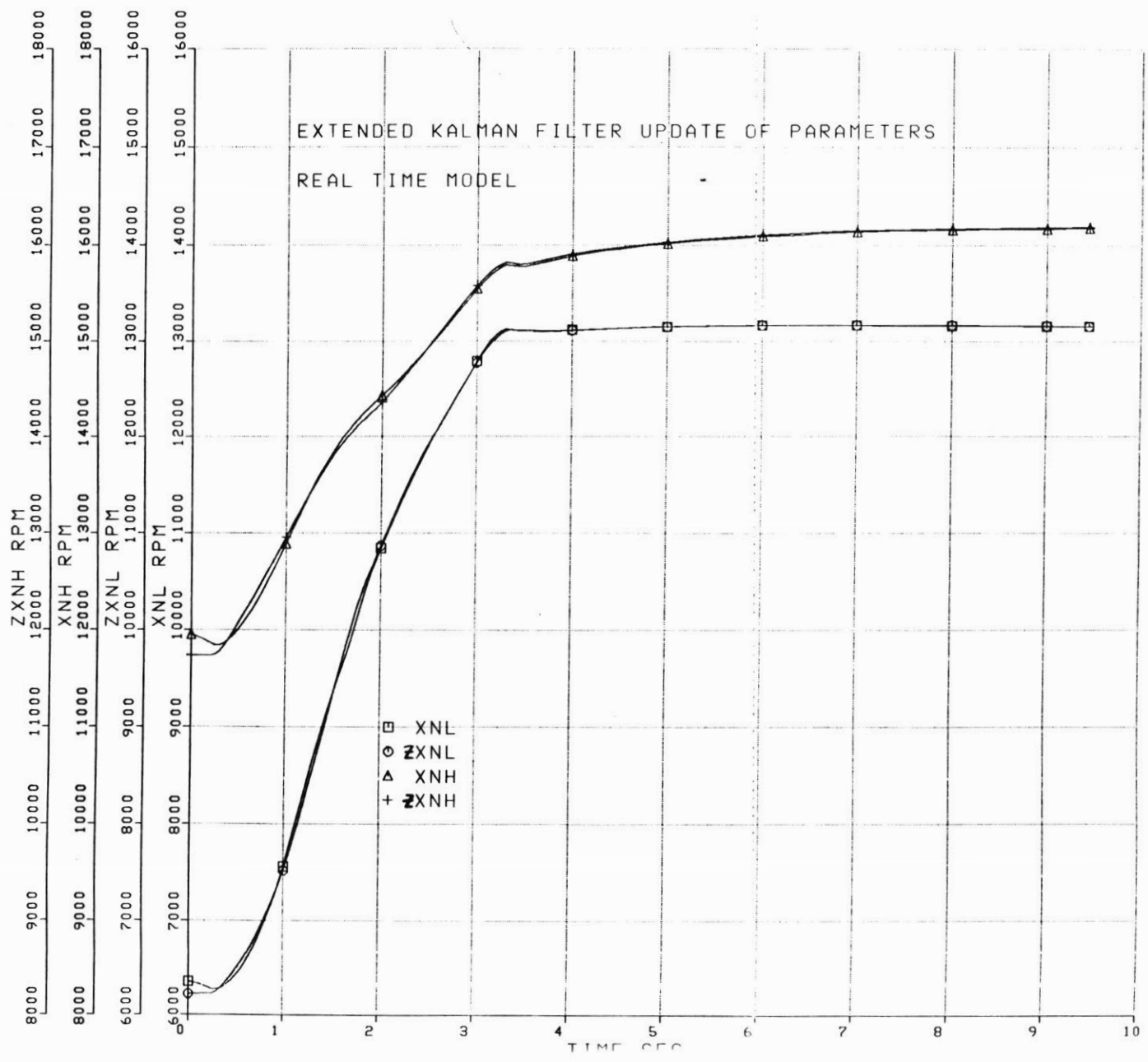


FIGURE 4.2-20

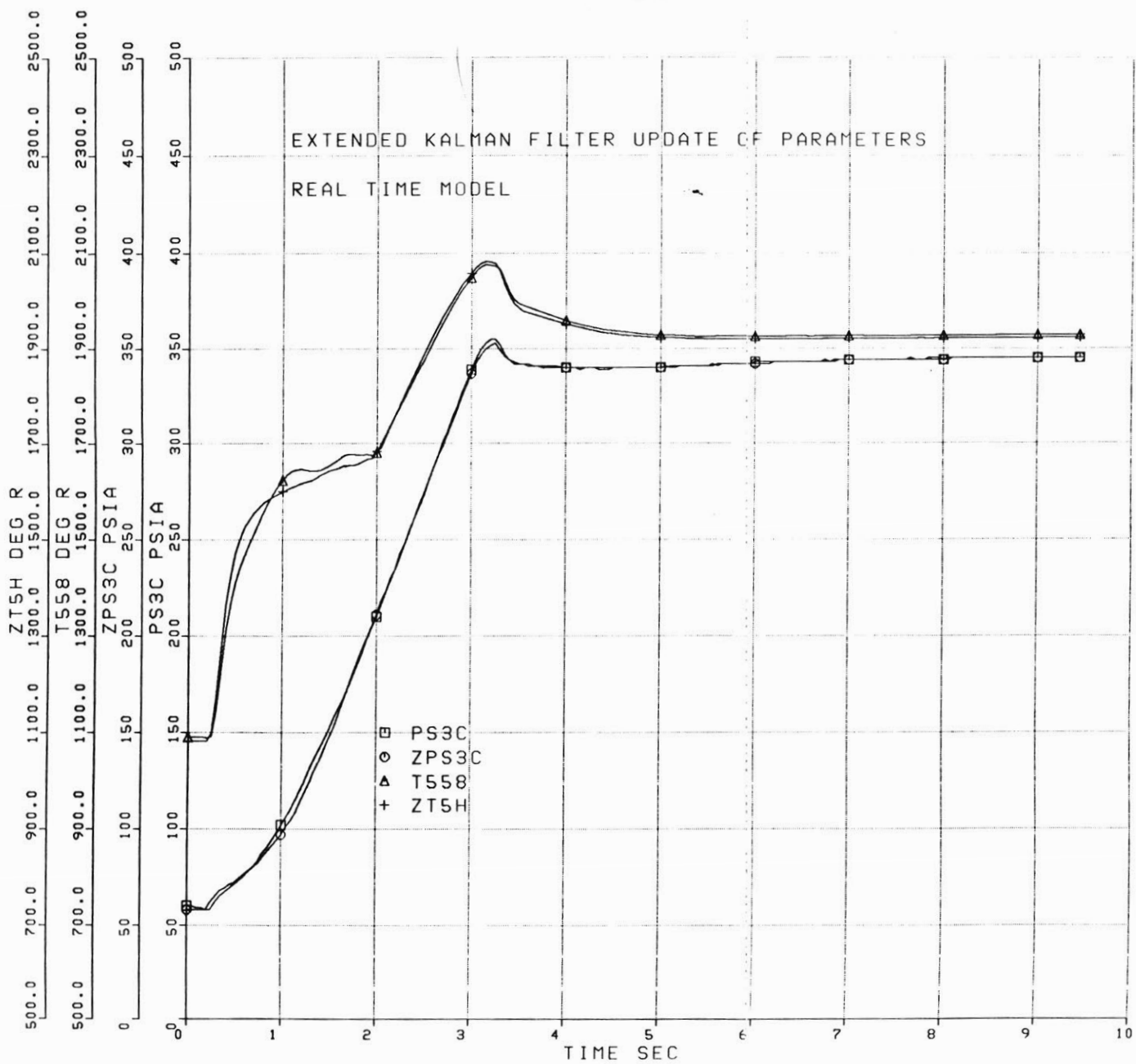


FIGURE 4.2-21

211

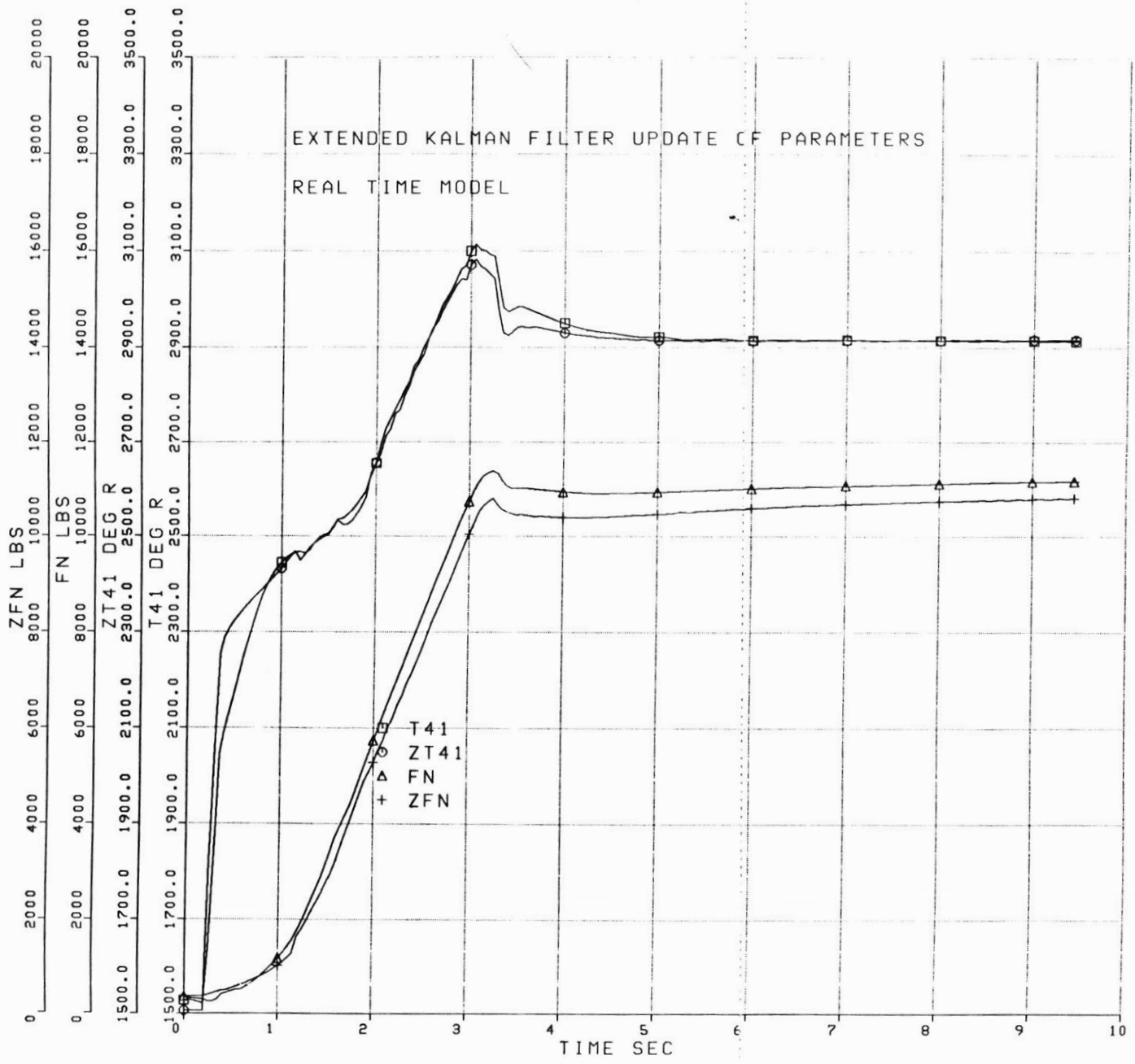


FIGURE 4.2-22

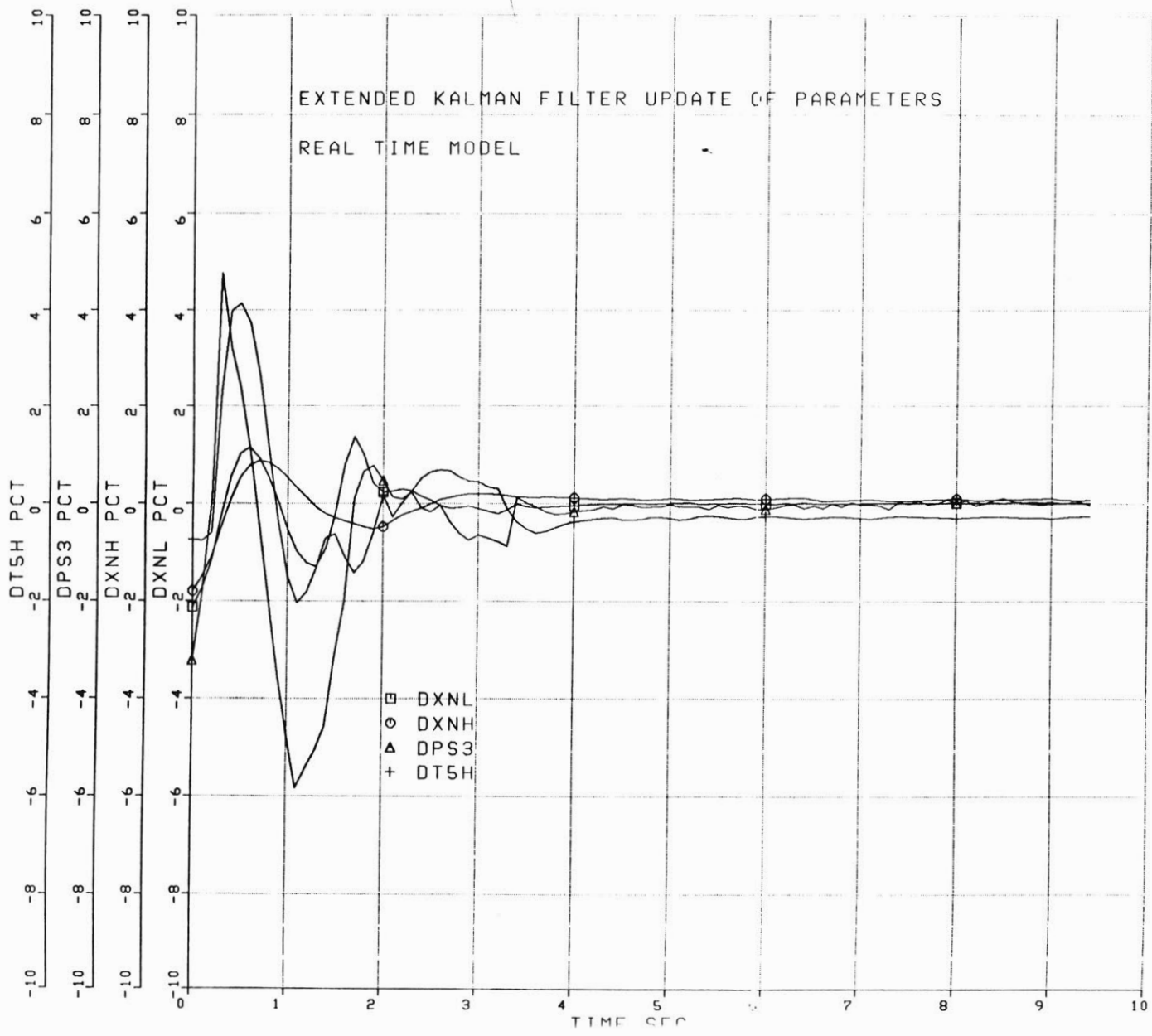


FIGURE 4.2-23

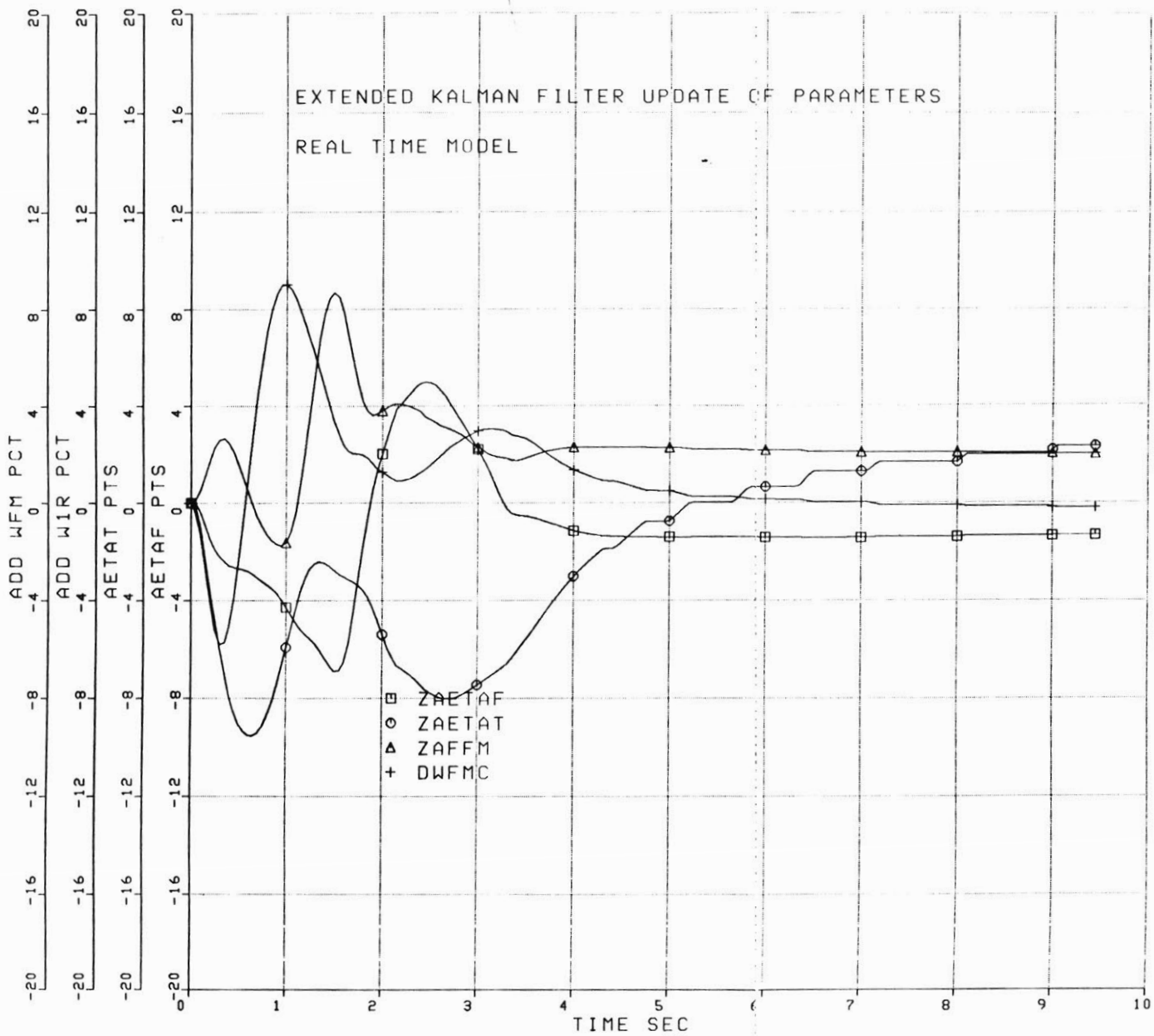


FIGURE 4.2-24

SUMMARY OF UPDATE METHODS' ERRORS

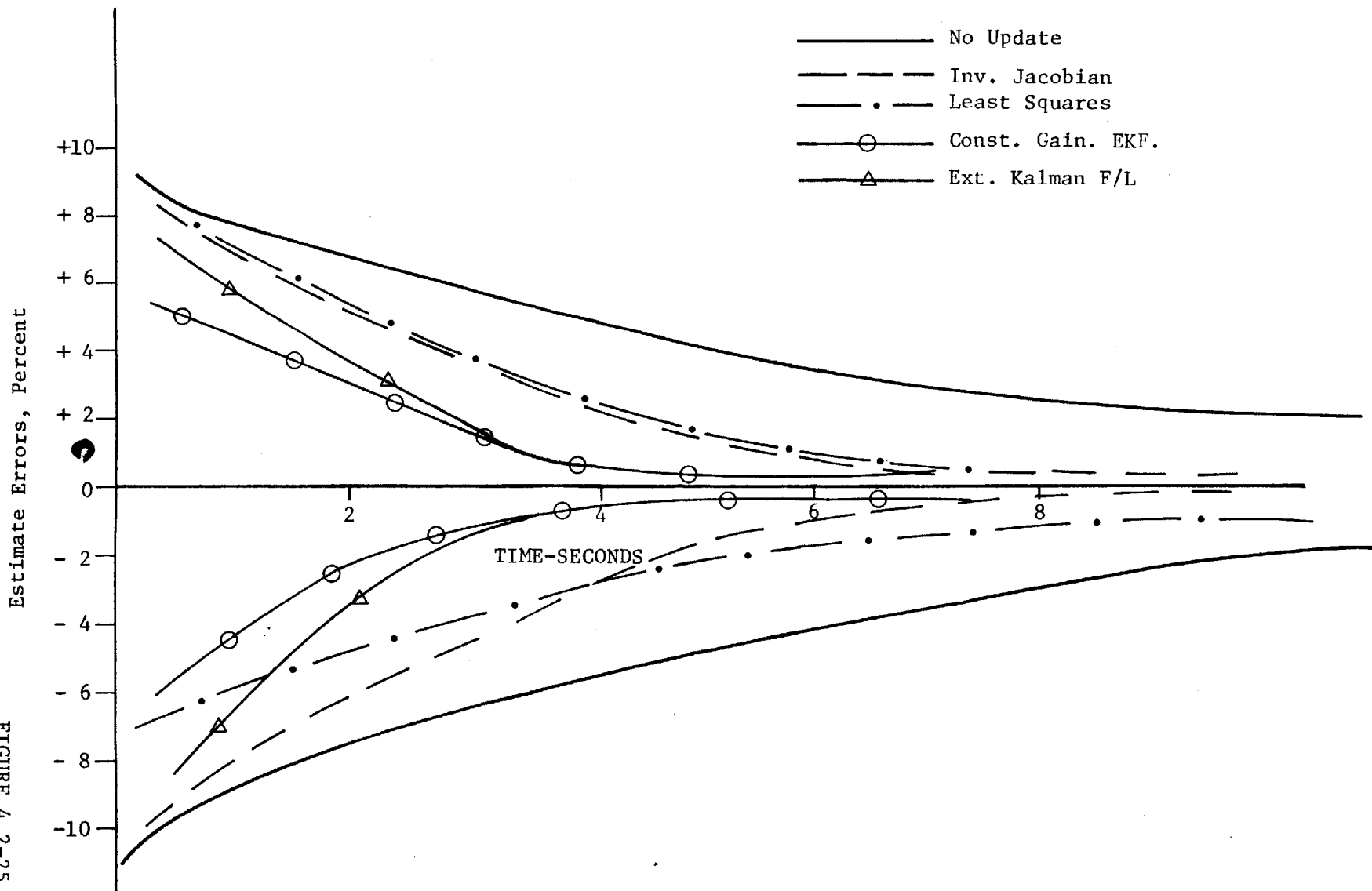


FIGURE 4.2-25

5. PROCESSOR REQUIREMENTS

This subject has been ignored through the preceding analysis. It is, however, a very important consideration in the design of the microcomputer based model. The update time of the numerical integrations is 10 milliseconds, and thus, all processing of the equation set must be completed in this time frame. In light of this requirement, the various update schemes are analyzed for processor time on a reference computer, and then the results are extrapolated for the real-world issues of the engine mounted controller.

5.1 Required Processor Time-Current Computer

The computer used to analyze processing time on a relative basis is the Honeywell model H600 computer. This is a very large scale machine, and as such, is not representative of current microcomputer technology. It has been in use at the General Electric Company in Lynn for the past five years to handle most computer processing tasks. Although not a micro, it serves as a basis for comparison between the four update schemes.

The ten second transients discussed in Chapter 4 are the foundation for analyzing processor time per time step in the real time model. The processor clock was started after the model had initialized at time zero, so as to give a good indication of transient processor time. The results are shown in Table 5.1.

TABLE 5.5-1 PROCESSOR TIME

<u>Method</u>	<u>P-Time per Update (MS)</u>
Base	7.83
Inverse Jacobian	8.41
Least Squares	11.55
Const. Gain EKF	8.83
Ext. Kalman Filter	19.91

The base case is for the real time model running an update. It does run in real time! The burden added by the update (approximately 25 mathematical operations) using the inverse Jacobian uses an additional 0.6 milliseconds (8%) per update. The recursive least squares derived gain adds a significant computer burden due to the calculation of the gain matrix each time step. Processor time increases by 3.7 MS or 48%. The efficiency of the constant gain extended Kalman filter shows an increase of 1 MS per update or 13%. Finally, the extended Kalman filter more than doubles the processor time (12.1 MS added or 250%), due to updating the covariance equation.

These results, along with the numerical results from Chapter 4 indicate that the constant gain extended Kalman filter is the most likely choice for the update method. The added processor burden is small, and the accuracy during transients is nearly the best.

5.2 Practical Issues of the Embedded Model

A re-look at Table 5.1-1 reveals that an advance in microprocessors increasing speed by only 200% would allow the extended Kalman filter

algorithm to be programmed into the model. Unfortunately, the task is not so simple. Current technology does allow this capability (or shortly will) by the use of VHSIC technology and parallel processing. However, these prototype processors operate under well-controlled environmental conditions of temperature and vibration.

The demands placed upon an airframe and/or engine mounted processor are very strong. The machine must withstand engine bay temperatures from sub-freezing to tropical temperatures. The bay pressures can range from 1 PSI to over 15 PSI. The maneuver loads can be as high as nine G's. Plus there is a broad spectrum of vibrational characteristics. When compared to the serene environment of the ground based, air conditioned computer used to generate the results, the complexity of the task becomes obvious.

Further, the reliability requirements also impose a technology challenge. If the Honeywell computer on the ground "crashes," there is some inconvenience to the user. If the engine controller "crashes" the airplane may also. Of course, there will be a back-up system, but the processor circuitry must be highly reliable in order to limit the high cost of each failure.

Thus, in conclusion of this part of the analysis, the burden imposed by practical considerations of the physical environment and reliability constraints make the extended Kalman filter still years down the road, and therefore the constant gain version is the choice.

6. SUMMARY AND CONCLUSIONS

6.1 Summary

The results of this work show that an embedded real time jet engine model can be logically adapted to successfully track the engine outputs within the constraints of real time operation. Since the particular model is predominantly algebraic equations, it does not lend itself to traditional state space linear methods. The procedure used was to select component characteristics, and adjust them dynamically to account for modelling errors. This set a variables was found to consist of an adder to the implied fan efficiency, an adder to the implied fan speed-flow relationship, an adder to the high pressure turbine efficiency, and a bias the control fuel flow measurement. Other component efficiencies and flows were considered, but rejected based on the changes in these parameters to correct model errors.

Several methods were tried to perform the dynamic update of the variables. The selected method was to augment the two dynamic states (the rotor speeds) by creating an augmented state vector that included the parameters and forming the constant gain extended Kalman filter. It is so called because the evaluation set is non-linear, but the filter gains are precomputer.

The adaptation algorithm can be used to monitor the condition of the engine as run time accumulates. This is accomplished by storing a reference variable vector at a reference power condition, and studying the time history of the vector. This is made possible by the fact that the update

responds in a unique (and correct) direction for changes in the engine of those parameters in the model update vector.

The update provides a significant improvement in synthesizing important unmeasurable engine parameters. Of particular interest is turbine inlet temperature, T41. The potential for synthetic control is present in this case, where the engine is controlled to the output on the model rather than a sensed parameter.

6.2 Conclusions

Specific conclusions are listed below.

1. Modelling errors that result in output differences between the engine and the model are best corrected by updating component representations in the model in real time for models that are non-state space representations.
2. A vector of parameters consisting of fan efficiency, high pressure turbine efficiency, fan speed flow relationship and a fuel flow bias is the best set to change in order to eliminate modelling errors.
3. A constant gain extended Kalman filter, which includes the two model dynamic states, and uses the vector as augmented states is the best way to dynamically update the model in consideration of real time constraints.
4. The resulting algorithm can successfully track an analytical model of the dynamic engine system, and provide insight into engine component health.

6.3 Recommendations for Further Study

Several questions were suggested during the results section. These concerns are listed here. The first area of study is the uniqueness of the vector direction for certain engine variations and sensor errors. It has been established that for a fuel flow sensor error, the direction is unique--it changes the fuel flow bias only. It has also been established that the vector responds in the correct direction for fan and turbine efficiency and fan air flow. The question is whether the direction for the N_1 sensor failure or error is unique. This information would further enhance failure detection and health monitoring.

The above analysis further suggests the failure detection logic should be studied. A detailed study of all failures could be undertaken to establish threshold levels. Then, in the event of failure detection, is the filter workable without the feedback of the failed sensor. A simple way to address this would be to look at the closed loop filter with one column set to zero. This would result in the particular error of the failed sensor having no effect on the update.

Another potential area of study is to analyze the update using engine test data. This would complicate the update by introducing noisy sensors and real uncertainty on measured parameters. In addition, data from an endurance test would highlight the ability to monitor engine health.

Finally, an investigation into the synthetic control capability is warranted. It is guessed that the update introduces phase shift into the control loop due to the integration. If the update is occurring near the control loop frequency, poor control may result. This may force a faster or slower update relative to the control frequency response.

REFERENCES

1. Linebrink, K.L., and Vizzini, R.W., "Full Authority Digital Electronic Control (FADEC) - Augmented Fighter Engine Demonstration," SEA Paper 821371 Oct. 1982.
2. "Digital Electronic Engine Control (DEEC) Flight Evaluation on an F15 Airplane," NASA CP-2298, 1984.
3. Reukauf, P.J., and Burcham, F.W., "Propulsion System/Flight Control Integration for Supersonic Aircraft," NASA CP-001, 1976.
4. Merrill, W.C., "Sensor Failure Detection for Jet Engines Using Analytical Redundancy," NASA TM 83695, AIAA-84-1452, June 1984.
5. Wallhagen, R.E., and Arpasi, D.J., "Self Teaching Digital Computer for Fail-Operational Control of a Turbojet Engine in a Sea-Level Test Stand," NASA TM X-3043, 1974.
6. Hrach, F.J., Arpasi, D.J., and Bruton, W.M., "Design and Evaluation of a Sensor Fail-Operational Control System for a Digitally Controlled Turbojet Engine," NASA TM X-3260, 1975.
7. Sahgal, R.K., and Miller, R.J., "Failure Accommodation in Gas Turbine Engines with Application Fan Turbine Inlet Temperature Reconstruction," Proceedings of Joint Automatic Control Conference, Dencer, Co., June 17-21, 1979, pp. 381-386.
8. Spang, H.A., and Corbey, R.C., "Failure Detection and Correction for Turbofan Engines," Joint Automatic Control Conference, San Francisco, Ca., June 22-24, 1977.
9. French, M.W., "Development of a Compact Real-Time Turbofan Engine Dynamic Simulation," SAE paper 821401, Oct. 1982.
10. Pisano, A.D., "Failure Indication and Corrective Action for Turboshaft Engines," AHS paper HPS-16, Nov. 1979.
11. Williams, L.W., "Instruction Manual for Transient Computer Program 82086D" General Electric Co. Memo SCO 82086D, 1983.
12. Sofanov, M.G., and Athans, M., "Robustness and Computational Aspects of Non-Linear and Stochastic Estimators and Regulators," Proceedings of IEEE Conference Decision and Control, Dec. 7-9, 1977.
13. Gelb et al., Applied Optimal Estimation, MIT Press, 1974.

14. Landau, Y.D., Adaptive Control, The Model Reference Approach, Marcel Dekker, New York, 1979.
15. Stewart, G.W., Introduction to Matrix Computations, Academic Press, New York, 1977.
16. Doyle, J.C., and Stein, G., "Multivariable Feedback Design Concepts for a Classical/Modern Synthesis," IEEE trans. on automatic control, Apr. 1981.
17. Messerole, J.S., "Detection Filuters for Fault Tolerant Control of Turbofan Engines," Ph.D. Thesis, Massachusetts Institute of Technology, 1981.
18. Sage, A.P., Optimum Systems Control, Prentice Hall, N.J., 1968.
19. Kwakernaak, H., and Sivan, R., Linear Optimal Control Systems, Wiley, New York, 1972.

APPENDIX 1

The following information shows the detailed results from Section 3.1. The purpose is to determine how far various parameters must be changed in order to eliminate modelling errors. The truth model in this case is the full range complex reference engine simulation. For each of the sets in Table 3.1-2, the model tracks the engine outputs of N_1 , N_2 , PS3C, and T56 by varying the four (or three) selected parameters of the set. This is a static test, so the method used to update dynamically is of no consequence. The exploration of the flight envelope includes altitudes to 60,000 feet and flight mach numbers to 2.0. It covers two power settings: intermediate rated power (IRP) at a power lever angle (PLA) of 87° for maximum thrust non-afterburning and maximum afterburner at a PLA of 130° .

The twelve tabulations show individual parameter changes at each of the ten flight conditions for the two power settings. The headings are translated as summarized below.

ALT	Altitude in feet
XM	Flight mach number
PLA	Power lever angle - degrees
ZAETAF	Adder to implied model fan efficiency - points
ZAETAT	Adder to implied model high pressure turbine eff. - points
ZAFFM	Adder to implied mode fan speed-flow - percent
ZAFF41	Adder to turbine nozzle flow function - percent
DWFMC	Adder (bias) to main fuel flow - percent
DASC	Adder (bias) to exhaust nozzle area - percent

EFN	Error in calculated thrust - percent
ET41	Error in calculated T41 - °R
EPX3C	Error in calculated PS3C - PCT
ENH	Error in calculated core speed - PCT

For example, with set 1 at sea-level-static, IRP power setting, the modelling errors (relative to the truth model) are equivalent to -1.2 points in fan efficiency, +1.3 points in turbine efficiency, 2.6 percent in fan speed-flow, and 0.7% in turbine nozzle area.

The magnitude of the improvement in predicting non-measured parameters judges the "goodness" of the update vector set. The non-measured parameters for the 4 element vectors are T41 and net thrust, FN. The elimination of a variable allows a comparison of N₂ syhtnesis and PS3C synthesis for the 3 element sets. The improvements are detailed in the Table A-13. It shows the set numbers along with the average synthesis errors (X) and the standard deviation (o) around the errors for the 20 flight condition/power settings. Set #0 is the base model without parameter adjustments.

TABLE A-1

SET 1: W1R,ETA-F,ETA-T,FF41

ALT	XM	PLA	ZAETAF	ZAETAT	ZAFFM	ZAFF41	DWFMC	DABC	EFN	ET41	EPS3C	ENH
0.	0.	87.	-1.203	1.278	2.626	0.744	0.	0.	3.89	-8.	-0.00	-0.00
0.	1.1	87.	2.663	-0.864	0.428	-2.068	0.	0.	-2.76	19.	0.00	-0.00
10000.	1.4	87.	5.220	1.727	3.284	-0.428	0.	0.	-4.89	-24.	0.00	0.00
15000.	0.	87.	-2.360	-0.144	0.488	0.804	0.	0.	2.56	6.	0.00	0.00
35000.	0.8	87.	-2.219	-0.344	-0.695	1.058	0.	0.	0.05	8.	0.00	-0.00
35000.	1.2	87.	-1.027	0.955	0.842	0.933	0.	0.	1.48	-9.	-0.00	0.00
35000.	1.6	87.	-0.064	1.388	2.409	-0.555	0.	0.	2.13	-4.	-0.00	-0.00
35000.	2.0	87.	4.314	1.365	1.577	-1.095	0.	0.	14.89	-16.	0.00	-0.00
60000.	1.0	87.	-4.098	-3.779	0.179	-0.137	0.	0.	-0.65	23.	-0.00	0.00
60000.	2.0	87.	4.945	1.820	1.382	-0.129	0.	0.	18.77	-26.	-0.02	-0.00
0.	0.	130.	-1.544	1.055	3.396	0.459	0.	0.	5.14	-1.	-0.00	0.00
0.	1.1	130.	3.731	-0.250	3.477	-1.244	0.	0.	-3.79	4.	0.00	0.00
10000.	1.4	130.	4.163	0.693	3.891	-1.196	0.	0.	-4.08	-8.	0.00	0.00
15000.	0.	130.	-2.087	-0.442	1.177	0.622	0.	0.	2.98	9.	0.00	0.00
35000.	0.8	130.	-2.195	-0.761	0.129	0.766	0.	0.	-2.48	12.	0.00	0.00
35000.	1.2	130.	-1.183	0.770	1.591	0.754	0.	0.	-3.61	-3.	0.00	0.00
35000.	1.6	130.	-0.408	0.896	2.720	-0.909	0.	0.	-5.54	8.	-0.00	-0.00
35000.	2.0	130.	3.369	0.474	2.735	-1.662	0.	0.	-6.41	-4.	0.00	-0.00
60000.	1.0	130.	-3.904	-3.141	-0.910	0.440	0.	0.	0.86	14.	0.00	0.00
60000.	2.0	130.	4.042	0.812	2.002	-0.781	0.	0.	-2.31	-13.	-0.01	-0.00

117

TABLE A-2

SET 2: W1R,ETA-F,ETA-T,DELTA WF

ALT	XM	PLA	ZAETAF	ZAETAT	ZAFFM	ZAFF41	DWFMC	DA8C	EFN	ET41	EPS3C	ENH
0.	0.	87.	-1.547	0.814	2.032	0.	-0.68	0.	3.03	-7.	-0.00	-0.00
0.	1.1	87.	4.613	0.583	2.687	0.	1.57	0.	-0.20	9.	0.00	0.00
10000.	1.4	87.	5.568	1.979	3.698	0.	0.39	0.	-4.39	-24.	0.00	0.00
15000.	0.	87.	-2.739	-0.639	-0.164	0.	-0.73	0.	1.67	7.	0.00	0.00
35000.	0.8	87.	-2.707	-1.000	-1.535	0.	-0.94	0.	-1.09	9.	0.00	-0.00
35000.	1.2	87.	-1.424	0.370	0.130	0.	-0.85	0.	0.35	-8.	-0.00	-0.00
35000.	1.6	87.	0.201	1.712	2.840	0.	0.52	0.	2.97	-5.	-0.00	-0.00
35000.	2.0	87.	5.328	2.030	2.659	0.	0.98	0.	17.40	-18.	0.00	0.00
60000.	1.0	87.	-4.052	-3.705	0.303	0.	0.13	0.	-0.48	23.	0.01	0.01
60000.	2.0	87.	4.949	1.831	1.445	0.	0.32	0.	18.92	-24.	-0.02	-0.01
0.	0.	130.	-1.751	0.774	3.025	0.	-0.43	0.	4.61	-1.	-0.00	-0.00
0.	1.1	130.	4.844	0.523	4.805	0.	1.07	0.	-2.45	1.	0.00	0.00
10000.	1.4	130.	5.113	1.356	5.054	0.	1.15	0.	-2.87	-8.	0.00	0.00
15000.	0.	130.	-2.375	-0.820	0.677	0.	-0.57	0.	2.31	9.	0.00	0.00
35000.	0.8	130.	-2.567	-1.232	-0.500	0.	-0.68	0.	-3.23	13.	0.00	-0.00
35000.	1.2	130.	-1.494	0.306	1.010	0.	-0.69	0.	-4.37	-2.	0.00	0.00
35000.	1.6	130.	0.024	1.426	3.434	0.	0.85	0.	-4.52	7.	-0.00	-0.00
35000.	2.0	130.	4.885	1.395	4.422	0.	1.61	0.	-4.31	-5.	0.00	0.00
60000.	1.0	130.	-4.061	-3.398	-1.228	0.	-0.40	0.	0.43	14.	0.01	0.00
60000.	2.0	130.	4.710	1.240	2.748	0.	0.77	0.	-1.34	-14.	-0.01	-0.01

118

XEROX 9700 (300) PM (S)

TABLE A-3

SET 3: ETA-F,ETA-T,FF41,DELTA A8

ALT	XM	PLA	ZAETAF	ZAETAT	ZAFFM	ZAFF41	DWFMC	DA8C	EFN	ET41	EPS3C	ENH
0.	0.	87.	-0.360	2.773	0.	2.008	0.	-5.77	3.76	-32.	0.00	-0.00
0.	1.1	87.	2.659	-0.834	0.	-2.079	0.	-0.70	-2.84	19.	-0.00	0.00
10000.	1.4	87.	6.737	3.291	0.	0.396	0.	-8.27	-3.62	-41.	0.01	0.00
15000.	0.	87.	-2.320	0.055	0.	0.985	0.	-0.85	2.42	3.	0.02	-0.00
35000.	0.8	87.	-2.284	-0.672	0.	0.752	0.	1.33	0.12	13.	-0.01	0.00
35000.	1.2.	87.	-0.850	1.400	0.	1.307	0.	-1.79	1.76	-16.	-0.00	-0.00
35000.	1.6	87.	2.244	4.318	0.	1.552	0.	-9.10	8.37	-48.	-0.00	-0.00
35000.	2.0	87.	4.983	1.974	0.	-0.870	0.	-3.92	18.38	-22.	0.01	-0.00
60000.	1.0	87.	-4.069	-3.703	0.	-0.068	0.	-0.38	-0.61	21.	0.00	0.00
60000.	2.0	87.	5.082	2.324	0.	0.112	0.	-3.05	21.28	-24.	-0.13	0.05
0.	0.	130.	-0.311	2.977	0.	2.101	0.	-9.00	5.05	-33.	0.00	0.00
0.	1.1	130.	4.070	0.316	0.	-1.129	0.	-7.29	-4.69	0.	0.00	0.00
10000.	1.4	130.	6.914	3.439	0.	0.506	0.	-13.56	-3.25	-43.	0.01	0.00
15000.	0.	130.	-1.969	0.052	0.	1.064	0.	-2.49	2.55	1.	0.00	0.00
35000.	0.8	130.	-2.226	-0.756	0.	0.766	0.	-0.17	-2.57	12.	-0.01	0.00
35000.	1.2	130.	-0.791	1.596	0.	1.456	0.	-4.05	-3.64	-17.	0.00	-0.00
35000.	1.6	130.	2.330	4.362	0.	1.572	0.	-12.43	-1.45	-43.	-0.00	0.00
35000.	2.0	130.	5.239	2.142	0.	-0.769	0.	-9.43	-2.91	-23.	0.00	-0.00
60000.	1.0	130.	-4.040	-3.522	0.	0.104	0.	2.26	1.09	21.	0.00	-0.00
60000.	2.0	130.	5.246	2.175	0.	0.011	0.	-6.87	0.42	-26.	-0.07	0.03

611

XENIX 9700 (0000) PM (00)

TABLE A-5

SET 5: W1R,ETA-F,ETA-T

ALT	XM	PLA	ZAETAF	ZAETAT	ZAFFM	ZAFF41	DWFMC	DABC	EFN	ET41	EPS3C	ENH
0.	0.	87.	-1.085	0.811	2.651	0.	0.	0.	3.94	-7.	0.68	-0.00
0.	1.1	87.	2.798	0.587	0.851	0.	0.	0.	-2.25	9.	-1.55	0.00
10000.	1.4	87.	5.162	1.980	3.270	0.	0.	0.	-4.91	-24.	-0.39	0.00
15000.	0.	87.	-2.250	-0.644	0.505	0.	0.	0.	2.59	7.	0.73	0.00
35000.	0.8	87.	-2.078	-1.006	-0.678	0.	0.	0.	0.08	9.	0.96	-0.00
35000.	1.2	87.	-0.884	0.364	0.865	0.	0.	0.	1.52	-8.	0.84	0.00
35000.	1.6	87.	-0.134	1.716	2.390	0.	0.	0.	2.08	-5.	-0.52	-0.00
35000.	2.0	87.	4.214	2.031	1.586	0.	0.	0.	14.93	-18.	-0.97	-0.00
60000.	1.0	87.	-4.126	-3.700	0.179	0.	0.	0.	-0.65	23.	-0.12	0.00
60000.	2.0	87.	4.865	1.881	1.327	0.	0.	0.	18.80	-26.	-0.11	-0.00
0.	0.	130.	-1.467	0.770	3.414	0.	0.	0.	5.17	-1.	0.42	0.00
0.	1.1	130.	3.646	0.530	3.556	0.	0.	0.	-3.71	1.	-1.05	0.00
10000.	1.4	130.	3.950	1.368	3.810	0.	0.	0.	-4.17	-9.	-1.13	0.00
15000.	0.	130.	-1.998	-0.825	1.190	0.	0.	0.	3.01	10.	0.57	0.00
35000.	0.8	130.	-2.088	-1.237	0.140	0.	0.	0.	-2.45	13.	0.70	0.00
35000.	1.2	130.	-1.062	0.299	1.611	0.	0.	0.	-3.57	-2.	0.68	0.00
35000.	1.6	130.	-0.520	1.435	2.700	0.	0.	0.	-5.59	7.	-0.84	-0.00
35000.	2.0	130.	3.081	1.415	2.629	0.	0.	0.	-6.54	-5.	-1.56	-0.00
60000.	1.0	130.	-3.818	-3.403	-0.896	0.	0.	0.	0.90	14.	0.40	0.00
60000.	2.0	130.	3.900	1.261	1.954	0.	0.	0.	-2.38	-14.	-0.72	0.00

121

TABLE A-6

SET 6: W1R,ETA-T,DELTA WF

ALT	XM	PLA	ZAETAF	ZAETAT	ZAFFM	ZAFF41	DWFMC	DABC	EFN	ET41	EPS3C	ENH
0.	0.	87.	0.	0.805	4.086	0.	1.54	0.	5.99	-7.	2.23	-0.00
0.	1.1	87.	0.	0.597	-2.001	0.	-2.56	0.	-5.58	9.	-4.07	0.00
10000.	1.4	87.	0.	2.044	-2.330	0.	-5.58	0.	-11.92	-26.	-5.88	0.00
15000.	0.	87.	0.	-0.668	3.546	0.	3.21	0.	6.64	8.	3.92	0.00
35000.	0.8	87.	0.	-1.042	2.133	0.	3.07	0.	3.81	10.	3.97	0.00
35000.	1.2	87.	0.	0.359	2.049	0.	1.33	0.	3.39	-8.	2.19	-0.00
35000.	1.6	87.	0.	1.715	2.569	0.	0.20	0.	2.45	-5.	-0.31	-0.00
35000.	2.0	87.	0.	2.050	-2.538	0.	-3.99	0.	5.44	-18.	-4.90	-0.00
60000.	1.0	87.	0.	-3.782	5.950	0.	6.39	0.	7.44	23.	6.22	0.00
60000.	2.0	87.	0.	1.810	-3.337	0.	-4.16	0.	7.24	-22.	-4.67	0.00
0.	0.	130.	0.	0.756	5.395	0.	2.11	0.	8.00	-0.	2.53	-0.00
0.	1.1	130.	0.	0.563	-0.292	0.	-3.46	0.	-7.80	0.	-4.47	0.00
10000.	1.4	130.	0.	1.426	-0.521	0.	-4.25	0.	-8.92	-10.	-5.28	0.00
15000.	0.	130.	0.	-0.848	3.881	0.	2.87	0.	6.58	10.	3.43	0.00
35000.	0.8	130.	0.	-1.273	2.908	0.	2.94	0.	0.82	13.	3.59	0.00
35000.	1.2	130.	0.	0.290	3.051	0.	1.61	0.	-1.64	-2.	2.32	-0.00
35000.	1.6	130.	0.	1.427	3.401	0.	0.81	0.	-4.57	7.	-0.03	-0.00
35000.	2.0	130.	0.	1.451	-0.472	0.	-2.90	0.	-10.45	-6.	-4.38	-0.00
60000.	1.0	130.	0.	-3.489	4.319	0.	5.85	0.	7.83	15.	6.26	0.00
60000.	2.0	130.	0.	1.275	-1.919	0.	-3.49	0.	-7.84	-14.	-4.39	0.00

122

TABLE A-7

SET 7: DELTA A8,ETA-F,ETA-T

ALT	XM	PLA	ZAETAF	ZAETAT	ZAFFM	ZAFF41	DWFMC	DA8C	EFN	ET41	EPS3C	ENH
0.	0.	87.	-0.139	1.434	0.	0.	0.	-5.72	3.75	-28.	1.74	-0.00
0.	1.1	87.	2.863	0.705	0.	0.	0.	-1.50	-2.35	9.	-1.52	0.00
10000.	1.4	87.	6.710	3.010	0.	0.	0.	-8.17	-3.68	-40.	0.32	0.00
15000.	0.	87.	-2.189	-0.560	0.	0.	0.	-0.87	2.45	4.	0.91	-0.00
35000.	0.8	87.	-2.171	-1.133	0.	0.	0.	1.30	0.19	13.	0.72	0.00
35000.	1.2	87.	-0.654	0.567	0.	0.	0.	-1.84	1.80	-14.	1.18	0.00
35000.	1.6	87.	2.418	3.376	0.	0.	0.	-9.19	8.54	-46.	1.45	-0.00
35000.	2.0	87.	4.980	2.557	0.	0.	0.	-4.07	18.73	-24.	-0.70	-0.00
60000.	1.0	87.	-4.086	-3.664	0.	0.	0.	-0.38	-0.63	21.	-0.06	0.00
60000.	2.0	87.	5.793	2.405	0.	0.	0.	-3.85	22.53	-32.	0.16	0.02
0.	0.	130.	-0.079	1.573	0.	0.	0.	-8.91	5.04	-29.	1.82	0.00
0.	1.1	130.	4.177	1.148	0.	0.	0.	-7.75	-4.52	-5.	-0.83	0.00
10000.	1.4	130.	6.873	3.076	0.	0.	0.	-13.41	-3.31	-41.	0.40	0.00
15000.	0.	130.	-1.831	-0.612	0.	0.	0.	-2.51	2.58	2.	0.97	0.00
35000.	0.8	130.	-2.114	-1.230	0.	0.	0.	-0.20	-2.53	12.	0.72	0.00
35000.	1.2	130.	-0.568	0.670	0.	0.	0.	-4.10	-3.59	-15.	1.31	0.00
35000.	1.6	130.	2.519	3.416	0.	0.	0.	-12.55	-1.32	-42.	1.47	0.00
35000.	2.0	130.	5.237	2.658	0.	0.	0.	-9.58	-2.78	-25.	-0.63	-0.00
60000.	1.0	130.	-4.021	-3.584	0.	0.	0.	2.26	1.09	21.	0.09	0.00
60000.	2.0	130.	5.539	2.235	0.	0.	0.	-7.32	0.71	-29.	-0.02	0.02

123

TABLE A-8

SET 8: ETA-T,DELTA A8,DELTA WF

ALT	XM	PLA	ZAETAF	ZAETAT	ZAFFM	ZAFF41	DWFMC	DA8C	EFN	ET41	EPS3C	ENH
0.	0.	87.	0.	1.454	0.	0.	0.18	-5.99	3.92	-29.	1.96	-0.00
0.	1.1	87.	0.	0.317	0.	0.	-2.38	3.44	-5.22	11.	-3.97	0.00
10000.	1.4	87.	0.	1.227	0.	0.	-3.85	4.16	-11.30	-6.	-5.09	0.00
15000.	0.	87.	0.	-0.222	0.	0.	2.87	-5.36	4.79	-5.	4.46	0.00
35000.	0.8	87.	0.	-0.749	0.	0.	2.83	-3.28	3.06	2.	4.36	-0.00
35000.	1.2	87.	0.	0.726	0.	0.	0.75	-3.20	3.08	-19.	2.22	-0.00
35000.	1.6	87.	0.	2.506	0.	0.	-1.68	-4.28	2.02	-24.	-1.30	-0.00
35000.	2.0	87.	0.	1.263	0.	0.	-2.53	4.74	4.06	-4.	-4.18	-0.00
60000.	1.0	87.	0.	-2.917	0.	0.	5.31	-8.92	5.77	-5.	6.67	0.00
60000.	2.0	87.	0.	0.650	0.	0.	-2.01	6.30	6.03	5.	-3.54	0.01
0.	0.	130.	0.	1.584	0.	0.	0.10	-9.10	5.14	-30.	1.95	-0.00
0.	1.1	130.	0.	0.512	0.	0.	-3.40	0.60	-7.71	1.	-4.43	0.00
10000.	1.4	130.	0.	1.243	0.	0.	-3.85	1.07	-8.71	-5.	-5.10	0.00
15000.	0.	130.	0.	-0.333	0.	0.	2.37	-6.34	4.32	-6.	3.92	0.00
35000.	0.8	130.	0.	-0.903	0.	0.	2.78	-4.73	-0.79	4.	4.23	0.01
35000.	1.2	130.	0.	0.806	0.	0.	0.64	-5.45	-2.84	-20.	2.21	0.00
35000.	1.6	130.	0.	2.511	0.	0.	-1.74	-6.51	-5.64	-19.	-1.37	-0.00
35000.	2.0	130.	0.	1.276	0.	0.	-2.55	0.95	-10.50	-2.	-4.25	-0.00
60000.	1.0	130.	0.	-3.039	0.	0.	4.80	-7.00	5.49	-5.	6.21	0.00
60000.	2.0	130.	0.	0.496	0.	0.	-1.95	3.80	-7.61	8.	-3.63	0.01

124

TABLE A-9

SET 9: W1R,FF41,ETA-T

ALT	XM	PLA	ZAETAF	ZAETAT	ZAFFM	ZAFF41	DWFMC	DA8C	EFN	ET41	EPS3C	ENH
0.	0.	87.	0.	0.311	2.735	0.504	0.	0.	4.13	-10.	0.00	-0.59
0.	1.1	87.	0.	1.280	0.329	-1.211	0.	0.	-2.45	15.	-0.00	0.69
10000.	1.4	87.	0.	5.109	2.582	0.444	0.	0.	-5.11	-15.	0.00	1.27
15000.	0.	87.	0.	-1.930	0.779	0.345	0.	0.	3.10	1.	0.00	-1.19
35000.	0.8	87.	0.	-1.930	-0.365	0.675	0.	0.	0.45	1.	0.02	-1.00
35000.	1.2	87.	0.	0.098	0.929	0.726	0.	0.	1.63	-11.	0.00	-0.69
35000.	1.6	87.	0.	1.339	2.411	-0.567	0.	0.	2.14	-4.	-0.00	-0.02
35000.	2.0	87.	0.	4.406	1.245	-0.041	0.	0.	15.15	-14.	-0.00	1.03
60000.	1.0	87.	0.	-6.674	0.586	-0.799	0.	0.	0.06	14.	0.01	-1.50
60000.	2.0	87.	0.	5.486	1.160	1.226	0.	0.	19.40	-29.	-0.00	1.28
0.	0.	130.	0.	-0.142	3.490	0.175	0.	0.	5.53	-4.	0.00	-0.62
0.	1.1	130.	0.	2.435	3.260	-0.302	0.	0.	-3.99	4.	0.00	0.93
10000.	1.4	130.	0.	3.200	3.367	-0.578	0.	0.	-4.70	-0.	0.00	0.99
15000.	0.	130.	0.	-1.979	1.356	0.254	0.	0.	3.54	4.	0.00	-1.09
35000.	0.8	130.	0.	-2.322	0.375	0.399	0.	0.	-1.95	5.	0.01	-1.07
35000.	1.2	130.	0.	-0.163	1.655	0.540	0.	0.	-3.35	-5.	0.00	-0.79
35000.	1.6	130.	0.	0.591	2.734	-0.979	0.	0.	-5.46	7.	0.00	-0.13
35000.	2.0	130.	0.	2.238	2.213	-1.220	0.	0.	-7.05	2.	-0.00	0.71
60000.	1.0	130.	0.	-5.821	-0.601	-0.133	0.	0.	1.87	4.	0.01	-1.29
60000.	2.0	130.	0.	2.656	1.333	-0.410	0.	0.	-2.97	-8.	-0.03	0.89

125

TABLE A-10

SET 10: W1R,ETA-T,DELTA WF

ALT	XM	PLA	ZAETAF	ZAETAT	ZAFFM	ZAFF41	DWFMC	DABC	EFN	ET41	EPS3C	ENH
0.	0.	87.	0.	-0.141	2.382	0.	-0.42	0.	3.64	-10.	0.00	-0.67
0.	1.1	87.	0.	2.656	1.281	0.	0.71	0.	-1.20	10.	-0.00	0.92
10000.	1.4	87.	0.	4.673	2.264	0.	-0.37	0.	-5.55	-15.	0.00	1.20
15000.	0.	87.	0.	-2.235	0.534	0.	-0.29	0.	2.78	1.	0.00	-1.28
35000.	0.8	87.	0.	-2.548	-0.849	0.	-0.51	0.	-0.13	2.	0.00	-1.21
35000.	1.2	87.	0.	-0.545	0.438	0.	-0.61	0.	0.85	-11.	0.00	-0.87
35000.	1.6	87.	0.	1.841	2.804	0.	0.49	0.	2.90	-4.	-0.00	0.06
35000.	2.0	87.	0.	4.453	1.275	0.	0.02	0.	15.21	-14.	0.00	1.03
60000.	1.0	87.	0.	-6.079	1.149	0.	0.71	0.	0.84	14.	0.00	-1.39
60000.	2.0	87.	0.	3.942	0.215	0.	-0.37	0.	16.70	-19.	-0.05	0.97
0.	0.	130.	0.	-0.294	3.363	0.	-0.15	0.	5.36	-4.	0.00	-0.65
0.	1.1	130.	0.	2.754	3.503	0.	0.21	0.	-3.74	3.	0.00	0.99
10000.	1.4	130.	0.	3.745	3.803	0.	0.49	0.	-4.24	0.	0.00	1.09
15000.	0.	130.	0.	-2.202	1.172	0.	-0.21	0.	3.32	4.	0.00	-1.16
35000.	0.8	130.	0.	-2.682	0.072	0.	-0.29	0.	-2.27	6.	0.00	-1.21
35000.	1.2	130.	0.	-0.633	1.277	0.	-0.46	0.	-3.82	-6.	0.00	-0.91
35000.	1.6	130.	0.	1.441	3.430	0.	0.85	0.	-4.53	7.	-0.00	0.01
35000.	2.0	130.	0.	3.379	3.135	0.	1.04	0.	-5.86	3.	-0.00	0.92
60000.	1.0	130.	0.	-5.730	-0.509	0.	0.13	0.	1.98	4.	0.00	-1.27
60000.	2.0	130.	0.	3.026	1.564	0.	0.43	0.	-2.98	-5.	-0.03	0.90

126

TABLE A-11

SET 11: FF41,ETA-T,DELTA AB

ALT	XM	PLA	ZAETAF	ZAETAT	ZAFFM	ZAFF41	DWFMC	DA8C	EFN	ET41	EPS3C	ENH
0.	0.	87.	0.	2.429	0.	1.902	0.	-5.79	3.80	-32.	0.00	-0.24
0.	1.1	87.	0.	1.321	0.	-1.207	0.	-0.55	-2.49	15.	-0.00	0.70
10000.	1.4	87.	0.	9.597	0.	2.691	0.	-8.25	-2.68	-43.	-0.01	1.89
15000.	0.	87.	0.	-1.603	0.	0.623	0.	-1.41	2.83	-3.	-0.00	-1.20
35000.	0.8	87.	0.	-2.390	0.	0.361	0.	0.88	0.36	4.	-0.01	-1.02
35000.	1.2	87.	0.	0.739	0.	1.171	0.	-1.95	1.92	-18.	0.00	-0.56
35000.	1.6	87.	0.	6.135	0.	1.964	0.	-8.82	7.89	-42.	-0.00	0.70
35000.	2.0	87.	0.	5.876	0.	0.619	0.	-3.59	18.91	-23.	-0.01	1.24
60000.	1.0	87.	0.	-6.286	0.	-0.513	0.	-1.28	0.14	9.	0.02	-1.45
60000.	2.0	87.	0.	3.962	0.	0.050	0.	-0.25	17.50	-7.	-0.02	0.86
0.	0.	130.	0.	2.683	0.	2.011	0.	-9.00	5.09	-33.	0.00	-0.21
0.	1.1	130.	0.	3.754	0.	0.227	0.	-7.36	-4.66	-4.	0.00	1.09
10000.	1.4	130.	0.	9.790	0.	2.802	0.	-13.82	-3.30	-44.	-0.00	1.93
15000.	0.	130.	0.	-1.357	0.	0.767	0.	-2.84	2.99	-5.	-0.00	-1.08
35000.	0.8	130.	0.	-2.564	0.	0.281	0.	-0.41	-2.24	5.	-0.04	-1.16
35000.	1.2	130.	0.	0.984	0.	1.324	0.	-4.16	-3.47	-18.	0.00	-0.53
35000.	1.6	130.	0.	6.246	0.	2.003	0.	-12.24	-2.01	-37.	-0.00	0.72
35000.	2.0	130.	0.	6.090	0.	0.712	0.	-9.14	-3.17	-23.	-0.01	1.28
60000.	1.0	130.	0.	-6.069	0.	-0.323	0.	1.43	2.06	8.	0.02	-1.32
60000.	2.0	130.	0.	5.611	0.	1.119	0.	-5.85	-0.59	-20.	-0.03	1.19

127

TABLE A-12

SET 12: ETA-T,DELTA WF,DELTA A8

ALT	XM	PLA	ZAETAF	ZAETAT	ZAFFM	ZAFF41	DWFMC	DA8C	EFN	ET41	EPS3C	ENH
0.	0.	87.	0.	0.428	0.	0.	-1.19	-3.86	2.62	-25.	0.00	-0.61
0.	1.1	87.	0.	2.831	0.	0.	0.65	-2.10	-1.44	9.	-0.00	0.93
10000.	1.4	87.	0.	5.825	0.	0.	-1.34	-4.70	-5.40	-31.	0.00	1.34
15000.	0.	87.	0.	-2.187	0.	0.	-0.41	-0.78	2.50	-1.	0.00	-1.32
35000.	0.8	87.	0.	-2.614	0.	0.	-0.29	1.24	0.22	6.	0.00	-1.12
35000.	1.2	87.	0.	-0.457	0.	0.	-0.74	-0.71	0.78	-14.	0.00	-0.86
35000.	1.6	87.	0.	3.562	0.	0.	-0.98	-6.28	4.46	-30.	-0.00	0.31
35000.	2.0	87.	0.	4.985	0.	0.	-0.28	-2.68	17.07	-19.	-0.00	1.10
60000.	1.0	87.	0.	-5.863	0.	0.	0.39	-1.86	0.53	7.	0.00	-1.38
60000.	2.0	87.	0.	4.045	0.	0.	-0.44	-0.48	17.01	-21.	-0.05	0.99
0.	0.	130.	0.	0.559	0.	0.	-1.24	-6.54	3.94	-26.	0.00	-0.57
0.	1.1	130.	0.	3.465	0.	0.	-0.13	-7.02	-4.79	-3.	0.00	1.05
10000.	1.4	130.	0.	5.873	0.	0.	-1.40	-9.59	-4.99	-32.	0.00	1.35
15000.	0.	130.	0.	-2.080	0.	0.	-0.50	-2.00	2.65	-2.	0.00	-1.23
35000.	0.8	130.	0.	-2.677	0.	0.	-0.31	-0.12	-2.31	5.	0.00	-1.21
35000.	1.2	130.	0.	-0.359	0.	0.	-0.85	-2.48	-4.28	-14.	0.00	-0.86
35000.	1.6	130.	0.	3.630	0.	0.	-1.00	-9.12	-4.10	-26.	-0.00	0.34
35000.	2.0	130.	0.	5.087	0.	0.	-0.34	-7.90	-4.19	-20.	-0.00	1.12
60000.	1.0	130.	0.	-5.822	0.	0.	0.27	0.99	2.23	7.	0.00	-1.28
60000.	2.0	130.	0.	4.106	0.	0.	-0.61	-4.03	-2.02	-22.	-0.03	1.03

128

TABLE A-13

Envelope Survey of Parameter Sets

Set #		$\Delta FN, \%$	$\Delta T41, \text{ }^\circ R$	EPS3C, %	EN ₂ , %
0 (base)	\bar{x}	-0.8	+15	-1.0	0.2
	σ	6.1	23	2.6	0.7
1	\bar{x}	+0.8	1.9	0	0
	σ	6.4	13	0	0
2	\bar{x}	+1.1	-1.1	0	0
	σ	6.4	13	0	0
3	\bar{x}	1.7	-11.3	0	0
	σ	7.3	21	0	0
4	\bar{x}	1.7	-9.3	0	0
	σ	6.9	25	0	0
5	\bar{x}	0.8	-1.4	-.15	0
	σ	6.4	13	.85	0
6	\bar{x}	0.3	-1.2	-.10	0
	σ	7.0	13	4.23	0
7	\bar{x}	2.1	-14	.48	0
	σ	7.2	22	.92	0
8	\bar{x}	-0.6	-7	.07	0
	σ	6.1	12	4.14	0
9	\bar{x}	1.0	-2.3	0	-.10
	σ	6.7	11	0	1.0
10	\bar{x}	1.0	-1.8	0	-.13
	σ	6.2	9	0	1.0
11	\bar{x}	1.9	-15	0	.13
	σ	6.2	19	0	1.1
12	\bar{x}	1.0	-13	0	-.06
	σ	6.3	15	0	1.1

The large deviations on T41 synthesis eliminate sets 3 and 4 (which include an A8 bias, in the parameter set). There is no improvement on the prediction versus the base case set 0. The same applies to sets 7 and 11.

Further eliminations are accomplished according to Figure A-1. It shows the sequential logic for judging the performance of the various sets. The remaining sets were judged upon the magnitude of variations required to track the engine. Variations on A8 bias eliminated sets 8 and 12, variations in turbine nozzle area eliminated sets 1 and 9, and the fan efficiency variations for set 11 deleted it from the 1st. At this point four sets remain.

The results from the sensor error sensitivities are shown in Tables A-14 to A-17. To evaluate these, the root sum square of the effects is taken for each set. Root sum square (RSS) is used because the sensor errors are assumed to be random and uncorrelated.

The root sum square is defined as

$$\sigma_i = \sqrt{\sum \left(\left(\frac{dx_i}{dy_j} \right) \Delta y_j \right)^2}$$

FLOWPATH FOR VARIABLE SET SELECTION

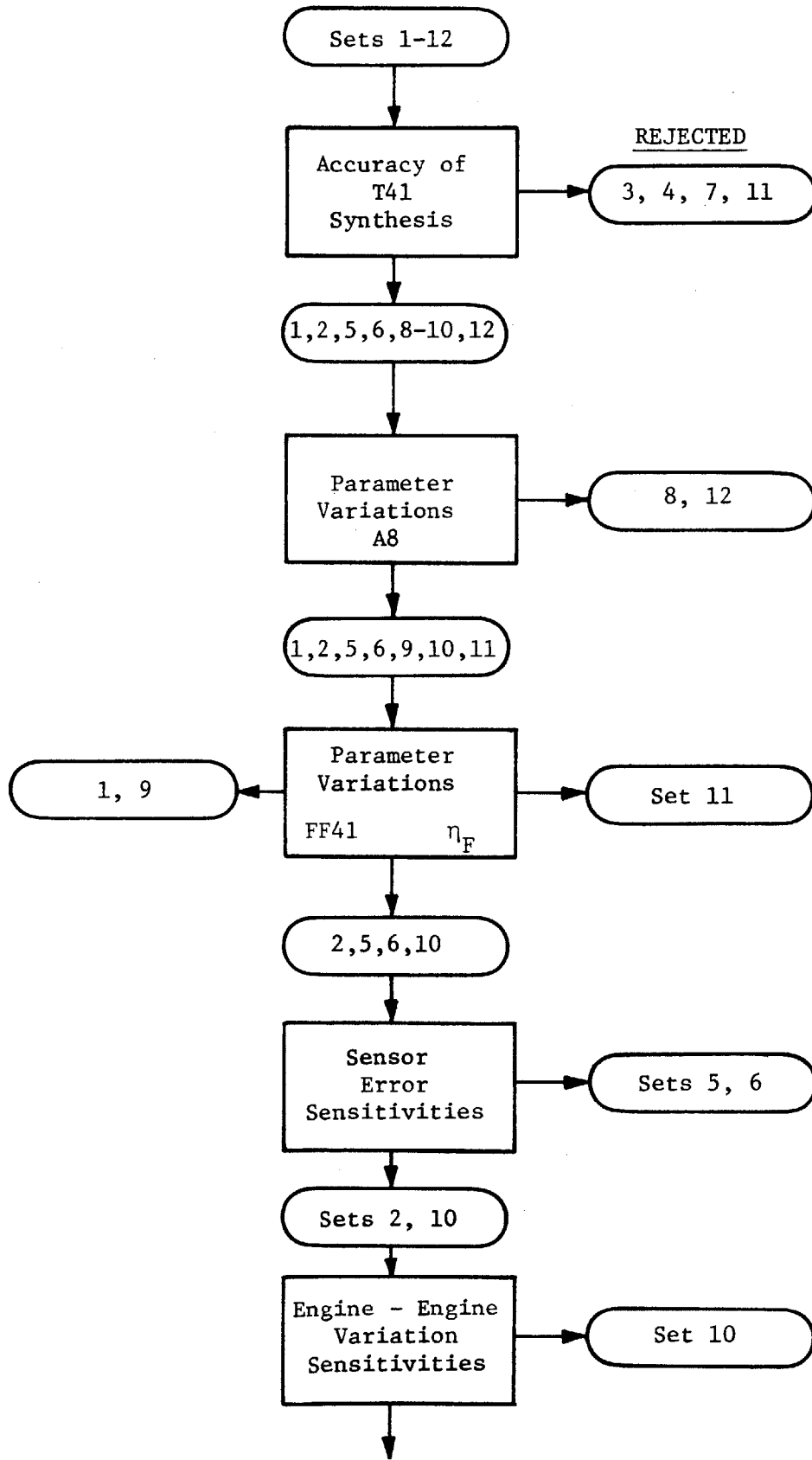


FIGURE A-1

TABLE A-14

SET 2:SENSOR ERRORS

ALT	XM	PLA	ZAETAF	ZAETAT	ZAFFM	ZAFF41	DWFMC	DABC	EFN	ET41	EPS3C	ENH
0.	0.	87.	-1.547	0.814	2.032	0.	-0.68	0.	3.03	-7.	-0.00	-0.00
0.	0.	87.	-1.538	0.692	2.025	0.	-5.42	0.	3.05	-8.	0.00	0.00
0.	0.	87.	-1.977	0.388	4.185	0.	-0.01	0.	3.74	8.	0.00	0.00
0.	0.	87.	-0.945	0.847	0.790	0.	-0.73	0.	3.02	-8.	-0.00	-0.00
0.	0.	87.	-2.351	1.355	1.849	0.	-0.83	0.	2.71	-6.	-0.00	-0.00
0.	0.	87.	-1.331	0.813	2.321	0.	-0.36	0.	3.46	-7.	-0.00	-0.00
0.	0.	87.	-2.202	0.307	1.811	0.	0.39	0.	3.09	17.	-0.00	-0.00
0.	0.	130.	-1.751	0.774	3.025	0.	-0.43	0.	4.61	-1.	-0.00	-0.00
0.	0.	130.	-1.739	0.611	3.023	0.	-5.18	0.	4.62	-1.	0.00	0.00
0.	0.	130.	-2.184	0.416	4.770	0.	0.12	0.	5.04	12.	0.00	0.00
0.	0.	130.	-1.142	0.806	1.778	0.	-0.47	0.	4.59	-1.	-0.00	-0.00
0.	0.	130.	-2.546	1.300	2.875	0.	-0.56	0.	4.26	1.	-0.00	-0.00
0.	0.	130.	-1.536	0.772	3.319	0.	-0.10	0.	5.04	-1.	-0.00	-0.00
0.	0.	130.	-2.421	0.251	2.912	0.	0.67	0.	4.53	24.	-0.00	-0.00

132

37952LV/ FP/ SET-2SEN

TABLE A-15

SET 5: SENSOR ERRORS

ALT	XM	PLA	ZAETAF	ZAETAT	ZAFFM	ZAFF41	DWFMC	DABC	EFN	ET41	EPS3C	ENH
0.	0.	87.	-1.085	0.811	2.651	0.	0.	0.	3.94	-7.	0.68	-0.00
0.	0.	87.	2.593	0.662	7.433	0.	0.	0.	10.58	-7.	5.68	0.00
0.	0.	87.	-1.971	0.387	4.194	0.	0.	0.	3.75	8.	0.01	0.00
0.	0.	87.	-0.476	0.844	1.424	0.	0.	0.	3.99	-8.	0.73	-0.00
0.	0.	87.	-1.801	1.351	2.598	0.	0.	0.	3.81	-6.	0.83	-0.00
0.	0.	87.	-1.085	0.811	2.651	0.	0.	0.	3.94	-7.	0.36	-0.00
0.	0.	87.	-2.453	0.310	1.464	0.	0.	0.	2.58	17.	-0.38	-0.00
0.	0.	130.	-1.467	0.770	3.414	0.	0.	0.	5.17	-1.	0.42	0.00
0.	0.	130.	2.142	0.562	8.217	0.	0.	0.	11.86	0.	5.41	0.00
0.	0.	130.	-2.267	0.416	4.654	0.	0.	0.	4.87	12.	-0.12	0.00
0.	0.	130.	-0.844	0.801	2.190	0.	0.	0.	5.22	-1.	0.47	-0.00
0.	0.	130.	-2.179	1.295	3.384	0.	0.	0.	5.01	1.	0.56	-0.00
0.	0.	130.	-1.467	0.770	3.414	0.	0.	0.	5.17	-1.	0.10	0.00
0.	0.	130.	-2.856	0.257	2.308	0.	0.	0.	3.63	24.	-0.66	-0.00

133

TABLE A-16

SET 6: SENSOR ERRORS

ALT	XM	PLA	ZAETAF	ZAETAT	ZAFFM	ZAFF41	DWFMC	DA8C	EFN	ET41	EPS3C	ENH
0.	0.	87.	0.	0.805	4.086	0.	1.54	0.	5.99	-7.	2.23	-0.00
0.	0.	87.	0.	0.685	4.064	0.	-3.32	0.	5.97	-8.	2.21	0.00
0.	0.	87.	0.	0.370	6.933	0.	2.87	0.	7.59	8.	2.86	0.00
0.	0.	87.	0.	0.841	2.061	0.	0.72	0.	4.95	-8.	1.45	-0.00
0.	0.	87.	0.	1.341	4.997	0.	2.57	0.	7.22	-5.	3.41	-0.00
0.	0.	87.	0.	0.805	4.086	0.	1.54	0.	5.99	-7.	1.90	-0.00
0.	0.	87.	0.	0.294	4.740	0.	3.57	0.	7.28	17.	3.16	-0.00
0.	0.	130.	0.	0.756	5.395	0.	2.11	0.	8.00	-0.	2.53	-0.00
0.	0.	130.	0.	0.595	5.372	0.	-2.80	0.	7.97	-1.	2.50	0.00
0.	0.	130.	0.	0.394	7.781	0.	3.29	0.	9.32	13.	3.14	-0.00
0.	0.	130.	0.	0.792	3.345	0.	1.29	0.	6.95	-1.	1.76	-0.00
0.	0.	130.	0.	1.273	6.349	0.	3.15	0.	9.22	1.	3.71	-0.00
0.	0.	130.	0.	0.756	5.395	0.	2.11	0.	8.00	-0.	2.20	-0.00
0.	0.	130.	0.	0.225	6.201	0.	4.21	0.	9.20	25.	3.49	-0.00

134

TABLE A-17

SET 10: SENSOR ERRORS

ALT	XM	PLA	ZAETAF	ZAETAT	ZAFFM	ZAFF41	DWFMC	DABC	EFN	ET41	EPS3C	ENH
0.	0.	87.	0.	-0.141	2.382	0.	-0.42	0.	3.64	-10.	0.00	-0.67
0.	0.	87.	0.	-0.253	2.372	0.	-5.18	0.	3.65	-11.	0.00	-0.66
0.	0.	87.	0.	-0.846	4.633	0.	0.32	0.	4.51	4.	0.00	-0.73
0.	0.	87.	0.	0.246	0.988	0.	-0.57	0.	3.40	-10.	0.00	-0.48
0.	0.	87.	0.	-0.141	2.382	0.	-0.42	0.	3.64	-10.	0.00	-1.16
0.	0.	87.	0.	-0.007	2.625	0.	-0.14	0.	3.98	-10.	0.00	-0.60
0.	0.	87.	0.	-1.032	2.311	0.	0.74	0.	3.95	12.	0.00	-0.76
0.	0.	130.	0.	-0.294	3.363	0.	-0.15	0.	5.36	-4.	0.00	-0.65
0.	0.	130.	0.	-0.445	3.358	0.	-4.92	0.	5.36	-5.	0.00	-0.64
0.	0.	130.	0.	-0.922	5.187	0.	0.47	0.	5.97	8.	0.00	-0.71
0.	0.	130.	0.	0.088	1.979	0.	-0.29	0.	5.09	-4.	0.00	-0.47
0.	0.	130.	0.	-0.294	3.363	0.	-0.15	0.	5.36	-4.	0.00	-1.14
0.	0.	130.	0.	-0.164	3.619	0.	0.14	0.	5.69	-4.	0.00	-0.58
0.	0.	130.	0.	-1.209	3.382	0.	1.05	0.	5.56	19.	0.00	-0.75

135

These are shown in Table A-18 below.

TABLE A-18

RSS of Sensor Error Sensitivities

Set #	$\Delta\eta_{F-PT}$	$\Delta\eta_{t-PT}$	$\Delta WIR \%$	$\Delta WF \%$	EFN %	ET41 °	EN ₂	EPS3C
2	1.29	0.86	2.51	1.34	0.92	28	--	--
5	4.12	0.86	5.31	--	6.78	28	--	5.2
6	--	0.87	3.65	2.77	2.61	28	--	1.8
10	--	1.20	2.64	1.43	1.01	26	.23	--

The parameter variations for sets 5 and 6 caused by sensor errors are too large and therefore the sets are eliminated. Finally, the two remaining sets are subjected to typical "known" engine to engine variations. The parameter changes for these variations are detailed in Tables A-19 and A-20, and summarized in Table A-21.

TABLE A-19

SET 2:ENG-ENG VARIATIONS

ALT	XM	PLA	ZAETAF	ZAETAT	ZAFFM	ZAFF41	DWFMC	DA8C	EFN	ET41	EPS3C	ENH
0.	0.	87.	-1.547	0.814	2.032	0.	-0.68	0.	3.03	-7.	-0.00	-0.00
0.	0.	87.	-0.971	0.859	1.840	0.	-0.77	0.	2.88	-8.	-0.00	-0.00
0.	0.	87.	-1.503	0.738	3.139	0.	-0.60	0.	3.06	-6.	-0.00	0.00
0.	0.	87.	-1.381	1.347	1.989	0.	-0.82	0.	2.94	-9.	-0.00	-0.00
0.	0.	87.	-0.662	0.655	2.206	0.	-0.63	0.	3.29	-10.	-0.00	0.00
0.	0.	87.	-1.278	1.546	2.074	0.	-0.80	0.	3.03	-14.	-0.00	-0.00
0.	0.	87.	-2.281	0.509	1.190	0.	-1.61	0.	1.72	-2.	-0.00	-0.00
0.	0.	87.	-1.093	1.008	1.645	0.	-0.86	0.	2.65	-13.	-0.00	-0.00
0.	0.	87.	-1.873	1.230	2.519	0.	-0.58	0.	3.48	-7.	-0.00	-0.00
0.	0.	87.	-1.845	0.521	1.750	0.	-0.95	0.	2.61	-9.	-0.00	-0.00

137

TABLE A-20

SET 10:ENG-ENG VARIATIONS

ALT	XM	PLA	ZAETAF	ZAETAT	ZAFFM	ZAFF41	DWFMC	DA8C	EFN	ET41	EPS3C	ENH
0.	0.	87.	0.	-0.141	2.382	0.	-0.42	0.	3.64	-10.	0.00	-0.67
0.	0.	87.	0.	0.268	2.066	0.	-0.61	0.	3.26	-10.	0.00	-0.47
0.	0.	87.	0.	-0.191	3.486	0.	-0.35	0.	3.64	-9.	0.00	-0.67
0.	0.	87.	0.	0.482	2.314	0.	-0.59	0.	3.48	-11.	0.00	-0.81
0.	0.	87.	0.	0.255	2.360	0.	-0.52	0.	3.55	-11.	0.00	-0.30
0.	0.	87.	0.	0.736	2.378	0.	-0.59	0.	3.53	-16.	0.00	-0.75
0.	0.	87.	0.	-0.904	1.701	0.	-1.23	0.	2.62	-7.	0.00	-0.76
0.	0.	87.	0.	0.339	1.900	0.	-0.68	0.	3.08	-16.	0.00	-0.56
0.	0.	87.	0.	0.046	2.948	0.	-0.26	0.	4.21	-11.	0.00	-0.97
0.	0.	87.	0.	-0.620	2.167	0.	-0.64	0.	3.34	-13.	0.00	-0.64

138

TABLE A-21
Effects of Engine to Engine Variations

Set 2: ΔWIR , $\Delta \eta_f$, $\Delta \eta_t$, ΔWF

	$\Delta \eta_f$	$\Delta \eta_t$	ΔWIR	ΔWF	EF_N	ET41
BASE	-1.55	0.81	2.03	-0.68	3.03	-7
$\eta_f \pm 0.6$ pts	-0.03	0.04	-0.19	-0.09	-0.15	-1
WIR $\pm 1.0\%$	0.04	-0.08	+0.11	+0.08	+0.03	+1
$\eta_c \pm 0.7$ pts	0.17	0.53	-0.04	-0.14	-0.09	-2
W25R $\pm 1.0\%$	0.89	-0.16	0.17	0.05	+0.23	-3
$\eta_t \pm 0.8\%$	0.27	-0.07	0.04	-0.12	0.00	-7
FF41 $\pm 1.0\%$	-0.73	-0.31	-0.84	-0.93	-1.31	+5
$\eta_{2t} \pm 1.0$ pts	0.45	0.19	-0.39	-0.18	-0.38	-6
FF45 $\pm 1.0\%$	-0.33	0.42	0.49	+0.10	0.45	0
Cooling $\pm .4\%$	-0.30	-0.29	-0.28	-0.27	-0.42	-2
RSS	1.35	0.84	1.12	1.02	1.52	11

Set 10: ΔWIR , $\Delta \eta_t$, ΔWF , Matching PS3C

	$\Delta \eta_t$	ΔWIR	ΔWF	EF_N	ET41	EN_2
BASE	-0.14	2.38	-0.42	3.64	-10	-.67
$\eta_f \pm 0.6$ pts	0.41	-0.32	-0.19	-0.38	0	+0.20
WIR $\pm 1.0\%$	0.05	0.10	0.07	0	+1	0
$\eta_c \pm 0.7$ pts	0.62	-0.07	-0.17	-0.64	-1	-0.14
W25R $\pm 1.0\%$	0.40	-0.02	-0.10	-0.09	-1	+0.37
$\eta_t \pm 0.8\%$	+0.08	0	-0.17	-0.11	-6	-0.03
FF41 $\pm 1.0\%$	-0.76	-0.68	-0.81	-0.02	+3	-0.09
$\eta_{2t} \pm 1.0$ pts	0.48	-0.48	-0.26	-0.56	-6	+0.11
FF45 $\pm 1.0\%$	0.19	0.57	0.16	+0.57	-1	-0.30
Cooling $\pm .4\%$	0.48	-0.22	-0.22	-0.30	+3	+0.03
RSS	1.34	1.09	0.95	0.96	9.7	0.62

In the last table, some explanation is necessary. The first part depicts the results for set 2. The first row shows the base deltas on the four parameters that correct the modelling errors. This applies to the "nominal" engine. The next row shows the deltas if the engine is 0.6 pts. better in fan efficiency than the nominal engine. The model responds by changing its fan efficiency by .57 points and the other variables by a small amount. In essence, the model identifies the difference in fan efficiency and then corrects itself accordingly. The third row shows a similar characteristic for fan speed flow changes, and the sixth for turbine efficiency changes. The root sum square of the random effects are summarized at the bottom.

The same information for set 10 is shown in the lower part. This set, with only two performance variables can only identify the two component changes. The thrust and T41 synthesis are about the same for the two methods. In conclusion set 2 is selected for its better ability in tracking performance changes due to the extra variable. Finally, the effects of engine to engine variations and sensor errors are combined as a final test.

TABLE A-22

Final Summary

	$\Delta\eta_f$	$\Delta\eta_t$	ΔWIR	ΔWF	EFN	ET41	EN ₂
Set 2:							
Sensors	1.29	0.86	2.51	1.34	0.92	28°	0
E-E var	1.35	0.84	1.12	1.02	1.52	11°	0
RSS	1.87	1.20	2.75	1.68	1.78	30°	0
Set 10:							
Sensors	--	1.20	2.64	1.43	1.01	26°	0.23
E-E var	--	1.34	1.09	0.95	0.96	10°	0.56
RSS	--	1.80	2.86	1.72	1.39	28°	0.61